[Electronic Supplementary Information to accompany *Chem. Sci.* manuscript SC-EDG-11-2011-000950]

Catalytically active supramolecular porphyrin boxes: acceleration of the methanolysis of phosphate triesters via a combination of increased local nucleophilicity and reactant encapsulation

Byungman Kang,[a] Josh W. Kurutz,[a] Kyoung-Tae Youm,[a,b] Ryan K. Totten,[a] Joseph T. Hupp,*[a] and SonBinh T. Nguyen*[a]

[a]*Department of Chemistry and International Institute for Nanotechnology, Northwestern University, 2145 Sheridan Road, Evanston, Illinois 60208-3113, USA.* [b]*Current address: Samsung Cheil Industries Inc., Uiwang, Gyeonggi 437-711, Republic of Korea*

Table of Contents *Page number*

I. General Information. ^{1}H and ^{13}C NMR spectra were recorded on either a Varian INOVA 500 FT-NMR (499.6 MHz for ^{1}H, 125.6 MHz for ^{13}C) or a Varian Mercury 400 FT-NMR spectrometer (400.6 MHz for ^{1}H, 100.7 MHz for ^{13}C). ^{1}H NMR data are reported as follows: chemical shift (multiplicity (br s = broad singlet, s = singlet, d = doublet, t = triplet, q = quartet, and m = multiplet), coupling constant and integration). ^{1}H and ^{13}C chemical shifts are reported in ppm downfield from tetramethylsilane (TMS, δ scale) using the residual solvent resonances as internal standards. ^{31}P NMR spectra were recorded on a Varian INOVA 400 FTNMR spectrometer (161.9 MHz for ^{31}P) and externally referenced to 85% phosphoric acid solution in D_2O.

Analytical gel-permeation chromatography (GPC) was carried out on a Varian ProStar HPLC system (Varian Inc., USA) equipped with a multi-wavelength detector using a Phenomenex Phenogel 100-Å column packed in CH_2Cl_2 with a 7.80-mm inner diameter and a 300-mm length. Samples were eluted using CH_2Cl_2 (flow rate = 1 mL/min) and monitored at 440 nm.

Matrix-assisted laser desorption ionization time-of-flight (MALDI-ToF) mass spectra were recorded on a Bruker Autoflex III MALDI spectrometer using either reflective positive or linear negative ionization method with either anthracene or dithranol matrices. The use of non-acidic anthracene matrix is critical for porphyrin containing Al-OMe: if the acidic 2-hydroxy-1-naphthoic acid matrix is used, extensive demetallation occurs. When the slightly less acidic matrix dithranol was used, demetallion was not observed but significant loss of the OMe axial ligand does occur and μ-oxo dimer can often be observed. High-resolution electrospray ionization mass spectrometric (HRESIMS) data were obtained by staff members in the Integrated Molecular Structure Education and Research Center (IMSERC), Northwestern University (Evanston, IL, USA).

UV-vis spectra were obtained in CH_2Cl_2 or $CHCl_3$ on a Varian Cary 500 spectrophotometer unless otherwise noted. Fluorescence emission spectra were obtained in a mixture of $CHCl_3$/MeOH (1:1 v/v) on a Jobin Yvon FluoroLog fluorometer (λ_{ex} = 442 nm, λ_{em} = 500 – 800 nm, slit width = 3 nm) (HORIBA Jobin Yvon Inc., Edison, NJ, USA). Dynamic light-scattering (DLS) measurements were performed on a Zetasizer Nano ZS (Malvern Instruments, Malvern, UK) with a He-Ne laser (633 nm). Non-invasive backscatter method (detection at 173° scattering angle) was used.

II. General procedures and materials. All air- or water-sensitive reactions were carried out under nitrogen using oven-dried glassware. All synthetic and catalytic experiments concerning porphyrin and porphyrin derivatives were carried out under light-deficient conditions: the hood lights were turned off and the reaction flasks are covered with aluminum foil to further minimize light exposure. Isolated porphyrin products were stored at low temperatures (-10 °C) in foil-covered vials. All flash-chromatography was carried out using silica gel (MP Silitech 60-200 mesh) under a positive pressure of nitrogen, unless otherwise noted. Analytical thin layer chromatography (TLC) was performed using glass-backed silica gel 60 F_{254} plates (Merck EMD-571507). Visualization of the TLC results was achieved either by observation under UV light (254 nm), or via treatment with 10 wt% phosphomolybdic acid in ethanol followed by heating.

Tetrahydrofuran and dichloromethane (Fisher Scientific) were dried over neutral alumina in a Dow-Grubbs solvent system[S1] installed by Glass Contours (now SG Water, Nashua, NH, USA). All other reagents and solvents were purchased from the Aldrich Chemical Company (Milwaukee, WI, USA) and used without further purification. Deuterated solvents were purchased from Cambridge Isotope Laboratories (Andover, MA, USA) and used without further purification.

III. Preparation of the template porphyrin Py-MesP.

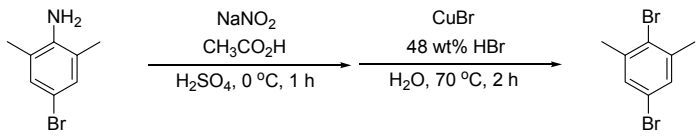

1

2,5-Dibromo-1,3-dimethylbenzene (1). This compound was synthesized following a modified literature procedure.[S2] Into a 500 mL round-bottom flask equipped with a magnetic stir bar was added conc. sulfuric acid (70

mL). The flask was cooled down in an ice bath while stirring and $NaNO_2$ (6.9 g, 0.10 mol) was added. After 30 min, a solution of 4-bromo-2,6-dimethylaniline (20 g, 0.10 mol) in glacial acetic acid (80 mL) was slowly added to the reaction solution. This mixture was allowed to stir at 0 ºC for 1 h before additional glacial acetic acid (50 mL) was added. The resulting suspension was then poured into a mixture of copper(I) bromide (17.2 g, 0.12 mol) and 48 wt% hydrobromic acid (70 mL). The combined mixture was allowed to warm to 70 °C and vigorously stirred for 2 h. The resulting mixture was diluted with ice water (200 mL) and extracted with hexanes (3 × 150 mL). The combined organic extracts were dried over $MgSO_4$, filtered, and concentrated under reduced pressure. Purification via silica gel column chromatography (column dimensions = 60 mm × 250 mm, hexanes eluent) afforded 12.7 g (48% yield, 0.048 mol) of **1** as a colorless oil. Spectroscopic data for **1** was in good agreement with literature data.[S2] R_f = 0.62 (hexanes). ^{1}H NMR (499.6 MHz, $CDCl_3$): δ 2.38 (s, 6H, C*H*$_3$), 7.21 (s, 2H, Ar-*H*). {^{1}H}^{13}C NMR (125.6 MHz, $CDCl_3$): δ 23.6 (*C*H$_3$), 120.2 (C_p), 126.3 (C_i), 130.8 (C_m), 140.2 (C_o).

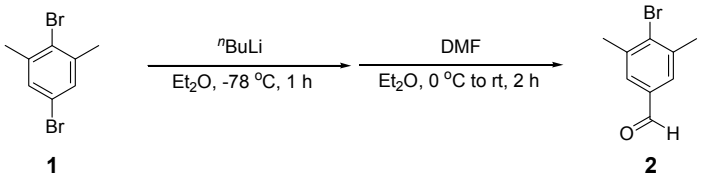

4-Bromo-3,5-dimethylbenzaldehyde (2). This compound was synthesized following a modified literature procedure.[S3] In a 100 mL round-bottom flask equipped with a magnetic stir bar, a solution of compound **1** (4.0 g, 15.1 mmol) in anhydrous Et_2O (50 mL) was allowed to cool to -78 °C under N_2 before ^{n}BuLi (9.4 mL of a 1.6 M solution in hexanes, 1.0 equiv) was added dropwise. After stirring for 1 h under N_2 at -78 °C, *N,N*-dimethylformamide (3.6 mL, 46.9 mmol, 3.1 equiv) was added and the reaction mixture was allowed to warm to room temperature. It was then acidified with 5 wt% HCl solution (10 mL) and extracted with diethyl ether (3 × 80 mL). The combined organic extracts were dried over $MgSO_4$, filtered, and concentrated under reduced pressure. Purification via silica gel column chromatography (column dimensions = 60 mm × 250 mm, eluent = EtOAc/hexanes 1:6 v/v) afforded 2.6 g (81% yield, 12.2 mmol) of **2** as colorless crystals. Spectroscopic data for **2** was in good agreement with literature data.[S3] R_f = 0.34 (EtOAc/hexanes = 1:6 v/v). ^{1}H NMR (499.6 MHz, $CDCl_3$): δ 2.47 (s, 6H, C*H*$_3$), 7.54 (s, 2H, Ar-*H*), 9.91 (s, 1H, C*H*O). {^{1}H}^{13}C NMR (125.6 MHz, $CDCl_3$): δ 24.1 (*C*H$_3$), 129.0 (C_o), 132.7 (C_p), 134.8 (C_i), 139.7 (C_m), 191.9 (*C*HO).

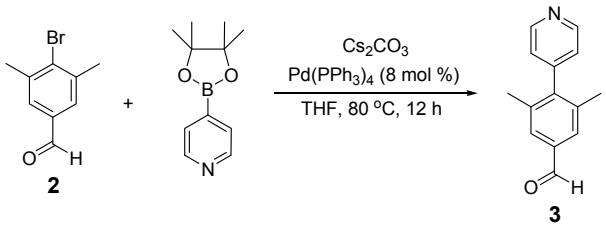

3,5-dimethyl-4-(4´-pyridyl)benzaldehyde (3). A 250 mL two-necked flask, equipped with a septum inlet and a reflux condenser, was degassed with N_2 and then charged with compound **2** (2.35 g, 11.0 mmol), Cs_2CO_3 (4.3 g, 13.2 mmol), and $Pd(PPh_3)_4$ (1.0 g, 0.87 mmol). A degassed solution of 4-pyridineboronic acid pinacol ester (2.7 g, 13.1 mmol) in THF (130 mL) was added rapidly through the septum inlet with a syringe. The mixture was heated to 80 °C for 12 h under stirring, cooled down to room temperature, and then poured into water (100 mL). The

resulting mixture was extracted with EtOAc (3 × 120 mL). The combined organic extracts were dried over $MgSO_4$, filtered, and concentrated under reduced pressure. Purification via silica gel column chromatography (column dimensions = 40 mm × 300 mm, eluent = EtOAc/hexanes 1:1 v/v) afforded 2.0 g (86% yield, 9.5 mmol) of **3** as a pale yellow solid. R_f = 0.35 (EtOAc/hexanes = 1:1 v/v). ^{1}H NMR (499.6 MHz, $CDCl_3$): δ 2.10 (s, 6H, CH_3), 7.10 (d, J = 5.5 Hz, 2H, pyridyl C*H*), 7.64 (s, 2H, Ar-*H*), 8.73 (d, J = 5.5 Hz, 2H, pyridyl C*H*), 10.01 (s, 1H, C*H*O). {^{1}H}^{13}C NMR (125.6 MHz, $CDCl_3$): δ 20.8 (CH_3), 123.8 (pyridyl C_m), 129.1 (Ar-C_o), 136.0 (Ar-C_i), 136.7 (Ar-C_m), 145.3 (Ar-C_p), 148.5 (pyridyl C_p), 150.6 (pyridyl C_o), 192.4 (*C*HO). HRESIMS: Calcd for $[C_{14}H_{13}NO+H]^+$: 212.1075, found: *m/z* 212.1081 $[M+H]^+$.

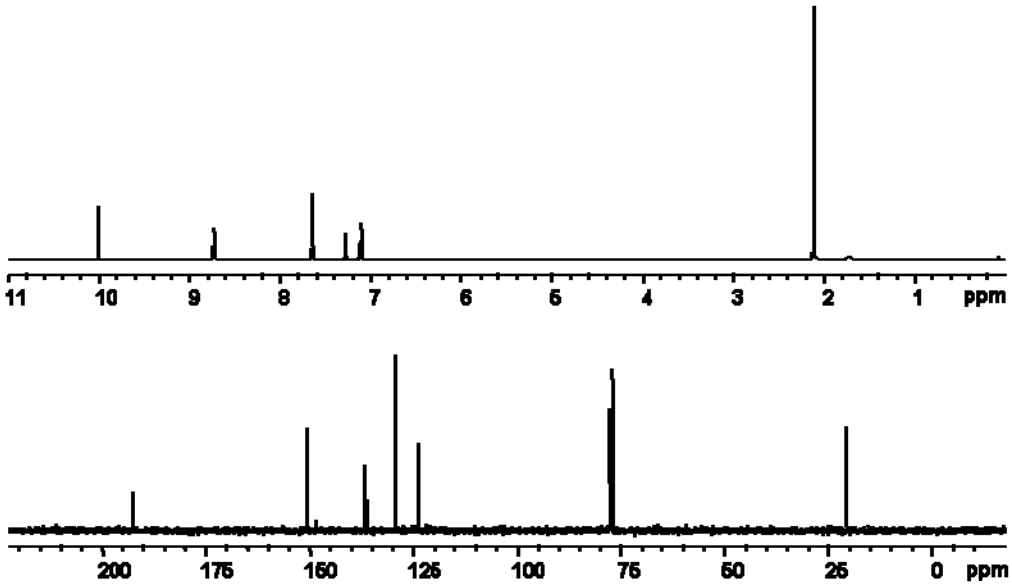

Fig. S1 The ^{1}H (top) and ^{13}C NMR (bottom) spectra for 3,5-dimethyl-4-(4′-pyridyl)benzaldehyde (**3**).

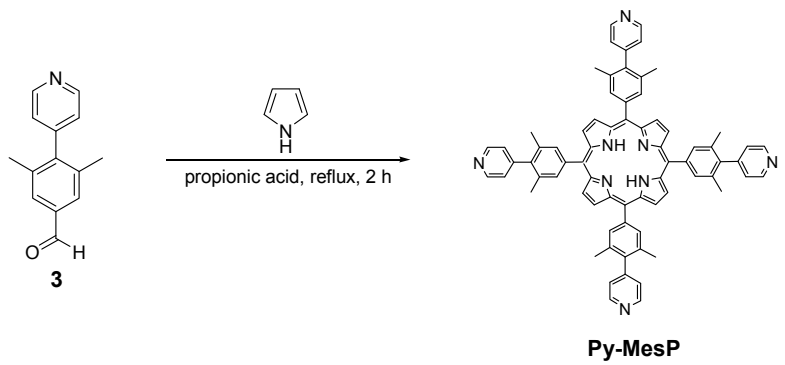

[5,10,15,20-Tetrakis(4-(4′-pyridyl)-3,5-(dimethyl)phenyl)]porphine (Py-MesP). In a 100 mL round-bottom flask equipped with a magnetic stir bar, freshly distilled pyrrole (0.41 mL, 5.92 mmol) was added dropwise to a solution of compound **3** (1.25 g, 5.92 mmol) in propionic acid (24 mL). The reaction mixture was refluxed for 2 h under N_2 and then cooled down to room temperature. Excess propionic acid was removed by vacuum distillation at 60 °C and 20 mm Hg. The resulting black residue was dissolved in dichloromethane (100 mL) and washed with saturated aqueous Na_2CO_3 (30 mL). The remaining organic layer was dried over $MgSO_4$, filtered, and concentrated under reduced pressure. Purification via silica gel column chromatography (column dimensions = 40 mm × 300 mm, eluent = MeOH/CH_2Cl_2 1:15 v/v) afforded 562 mg (9.2% yield, 0.54 mmol) of Py-MesP as a purple solid. R_f

= 0.25 (MeOH/CH_2Cl_2 = 1:15 v/v). ^{1}H NMR (499.6 MHz, $CDCl_3$): δ -2.69 (s, 2H, N*H*), 2.35 (s, 24H, CH_3), 7.50 (d, *J* = 5.0 Hz, 8H, β-pyridyl-*H*), 8.04 (s, 8H, Ar-*H*), 8.87 (d, *J* = 4.5 Hz, 8H, α-pyridyl-*H*), 9.03 (s, 8H, β-*H*). {^{1}H}^{13}C NMR (125.6 MHz, $CDCl_3$): δ 21.1 (CH_3), 120.2 (C_3), 125.0 (pyridyl-C_m), 133.7 (C_5, Ar-C_i), 134.5 (C_4, Ar-C_o), 138.7 (Ar-C_m), 141.9 (Ar-C_p), 149.6 (pyridyl-C_p), 150.5 (pyridyl-C_o). MALDI-ToF (reflective positive mode): Calcd for $C_{72}H_{58}N_8$: 1034.47, found: *m/z* 1034.07 $[M]^+$. UV-vis (nm, (ε ×10^4 /$M^{-1}cm^{-1}$)): 420 (22.7), 516 (0.9), 553 (0.5), 590 (0.3), 648 (0.3).

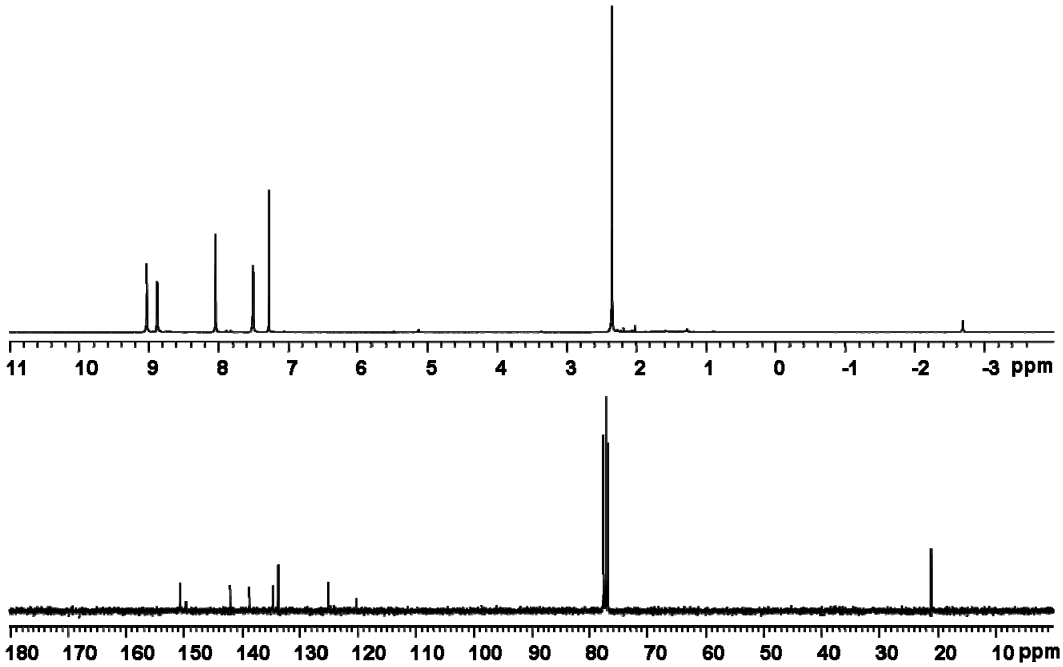

Fig. S2 The ^{1}H (top) and ^{13}C NMR (bottom) spectra for [5,10,15,20-tetrakis(4-(4´-pyridyl)-3,5-(dimethyl)phenyl)]porphine (**Py-MesP**).

IV. Preparation of porphyrins possessing pentenyloxyphenyl substituents.

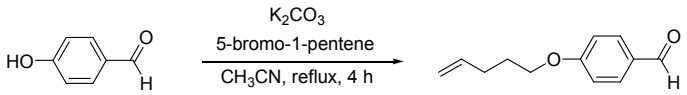

4

4-(1-Pentenyloxy)benzaldehyde (4). This compound was synthesized following a modified literature procedure.[S4] Into a 250 mL round bottom flask equipped with a magnetic stir bar and a water-cooled reflux condenser were combined 4-hydroxybenzaldehyde (5.0 g, 40.9 mmol), K_2CO_3 (11.9 g, 86.1 mmol), anhydrous acetonitrile (150 mL), and 5-bromo-1-pentene (9.1 g, 61.1 mmol). The resulting mixture was then refluxed for 4 h under N_2. The solution was cooled to room temperature, filtered, and washed with dichloromethane (3 × 50 mL). The combined organics were evaporated to dryness under reduced pressure. The resultant residue was dissolved in dichloromethane (150 mL) and washed with water (50 mL). Organic layer was dried over $MgSO_4$, filtered, and concentrated under reduced pressure. Purification via silica gel column chromatography (column dimensions = 60 mm × 250 mm, eluent = EtOAc/hexanes 1:3 v/v) afforded 7.5 g (97% yield, 39.7 mmol) of **4** as a pale yellow oil. Spectroscopic data for **4** was in good agreement with literature data.[S4] R_f = 0.50 (EtOAc/hexanes = 1:3 v/v). ^{1}H NMR (499.6 MHz, $CDCl_3$): δ 1.93 (m, 2H, CH_2CH$_2$O), 2.26 (dd, J_1 = 13.5 Hz, J_2 = 6.5 Hz, 2H, CH$_2$=CHCH_2),

4.06 (t, J = 6.5 Hz, 2H, CH_2CH_2O), 5.03 (dd, J_1 = 25.5 Hz, J_2 = 10.0 Hz, 1H, CH_2=$CHCH_2$), 5.08 (dd, J_1 = 25.5 Hz, J_2 = 17.0 Hz, 1H, CH_2=$CHCH_2$), 5.86 (m, 1H, CH_2=$CHCH_2$), 6.99 (d, J = 8.0 Hz, 2H, Ar-*H*), 7.83 (d, J = 8.5 Hz, 2H, Ar-*H*), 9.88 (s, 1H, C*H*O). $\{^1H\}^{13}C$ NMR (125.6 MHz, $CDCl_3$): δ 28.3 (CH_2CH_2O), 30.1 (CH_2=$CHCH_2$), 67.7 (CH_2CH_2O), 114.9 (Ar-C_o), 115.6 (CH_2=$CHCH_2$), 129.9 (Ar-C_p), 132.1 (Ar-C_m), 137.6 (CH_2=$CHCH_2$), 164.3 (Ar-C_i), 191.0 (*C*HO).

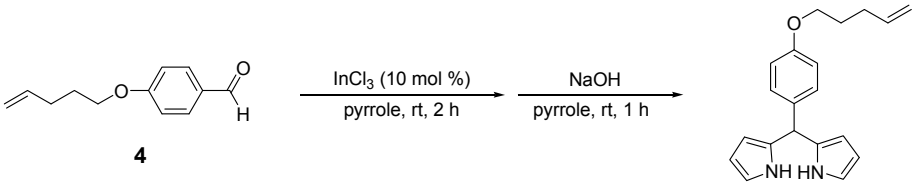

4 **5**

(4-(1-Pentenyloxy)phenyl)dipyrromethane (5). Compound **4** (3.0 g, 15.8 mmol) was combined with freshly distilled pyrrole (110 mL) in a 200 mL Schlenk flask equipped with a magnetic stir bar. This mixture was degassed for 20 min with a stream of N_2. Solid $InCl_3$ (349 mg, 1.58 mmol) was then added in one portion, and the reaction mixture was stirred under N_2 at room temperature. After 2 h, solid NaOH (1.9 g, 47.5 mmol) was added to quench the reaction, followed by additional stirring for 1h at room temperature. The reaction mixture was filtered and evaporated to dryness by rotary evaporation. Excess pyrrole was removed by vacuum distillation at 60 °C and 20 mm Hg. The resulting residue was then subjected to silica gel column chromatography (column dimensions = 60 mm × 250 mm, eluent = hexanes/CH_2Cl_2/EtOAc 7:2:1 v/v/v) to yield the desired product as a yellow solid (3.1 g, 64%, 10.1 mmol). Spectroscopic data for **5** was in good agreement with literature data.[S5] R_f = 0.38 (hexanes/CH_2Cl_2/EtOAc = 7:2:1 v/v/v). ^1H NMR (499.6 MHz, CD_2Cl_2): δ 1.88 (m, 2H, CH_2CH_2O), 2.24 (dd, J_1 = 14.0 Hz, J_2 = 7.0 Hz, 2H, CH_2=$CHCH_2$), 3.97 (t, J = 6.5 Hz, 2H, CH_2CH_2O), 5.01 (dd, J_1 = 34.2 Hz, J_2 = 10.0 Hz, 1H, CH_2=$CHCH_2$), 5.08 (dd, J_1 = 34.2 Hz, J_2 = 17.5 Hz, 1H, CH_2=$CHCH_2$), 5.39 (s, 1H, C*H*), 5.87 (s, 2H, pyrrole C*H*), 5.91 (m, 1H, CH_2=$CHCH_2$), 6.12 (d, J = 3.0 Hz, 2H, pyrrole C*H*), 6.67 (s, 2H, pyrrole C*H*), 6.86 (d, J = 8.5 Hz, 2H, Ar-*H*), 7.12 (d, J = 8.5 Hz, 2H, Ar-*H*), 7.98 (br s, 2H, N*H*). $\{^1H\}^{13}C$ NMR (125.6 MHz, CD_2Cl_2): δ 29.0 (CH_2CH_2O), 30.6 (CH_2=$CHCH_2$), 43.7 (*C*H), 67.8 (CH_2CH_2O), 107.3 (pyrrole C_2), 108.7 (pyrrole C_3), 115.0 (Ar-C_o), 115.4 (CH_2=$CHCH_2$), 117.5 (pyrrole C_4), 129.8 (Ar-C_p), 133.5 (Ar-C_m), 134.9 (pyrrole C_1), 138.6 (CH_2=$CHCH_2$), 158.6 (Ar-C_i).

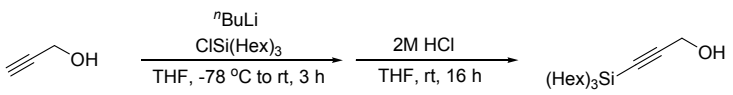

6

3-Trihexylsilyl-2-propyn-1-ol (6). This compound was synthesized following a modified literature procedure.[S6] In a 500 mL round-bottom flask equipped with a magnetic stir bar, a solution of propargyl alcohol (1.0 g, 17.8 mmol) in anhydrous THF (150 mL) was allowed to cool to -78 °C under N_2 before ^nBuLi (23.4 mL of a 1.6 M solution in hexanes, 2.1 equiv) was added dropwise. After stirring for 30 min at -78 °C under N_2, chlorotrihexylsilane (12.2 g, 38.3 mmol) was slowly added to the mixture. The reaction mixture was then allowed to warm to room temperature and stirred under N_2 for additional 3 h. It was then acidified with 2 M HCl solution (60 mL) and the reaction was stirred for 12 h at room temperature. The solution was extracted with Et_2O (3 × 150

mL) and the combined organic extracts were washed with saturated aqueous $NaHCO_3$ (100 mL) and brine (100 mL) before being dried over $MgSO_4$. Purification via silica gel column chromatography (column dimensions = 60 mm × 250 mm, eluent = EtOAc/hexanes 1:10 v/v) afforded 5.1 g (85%, 15.1 mmol) of **6** as a pale yellow oil. R_f = 0.45 (EtOAc/hexanes = 1:8 v/v). ^{1}H NMR (499.6 MHz, $CDCl_3$): δ 0.60 (t, *J* = 9.0 Hz, 6H, C*H*$_2$Si), 0.88 (t, *J* = 7.0 Hz, 9H, C*H*$_3$), 1.30 (m, 24H, C*H*$_2$), 1.82 (s, 1H, O*H*), 4.26 (s, 2H, C*H*$_2$OH). {^{1}H}^{13}C NMR (125.6 MHz, $CDCl_3$): δ 13.4 (*C*H$_2$Si), 14.3 (*C*H$_3$), 22.8 (*C*H$_2$), 23.9 (*C*H$_2$), 31.7 (*C*H$_2$), 33.3 (*C*H$_2$), 51.8 (*C*H$_2$OH), 89.0 (SiC≡*C*), 105.0 (Si*C*≡C).

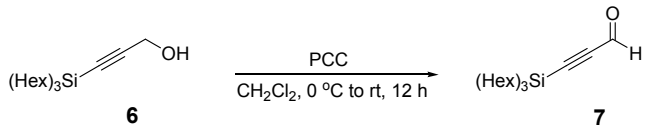

3-Trihexylsilyl-2-propynal (7). In a 250 mL round-bottom flask equipped with a magnetic stir bar, a solution of compound **6** (3.8 g, 11.2 mmol) in CH_2Cl_2 (5 mL) was added dropwise at 0 °C to a suspension of pyridinum chlorochromate (4.8 g, 22.4 mmol) in CH_2Cl_2 (150 mL). After stirring for 9 h, the dark suspension was filtered through a pad of silica gel, which was then washed with CH_2Cl_2 (200 mL). The volatiles were evaporated from the filtrate using a rotary evaporator. Purification via silica gel column chromatography (column dimensions = 60 mm × 250 mm, eluent = EtOAc/hexanes 1:25 v/v) afforded 3.27 g (87%, 9.7 mmol) of **7** as a colorless oil. Spectroscopic data for **7** was in good agreement with literature data.[S7] R_f = 0.45 (EtOAc/hexanes = 1:40 v/v). ^{1}H NMR (499.6 MHz, $CDCl_3$): δ 0.69 (t, *J* = 9.0 Hz, 6H, C*H*$_2$Si), 0.89 (t, *J* = 6.5 Hz, 9H, C*H*$_3$), 1.32 (m, 24H, C*H*$_2$), 9.18 (s, 1H, C*H*O). {^{1}H}^{13}C NMR (125.6 MHz, $CDCl_3$): δ 12.7 (*C*H$_2$Si), 14.3 (*C*H$_3$), 22.8 (*C*H$_2$), 23.8 (*C*H$_2$), 31.6 (*C*H$_2$), 33.2 (*C*H$_2$), 102.5 (SiC≡*C*), 103.7 (Si*C*≡C), 176.8 (*C*HO).

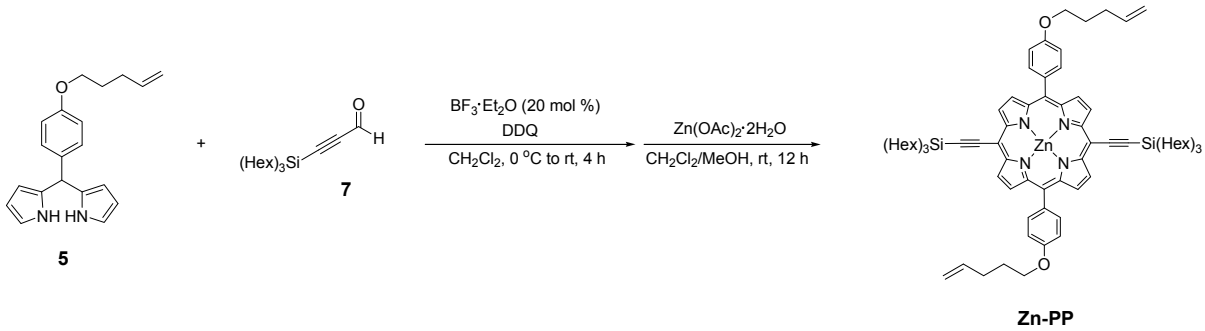

[[5,15-Bis(4-(1-pentenyloxy)phenyl)-10,20-bis((trihexylsilyl)ethynyl)]porphinato]zinc(II) (Zn-PP).

In a 1 L Schlenk flask equipped with a magnetic stir bar were combined compound **5** (1.90 g, 6.2 mmol), 3-trihexylsilyl-2-propynal **7** (2.09 g, 6.2 mmol), and CH_2Cl_2 (900 mL). The resulting mixture was degassed with a stream of N_2 for 10 min and cooled to 0 °C. After $BF_3 \cdot Et_2O$ (0.15 mL) was added, the reaction mixture was stirred under N_2 for 30 min at 0 °C before being warmed up to room temperature. After stirring for an additional 30 min at room temperature, DDQ (2.81 g, 12.4 mmol) was added as a solid and stirring was continued for an additional 3 h. A solution of $Zn(OAc)_2 \cdot 2H_2O$ (2.04 g, 9.3 mmol) in MeOH (30 mL) was then added and the reaction mixture was allowed to stir for 12 h more before being evaporated to dryness using a rotary evaporator. The crude product was purified by silica gel column chromatography (column dimensions = 40 mm × 300 mm, eluent = THF/hexanes 1:15 v/v) to yield the desired product as a purple solid (1.83 g, 22%, 1.4 mmol). R_f = 0.37 (THF/hexanes = 1:20 v/v). ^{1}H

NMR (499.6 MHz, $CDCl_3$): δ 0.91 (t, J = 7.0 Hz, 18H, ^{n}Hex CH_3), 1.03 (m, 12H, ^{n}Hex CH_2), 1.35-1.44 (m, 24H, ^{n}Hex CH_2), 1.55 (m, 12H, ^{n}Hex CH_2), 1.77 (m, 12H, ^{n}Hex CH_2), 2.13 (m, 4H, CH_2CH$_2$O), 2.45 (m, 4H, CH$_2$=CHCH_2), 4.30 (t, J = 6.0 Hz, 4H, CH$_2$CH_2O), 5.13 (dd, J_1 = 44.5 Hz, J_2 = 10.5 Hz, 2H, CH_2=CHCH$_2$), 5.22 (dd, J_1 = 44.5 Hz, J_2 = 17.5 Hz, 2H, CH_2=CHCH$_2$), 6.01 (m, 2H, CH$_2$=CHCH$_2$), 7.30 (d, J = 8.5 Hz, 4H, Ar-H), 8.09 (d, J = 8.0 Hz, 4H, Ar-H), 8.94 (d, J = 4.5 Hz, 4H, β-H_2), 9.70 (d, J = 4.5 Hz, 4H, β-H_1). {^{1}H}^{13}C NMR (125.6 MHz, $CDCl_3$): δ 16.5 (CH$_2$Si), 16.8 (CH$_3$), 25.3 (CH$_2$), 27.0 (CH$_2$), 31.3 (CH$_2$CH$_2$O), 32.9 (CH$_2$=CHCH$_2$), 34.3 (CH$_2$), 36.0 (CH$_2$), 70.2 (CH$_2$$CH_2$O), 103.1 (SiC≡$C$), 104.3 (Si$C$≡C), 111.1 ($C_{10}$), 115.4 ($CH_2$=CHCH$_2$), 118.0 (Ar-$C_o$), 125.1 ($C_5$), 133.8 (Ar-$C_p$), 135.4 (Ar-$C_m$), 137.1 ($C_3$), 138.1 ($C_2$), 140.6 (CH$_2$=$CHCH_2$), 153.2 ($C_1$), 154.9 ($C_4$), 161.5 (Ar-$C_i$). MALDI-ToF (reflective positive mode): Calcd for $C_{82}H_{112}N_4O_2Si_2Zn$: 1304.76, found: m/z 1304.72 $[M]^+$. UV-vis (nm, (ε ×10^4 /M^{-1}cm^{-1})): 436 (43.2), 538 (0.4), 577 (1.5), 625 (3.6).

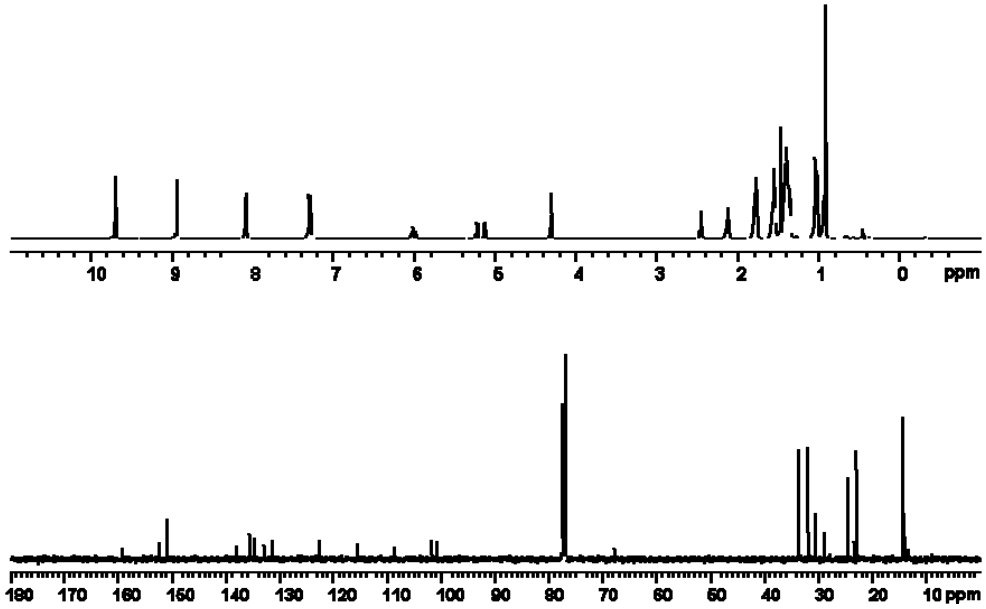

Fig. S3 The ^{1}H (top) and ^{13}C NMR (bottom) spectra for [[5,15-bis(4-(1-pentenyloxy)phenyl)-10,20-bis((trihexylsilyl)ethynyl)]porphinato]zinc(II) (**Zn-PP**).

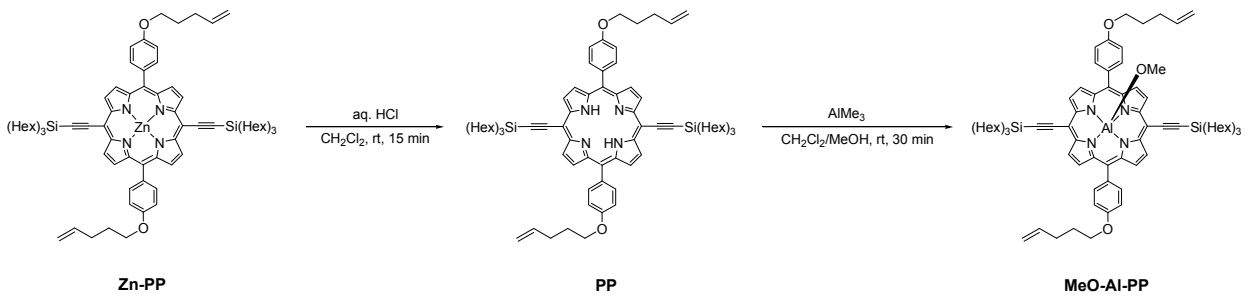

[[5,15-Bis(4-(1-pentenyloxy)phenyl)-10,20-bis((trihexylsilyl)ethynyl)]porphinato]aluminum(III) methoxide (MeO-Al-PP). To a magnetically stirred solution of **Zn-PP** (100 mg, 76.5 μmol) in CH_2Cl_2 (25 mL) in a 50 mL round bottom flask was added aqueous HCl (5 mL of an 18.5 wt% solution). After stirring for 15 min at room temperature, the resulting mixture was washed consecutively with water (40 mL), saturated aqueous $NaHCO_3$ (30 mL), and brine (30 mL) before being dried over Na_2SO_4 and filtered. The filtrate was then evaporated to dryness using a rotary evaporator and the remaining residue was subjected to silica gel column chromatography (column

dimensions = 20 mm × 200 mm, eluent = CH_2Cl_2/hexanes 1:2 v/v) to yield the demetallated product (PP) as a purple solid (88 mg, 92%, 70.7 μmol). R_f = 0.34 (CH_2Cl_2/hexanes = 1:3 v/v). ^{1}H NMR (499.6 MHz, $CDCl_3$): δ -2.12 (s, 2H, N*H*), 0.91 (t, *J* = 6.0 Hz, 18H, ^{n}Hex CH_3), 1.02 (m, 12H, ^{n}Hex CH_2), 1.35-1.45 (m, 24H, ^{n}Hex CH_2), 1.54 (m, 12H, ^{n}Hex CH_2), 1.77 (m, 12H, ^{n}Hex CH_2), 2.13 (m, 4H, CH_2CH$_2$O), 2.45 (m, 4H, CH$_2$=CHCH_2), 4.30 (t, *J* = 6.0 Hz, 4H, CH$_2$CH_2O), 5.13 (dd, J_1 = 44.2 Hz, J_2 = 11.0 Hz, 2H, CH_2=CHCH$_2$), 5.22 (dd, J_1 = 44.2 Hz, J_2 = 16.5 Hz, 2H, CH_2=CHCH$_2$), 6.01 (m, 2H, CH$_2$=C*H*CH$_2$), 7.31 (d, *J* = 8.0 Hz, 4H, Ar-*H*), 8.09 (d, *J* = 9.0 Hz, 4H, Ar-*H*), 8.85 (d, *J* = 5.0 Hz, 4H, β-H_2), 9.61 (d, *J* = 4.5 Hz, 4H, β-H_1). {^{1}H}^{13}C NMR (125.6 MHz, $CDCl_3$): δ 14.0 (*C*H$_2$Si), 14.4 (*C*H$_3$), 22.9 (*C*H$_2$), 24.6 (*C*H$_2$), 28.9 (*C*H$_2$CH$_2$O), 30.5 (CH$_2$=CH*C*H$_2$), 31.9 (*C*H$_2$), 33.6 (*C*H$_2$), 67.8 (CH$_2$*C*H$_2$O), 101.2 (SiC≡*C*), 101.4 (Si*C*≡C), 108.2 (C_{10}), 113.2 (*C*H$_2$=CHCH$_2$), 115.6 (Ar-C_o), 121.8 (C_5), 133.8 (Ar-*Cp* and C_1), 135.8 (Ar-C_m and CH$_2$=*C*HCH$_2$), 138.1 (C_2 and C_3), 159.3 (Ar-*Ci* and C_4). MALDI-ToF (reflective positive mode): Calcd for $C_{82}H_{114}N_4O_2Si_2$: 1243.98, found: *m/z* 1243.36 [M]$^+$. UV-vis (nm, (ε ×10^4 /M^{-1}cm^{-1})): 434 (53.5), 546 (1.8), 586 (7.4), 623 (1.0), 682 (3.2).

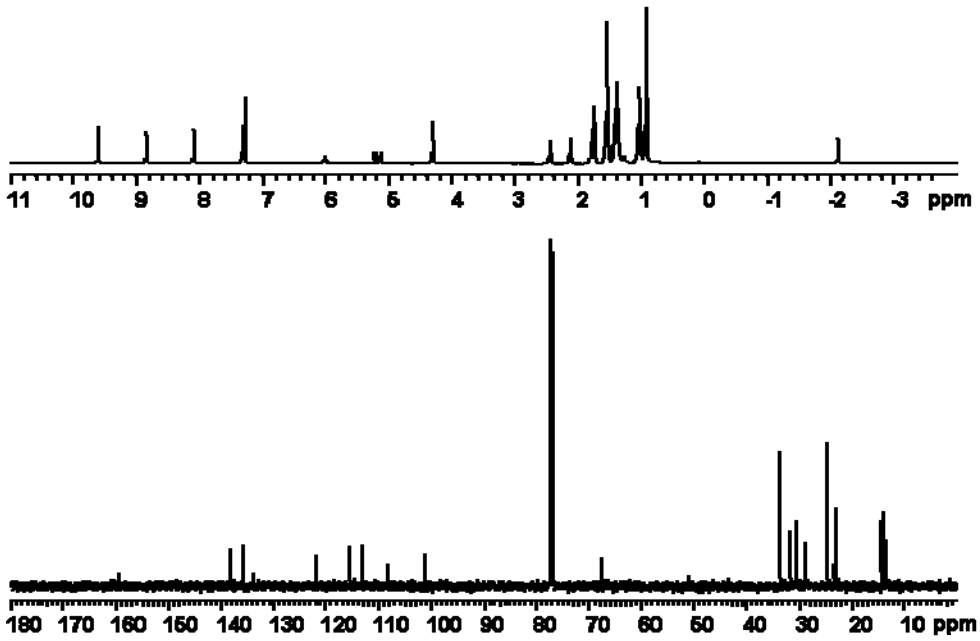

Fig. S4 The ^{1}H (top) and ^{13}C NMR (bottom) spectra for [5,15-bis(4-(1-pentenyloxy)phenyl)-10,20-bis((trihexylsilyl)ethynyl)]porphine (**PP**).

Under N_2 atmosphere, a 50 mL Schlenk flask equipped with a magnetic stir bar was loaded with a solution of free base porphyrin (PP) (40 mg, 3.22 μmol) in anhydrous CH_2Cl_2 (15 mL). A solution of $AlMe_3$ (48 μL, 2.0 M in heptane) was then added to the reaction mixture using a gas-tight syringe under N_2. After stirring for 30 min under N_2, MeOH (20 mL) was added to quench the reaction and the mixture was evaporated to dryness under reduced pressure. The residue was subject to size-exclusion chromatography (column dimensions = 30 mm × 250 mm, Bio-Rad Bio-Beads S-X1, eluent = CH_2Cl_2/MeOH 15:1 v/v) to afford **MeO-Al-PP** as a purple solid (41 mg, 98%, 3.15 μmol). ^{1}H NMR (499.6 MHz, $CDCl_3$): δ 1.01 (br s, 18H, ^{n}Hex CH_3), 1.15 (br s, 12H, ^{n}Hex CH_2), 1.45-1.54 (br m, 27H, ^{n}Hex CH_2), 1.68 (br s, 12H, ^{n}Hex CH_2), 1.89 (br s, 12H, ^{n}Hex CH_2), 2.16 (br s, 4H, CH_2CH$_2$O), 2.48 (br s, 4H, CH$_2$=CHCH_2), 4.31 (br s, 4H and 3H, CH$_2$CH_2O and OCH_3), 5.17 (dd, J_1 = 42.8 Hz, J_2 = 11.0 Hz, 2H, CH_2=CHCH$_2$), 5.26 (dd, J_1 = 42.8 Hz, J_2 = 16.5 Hz, 2H, CH_2=CHCH$_2$), 6.05 (br m, 2H, CH$_2$=C*H*CH$_2$), 6.97 (br s,

4H, Ar-*H*), 7.62 (br s, 2H, Ar-*H*), 8.47 (br s, 4H, β-H_2), 8.91 (br s, 2H, Ar-*H*), 9.09 (br s, 4H, β-H_1). $\{^1H\}^{13}C$ NMR (125.6 MHz, $CDCl_3/CD_3OD$): δ 13.7 (CH_2Si), 13.8 (CH_3), 22.6 (CH_2), 24.3 (CH_2), 28.5 (CH_2CH_2O), 30.2 (CH_2=CHCH_2), 31.6 (CH_2), 33.3 (CH_2), 58.1 (OCH_3), 67.4 (CH_2CH_2O), 98.9 (SiC≡*C*), 100.8 (Si*C*≡C), 107.2 (C_{10}), 112.7 (CH_2=$CHCH_2$), 115.1 (Ar-C_o), 119.4 (C_5), 129.5 (Ar-C_p), 131.3 (Ar-C_m), 132.8 (C_3), 136.1 (C_2), 137.6 (CH_2=*C*HCH_2), 145.6 (C_1), 146.9 (C_4), 158.9 (Ar-C_i). MALDI-ToF (reflective negative mode, anthracene matrix): Calcd for $C_{83}H_{115}N_4O_3Si_2Al$: 1298.83, found: *m/z* 1303.13 $[M]^-$, 1286.16 $[M - CH_3]^-$. ESIMS: Calcd for $C_{83}H_{115}N_4O_3Si_2Al$: 1298.83, found: *m/z* 1299.17 $[M]^+$. UV-vis (nm, (ε × 10^4 /$M^{-1}cm^{-1}$)): 437 (35.5), 535 (0.5), 586 (1.4), 637 (4.1).

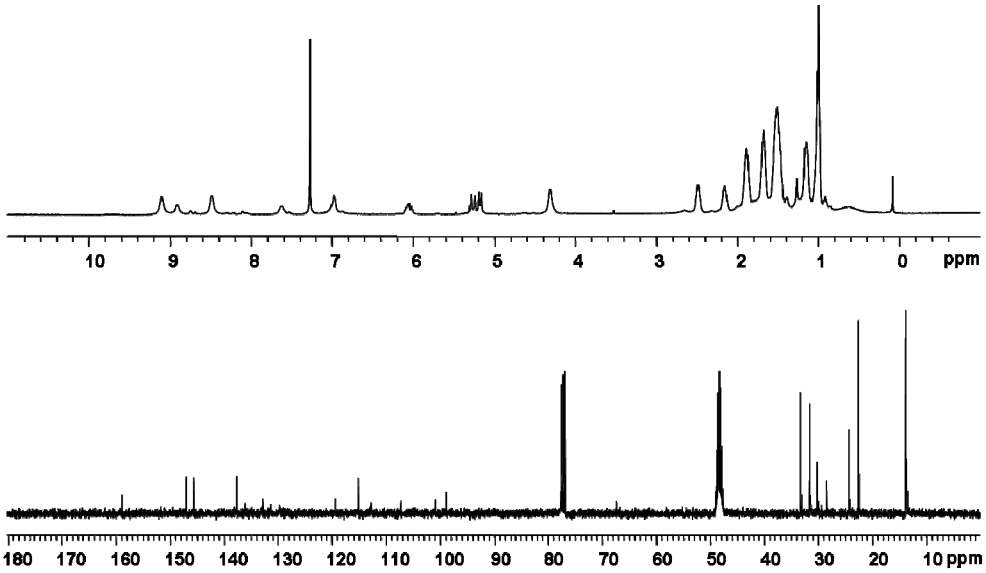

Fig. S5 The ^1H (top) and ^{13}C NMR (bottom) spectra for [[5,15-bis(4-(1-pentenyloxy)phenyl)-10,20-bis((trihexylsilyl)ethynyl)]porphinato]aluminum(III) methoxide (**MeO-Al-PP**).

V. Preparation of covalently linked porphyrin molecular boxes.

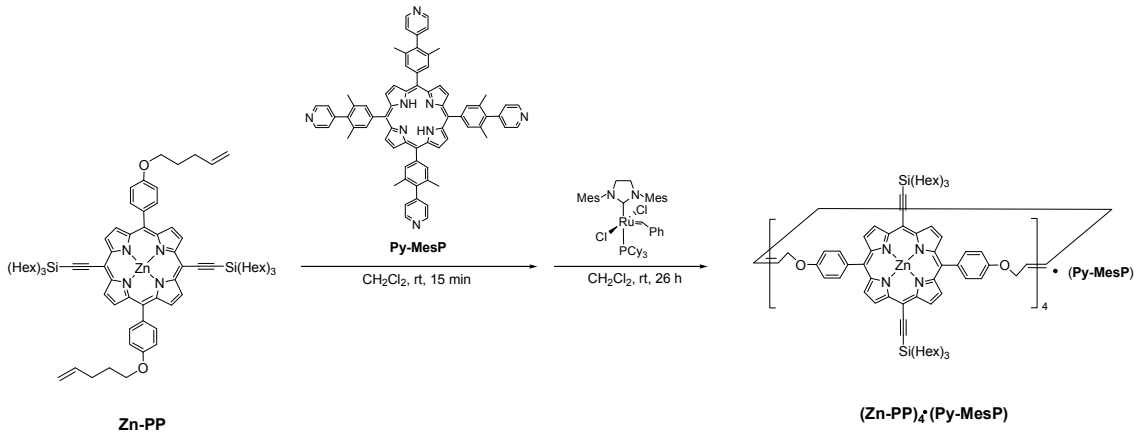

Covalently linked Zn-molecular box incorporating Py-MesP template (Zn-PP)$_4$·(Py-MesP). Into a 250 mL Schlenk flask equipped with a magnetic stir bar were combined **Zn-PP** (100 mg, 76.5 μmol), anhydrous CH_2Cl_2 (150 mL), and the **Py-MesP** template (19.1 mg, 19.1 μmol). The resulting mixture was degassed with N_2 for 10 min and then allowed to stir under N_2 for an additional 20 min. A degassed CH_2Cl_2 (2 mL) solution of Grubbs'

second-generation catalyst (16.3 mg, 25 mol%) was then added via cannula to the reaction mixture and the resulting mixture was allowed to stir under N_2 for 14 h. A second catalyst aliquot (6.5 mg, 10 mol%, in 2 mL of N_2-degassed CH_2Cl_2) was then added via cannula and stirring was continued for 12 h more at room temperature. (Note: without the additional catalyst, the primary product, as analyzed by MALDI-ToF MS, are dimers.) The reaction was then quenched by adding ethyl vinyl ether (15 mL) and opening to air. Solvents were removed from the quenched reaction mixture under reduced pressure using a rotary evaporator and the resulting residue was subjected to size-exclusion chromatography (column dimensions = 40 mm × 300 mm, Bio-Rad Bio-Beads S-X1, CH_2Cl_2 eluent). The molecular box was collected from a dark purple band, which was purified once again by silica gel column chromatography (column dimensions = 20 mm × 200 mm, eluent = CH_2Cl_2/hexanes 1:2 v/v) to afford (**Zn-PP**)$_4$·(**Py-MesP**) as a purple solid (59 mg, 74% based on the recovered **Zn-PP** monomer (32 mg)). R_f = 0.40 (CH_2Cl_2/hexanes = 1:2 v/v). ^{1}H NMR (499.6 MHz, $CDCl_3$): δ -3.39 (s, 2H, N*H*), 0.88 (m, 72H, ^{n}Hex CH_3), 0.99 (m, 48H, ^{n}Hex CH_2), 1.27-1.37 (m, 96H, ^{n}Hex CH_2), 1.52 (m, 48H, ^{n}Hex CH_2), 1.75 (m, 48H, ^{n}Hex CH_2), 2.22 (m, 16H, CH_2CH$_2$O), 2.54 (m, 16H, CH=CHCH_2), 2.74 (d, *J* = 5.0 Hz, 8H, α-pyridyl-*H*), 4.39 (m, 16H, CH$_2$CH_2O), 5.58 (d, *J* = 5.0 Hz, 8H, β-pyridyl-*H*), 5.75 (s, vinyl-*H*), 5.87 (s, vinyl-*H*), 7.28 (s, 16H, Ar-*H*), 7.38 (br s, 8H, Py-MesP Ar-*H*), 8.11 (br s, 8H, Py-MesP β-*H*), 8.29 (s, 16H, Ar-*H*), 8.97 (d, *J* = 4.5 Hz, 16H, β-H_2), 9.67 (d, *J* = 4.0 Hz, 16H, β-H_1). {^{1}H}^{13}C NMR (125.6 MHz, $CDCl_3$): δ 14.1 (*C*H$_2$Si), 14.4 (*C*H$_3$), 20.5 (Py-MesP-*C*H$_3$), 22.9 (*C*H$_2$), 24.6 (*C*H$_2$), 29.6 (*C*H$_2$CH$_2$O), 29.9 (*C*H$_2$CH=CH*C*H$_2$), 31.8 (*C*H$_2$), 33.5 (*C*H$_2$), 68.0 (CH$_2$*C*H$_2$O), 99.5 (SiC≡*C*), 101.1 (Si*C*≡C), 109.9 (C_{10}), 119.3 (Py-MesP-C_3), 122.3 (Ar-C_o), 123.6 (C_5), 126.0 (pyridyl-C_m), 130.1 (CH$_2$*C*H=*C*HCH$_2$), 130.6 (Ar-C_p), 131.1 (Ar-C_m), 132.6 (C_3), 132.7 (C_2), 133.6 (Py-MesP-C_5, Py-MesP-Ar-C_i), 135.4 (Py-MesP-C_4, Py-MesP-Ar-C_o), 136.4 (Py-MesP-Ar-C_m), 141.5 (Py-MesP-Ar-C_p), 149.9 (pyridyl-C_p), 150.8 (pyridyl-C_o), 152.0 (C_1), 152.5 (C_4), 159.1 (Ar-C_i). MALDI-ToF (linear negative mode): Calcd for [M - (Py-MesP)]$^-$: 5117.28, found: *m/z* 5116.91 [M - (Py-MesP)]$^-$. UV-vis (nm, (ε ×10^5 /M^{-1}cm^{-1})): 420 (3.2), 440 (5.9), 455 (3.8), 517 (0.1), 550 (0.1), 595 (0.2), 646 (0.8).

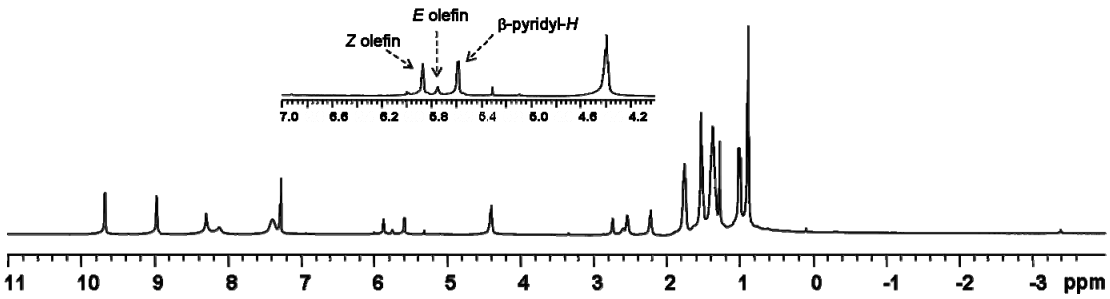

Fig. S6 The ^{1}H NMR spectrum for covalently linked Zn-molecular box incorporating Py-MesP template (**Zn-PP**)$_4$·(**Py-MesP**).

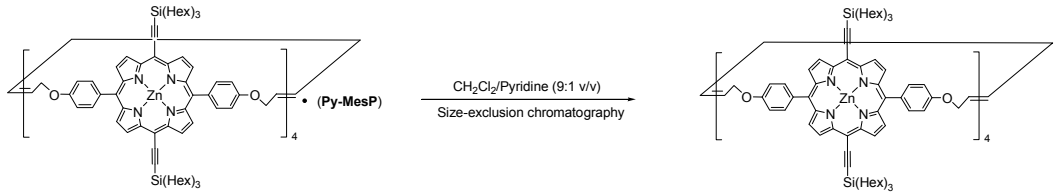

(Zn-PP)$_4$·(Py-MesP) **(Zn-PP)$_4$**

Detemplated hollow Zn-molecular box (Zn-PP)$_4$. **(Zn-PP)$_4$·(Py-MesP)** (20 mg, 3.25 μmol) was dissolved in CH_2Cl_2/pyridine (9:1 v/v) and then subjected to size-exclusion chromatography (column dimensions = 20 mm × 200 mm, Bio-Rad Bio-Beads S-X1, eluent = CH_2Cl_2/pyridine 9:1 v/v). Template-free hollow molecular box (**Zn-PP)$_4$** was collected from a dark purple band and the volatiles were removed under reduced pressure. To remove excess pyridine completely, the isolated purple solid was evacuated for 4 h at 60 ºC (16 mg, 96%, 3.13 μmol). R_f = 0.15 (CH_2Cl_2/hexanes = 1:2 v/v). ^{1}H NMR (499.6 MHz, $CDCl_3$): δ 0.94 (m, 72H, ^{n}Hex CH_3), 1.22-1.61 (m, 240H, ^{n}Hex CH_2), 2.28 (m, 16H, CH_2CH$_2$O), 2.59 (m, 16H, CH=CHCH_2), 4.46 (m, 16H, CH$_2$CH_2O), 5.84 (s, vinyl-*H*), 5.91 (s, vinyl-*H*), 7.38 (d, *J* = 7.0 Hz, 16H, Ar-*H*), 8.04 (d, *J* = 7.5 Hz , 16H, Ar-*H*), 8.52 (s, 16H, β-H_2), 8.72 (m, 16H, β-H_1). {^{1}H}^{13}C NMR (125.6 MHz, $CDCl_3$): δ 14.0 (*C*H$_2$Si), 14.4 (*C*H$_3$), 22.9 (*C*H$_2$), 24.6 (*C*H$_2$), 29.6 (*C*H$_2$CH$_2$O), 29.9 (*C*H$_2$CH=CH*C*H$_2$), 31.9 (*C*H$_2$), 33.6 (*C*H$_2$), 67.8 (CH$_2$*C*H$_2$O), 99.9 (Si*C*≡*C*), 101.1 (Si*C*≡C), 112.9 (C_{10}), 122.3 (Ar-C_o), 122.4 (C_5), 130.2 (CH$_2$*C*H=*C*HCH$_2$), 130.9 (Ar-C_p), 132.5 (Ar-C_m), 134.9 (C_3), 135.9 (C_2), 150.5 (C_1), 152.0 (C_4), 159.0 (Ar-C_i). MALDI-ToF (linear negative mode): Calcd for $C_{320}H_{432}N_{16}O_8Si_8Zn_4$: 5117.28, found: *m/z* 5115.17 [M]$^-$. UV-vis (nm, (ε ×10^5 /M^{-1}cm^{-1})): 440 (25.1), 539 (0.3), 579 (0.9), 627 (2.5).

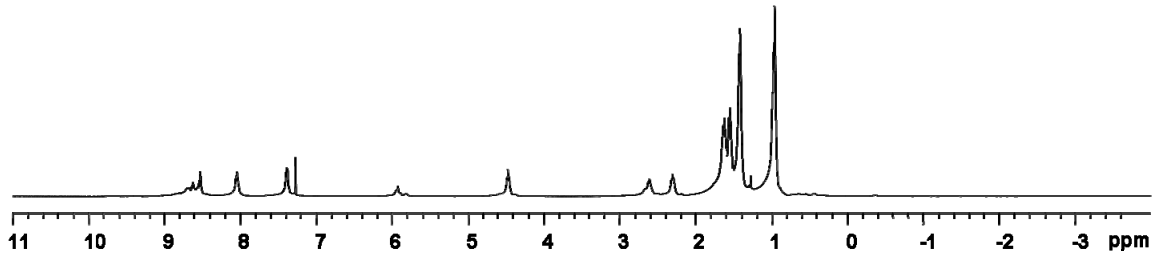

Fig. S7 The ^{1}H NMR spectrum for detemplated hollow Zn-molecular box (**Zn-PP)$_4$**.

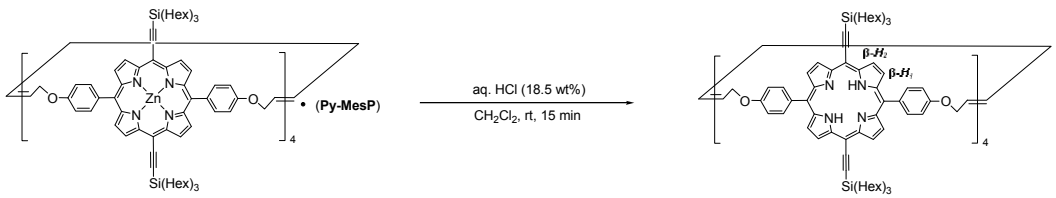

(Zn-PP)$_4$·(Py-MesP) **(PP)$_4$**

Demetallated hollow molecular box comprising of free base porphyrin (PP)$_4$. To a magnetically stirred solution of (**Zn-PP)$_4$·(Py-MesP**) (80 mg, 13.0 μmol) in CH_2Cl_2 (30 mL) in a 50 mL round bottom flask was added aqueous HCl (4 mL, 18.5 wt%). After stirring for 15 min at room temperature, the resulting mixture was washed consecutively with water (50 mL), saturated $NaHCO_3$ (30 mL), and brine (30 mL) before being dried over Na_2SO_4 and filtered. The filtrate was then evaporated to dryness using a rotary evaporator and the remaining residue was subjected to silica gel column chromatography (column dimensions = 20 mm × 200 mm, eluent = CH_2Cl_2/hexanes

1:1.5 v/v) to yield the demetallated product **(PP)$_4$** as a purple solid (59 mg, 93%, 12.1 μmol). ^{1}H NMR (499.6 MHz, $CDCl_3$): δ -2.15 (s, 8H, N*H*), 0.89 (m, 72H, ^{n}Hex CH_3), 0.99 (m, 48H, ^{n}Hex CH_2), 1.37 (m, 96H, ^{n}Hex CH_2), 1.52 (m, 48H, ^{n}Hex CH_2), 1.73 (m, 48H, ^{n}Hex CH_2), 2.19 (m, 16H, CH_2CH$_2$O), 2.50 (m, 16H, CH=CHCH_2), 4.37 (m, 16H, CH$_2$CH_2O), 5.75 (s, vinyl-*H*), 5.82 (s, vinyl-*H*), 7.36 (d, *J* = 7.5 Hz, 16H, Ar-*H*), 8.12 (d, *J* = 7.5 Hz , 16H, Ar-*H*), 8.87 (s, 16H, β-H_2), 9.61 (s, 16H, β-H_1). {^{1}H}^{13}C NMR (125.6 MHz, $CDCl_3$): δ 14.0 (*C*H$_2$Si), 14.4 (*C*H$_3$), 22.9 (*C*H$_2$), 24.6 (*C*H$_2$), 29.4 (*C*H$_2$CH$_2$O), 29.8 (*C*H$_2$CH=CH*C*H$_2$), 31.9 (*C*H$_2$), 33.6 (*C*H$_2$), 67.8 (CH$_2$*C*H$_2$O), 101.2 (SiC≡*C*), 101.4 (Si*C*≡C), 113.2 (C_{10}), 121.7 (Ar-C_o), 123.6 (C_5), 128.2 (CH$_2$*C*H=*C*HCH$_2$), 130.6 (Ar-C_p), 133.9 (Ar-C_m), 134.7 (C_3), 135.8 (C_2), 151.2 (C_1), 152.6 (C_4), 159.1 (Ar-C_i). MALDI-ToF (linear negative mode): Calcd for $C_{320}H_{440}N_{16}O_8Si_8$: 4863.70, found: *m/z* 4862.71 [M]$^-$. UV-vis (nm, (ε ×10^5 /M^{-1}cm^{-1})): 434 (17.6), 545 (0.6), 586 (2.4), 622 (0.4), 681 (1.0).

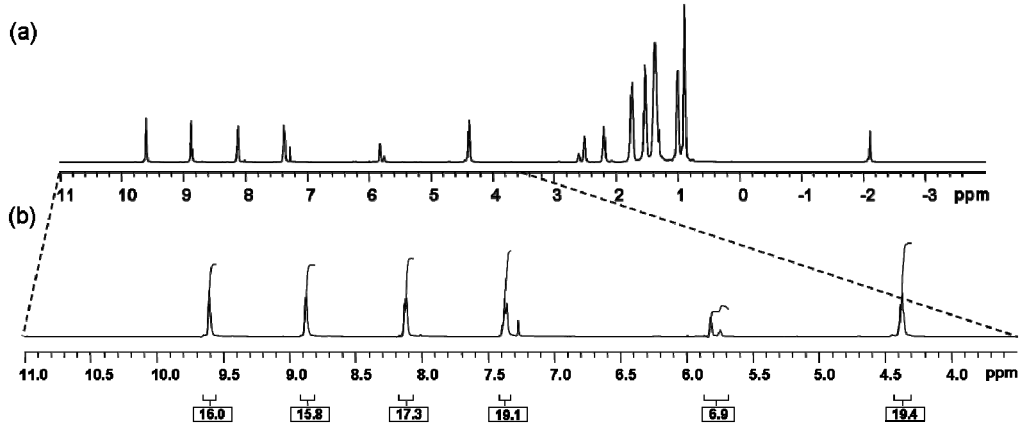

Fig. S8 (a) The ^{1}H NMR spectrum for demetallated hollow molecular box comprising of free base porphyrin **(PP)$_4$**. (b) The expanded region of ^{1}H NMR spectrum with the detailed integration values.

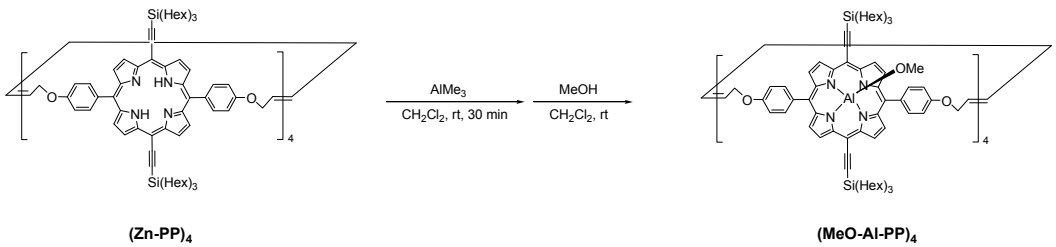

Covalently linked hollow Al-molecular box (MeO-Al-PP)$_4$. Under a N_2 atmosphere, a 50 mL Schlenk flask equipped with a magnetic stir bar was loaded with a solution of free base porphyrin **(PP)$_4$** (45 mg, 9.25 μmol) in anhydrous CH_2Cl_2 (15 mL). A solution of $AlMe_3$ (46 μL, 2.0 M in heptane) was then added to the reaction mixture using a gas-tight syringe under N_2. After stirring for 30 min under N_2, MeOH (20 mL) was added to quench the reaction and the mixture was evaporated to dryness under reduced pressure. The residue was subject to size-exclusion chromatography (column dimensions = 30 mm × 250 mm, Bio-Rad Bio-Beads S-X1, eluent = CH_2Cl_2/MeOH 15:1 v/v) to afford (MeO-Al-PP)$_4$ as a purple solid (46 mg, 98%, 9.04 μmol,). ^{1}H NMR (499.6 MHz, $CDCl_3$/CD_3OD, 50 ºC): δ 0.79-0.91 (br m, 72H, ^{n}Hex CH_3), 0.94-1.13 (br m, 48H, ^{n}Hex CH_2), 1.22-1.42 (br m, 96H, ^{n}Hex CH_2), 1.51 (br m, 48H, ^{n}Hex CH_2), 1.71 (br m, 48H, ^{n}Hex CH_2), 2.21 (br m, 16H, CH_2CH$_2$O), 2.51 (br m, 16H, CH=CHCH_2), 4.20-4.45 (br s, 16H and 12H, CH$_2$CH_2O and OCH_3), 5.84 (br s, vinyl-*H*), 7.21 (br s, 16H, Ar-*H*), 7.33-7.54 (br m, 16H, Ar-*H*), 8.54 (br s, 16H, β-H_2), 9.38 (br s, 16H, β-H_1). {^{1}H}^{13}C NMR (125.6 MHz, $CDCl_3$/CD_3OD): δ 13.7 (*C*H$_2$Si), 14.1 (*C*H$_3$), 22.6 (*C*H$_2$), 24.3 (*C*H$_2$), 29.6 (*C*H$_2$CH$_2$O), 31.5 (*C*H$_2$CH=CH*C*H$_2$),

31.8 (CH_2), 33.3 (CH_2), 58.5 (OCH_3), 67.7 (CH_2CH_2O), 99.8 (SiC≡*C*), 100.5 (Si*C*≡C), 107.5 (C_{10}), 112.8 (Ar-C_o), 120.9 (C_5), 128.8 ($CH_2CH{=}CHCH_2$), 130.4 (Ar-C_p), 131.1 (Ar-C_m), 134.9 (C_3), 136.3 (C_2), 145.6 (C_1), 147.6 (C_4), 158.9 (Ar-C_i). MALDI-ToF (reflective positive mode, pyrene matrix): Calcd for $C_{324}H_{444}N_{16}O_{12}Si_8Al_4$: 5087.70, found: *m/z* 5056.99 $[M - OMe]^+$, 5043.45 $[M - OMe - CH_3]^+$, 5030.55 $[M - AlOMe]^+$, 5015.20 $[M - AlOMe - CH_3]^+$, 5000.05 $[M - AlOMe - OMe]^+$. MALDI-ToF (reflective positive mode, dithranol matrix): Calcd for $C_{324}H_{444}N_{16}O_{12}Si_8Al_4$: 5087.70, found: *m/z* 4999.19 $[M - AlOMe - OMe]^+$, 4938.96 $[M -2(AlOMe) - OMe]^+$, 4879.25 $[M – 3(AlOMe) - OMe]^+$. The use of the neutral pyrene matrix is critical; if another matrix containing acidic proton (such as dithranol matrix) was used, loss of the Al-OMe moities is observed. ESIMS (positive mode): Calcd for $C_{324}H_{444}N_{16}O_{12}Si_8Al_4$: 5087.7023, found: *m/z* 2526.5710 $[M + H - OMe]^{2+}$, 2512.5700 $[M – 2OMe]^{2+}$. UV-vis (nm, ($\varepsilon \times 10^4$ /$M^{-1}cm^{-1}$)): 332 (7.5), 424 (75.2), 586 (4.4), 639 (11.4).

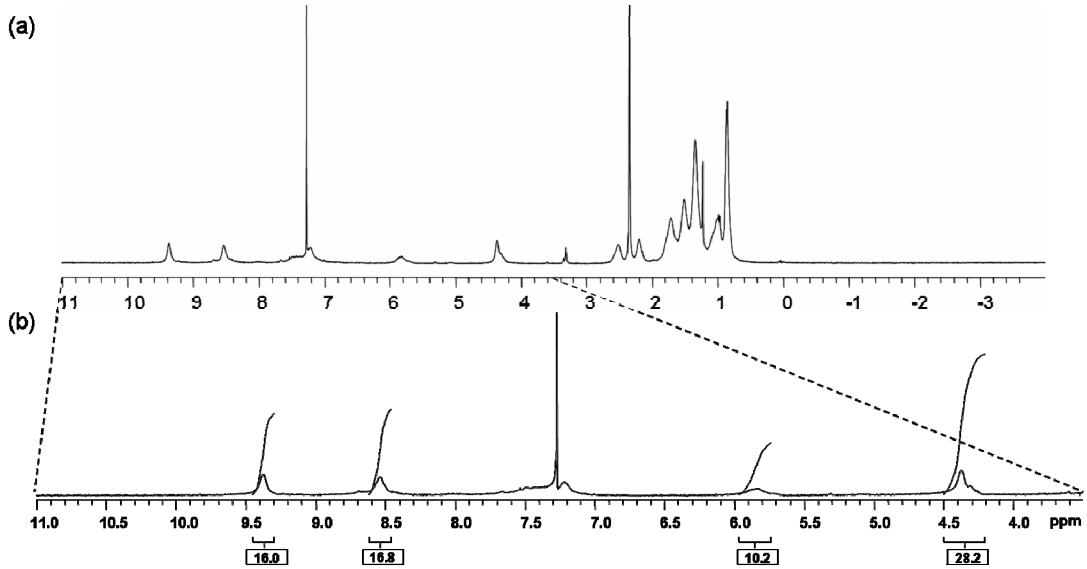

Fig. S9 (a) The ^1H NMR spectrum for covalently linked hollow Al-molecular box (**MeO-Al-PP**)$_4$. (b) An expanded region of the ^1H NMR spectrum with the detailed integration values.

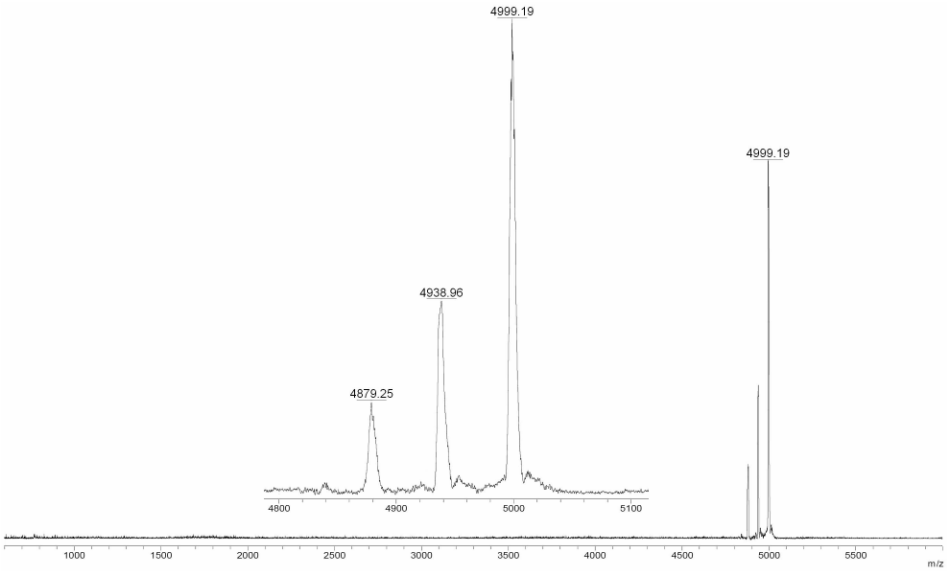

Fig. S10 MALDI-ToF MS spectrum of (**MeO-Al-PP**)$_4$. in the presence of dithranol matrix. Inset: an expanded region of the MALDI-ToF MS spectrum around the most intense peaks with a detailed peak assignment.

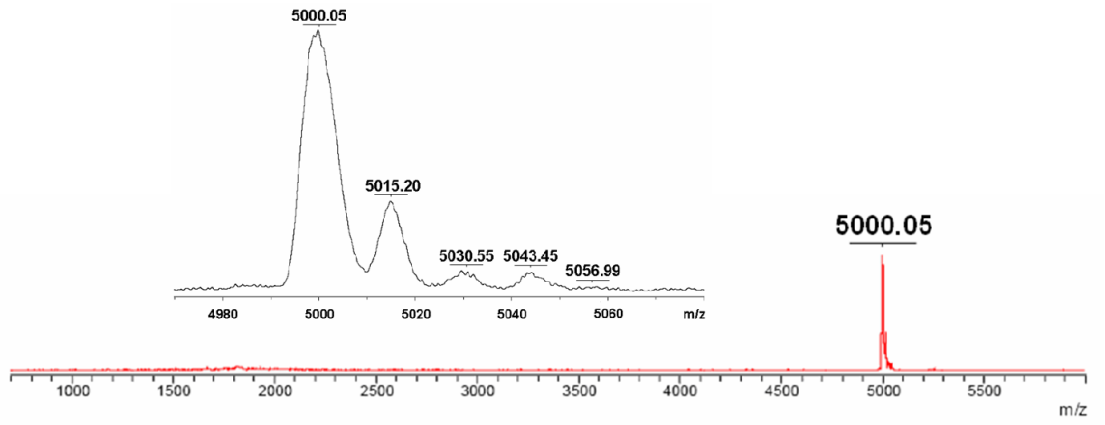

Fig. S11 MALDI-ToF MS spectrum of (**MeO-Al-PP**)$_4$. in the presence of pyrene matrix. Inset: an expanded region of the MALDI-ToF MS spectrum around the most intense peaks with a detailed peak assignment.

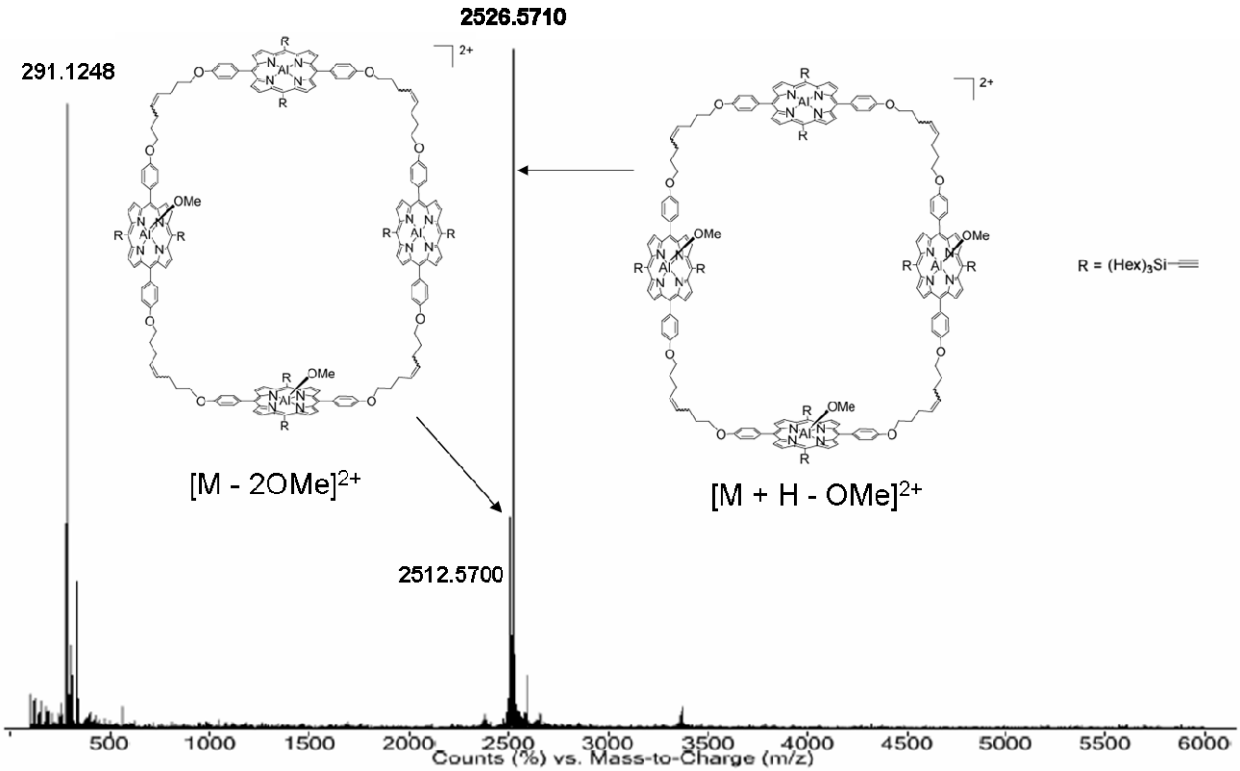

Fig. S12 High Resolution (HR) ESIMS spectrum of (**MeO-Al-PP**)$_4$.(positive mode).

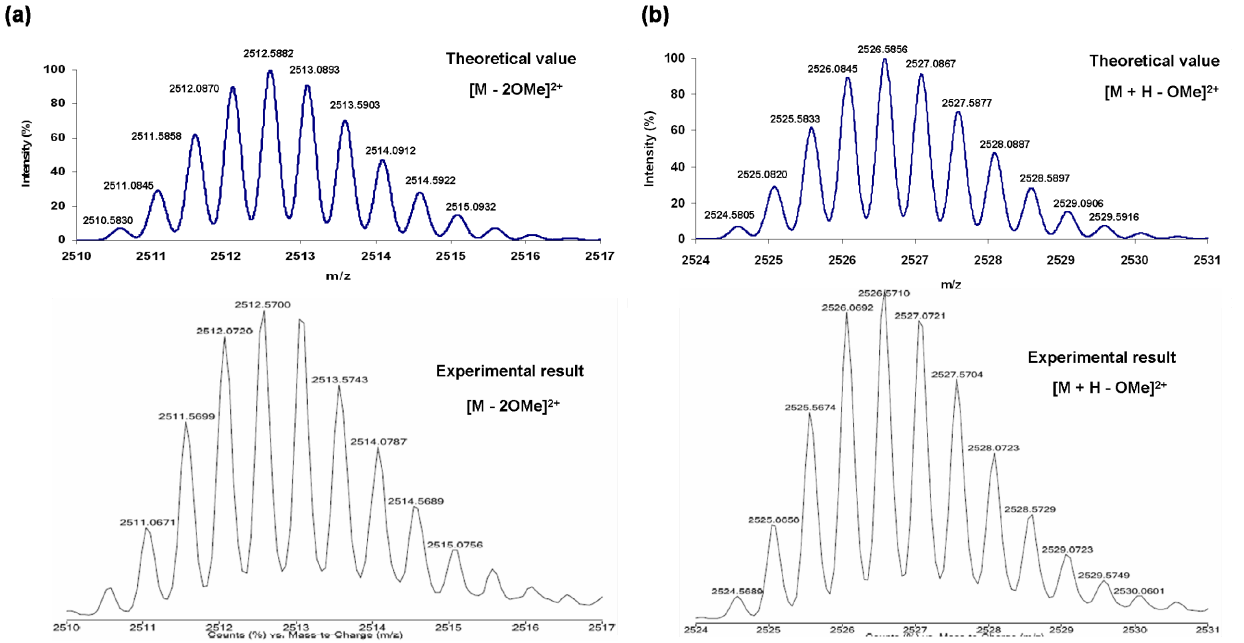

Fig. S13 Theoretical (top) and experimental (bottom) isotope distribution patterns of the *m/z* = +2 peaks in HRESI mass spectrum: 2512 ($[M + H - OMe]^{2+}$) and 2526 ($[M - 2OMe]^{2+}$), showing matching isotopic distribution patterns for $[M + H - OMe]^{2+}$ (a) and $[M - 2OMe]^{2+}$ (b)..

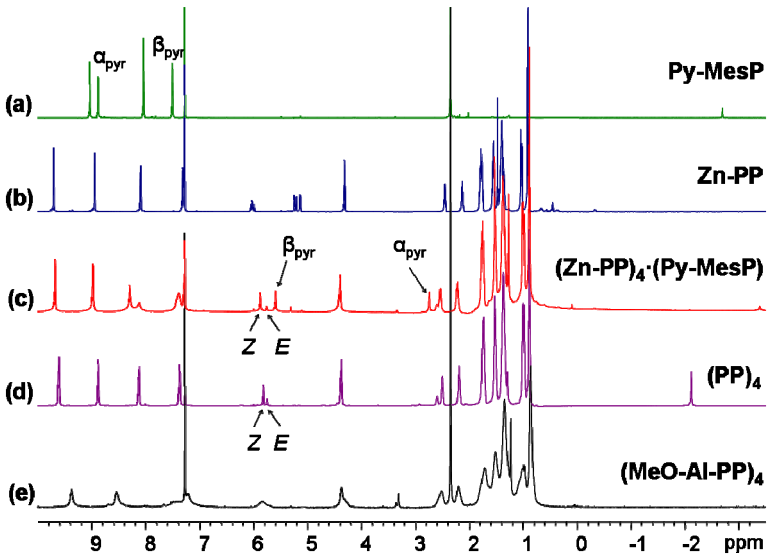

Fig. S14 ^{1}H NMR spectra of: (a) **Py-MesP** template, (b) **Zn-PP**, (c) (**Zn-PP**)$_4$·(**Py-MesP**), (d) (**PP**)$_4$, and (e) (**MeO-Al-PP**)$_4$. Spectra a-d were obtained in $CDCl_3$, whereas spectrum e were obtained in a mixture of $CDCl_3$ and CD_3OD (8.8:1 v/v) due to insufficient solubility of the assembly. This figure is a larger version of Fig. 1 in the main text.

Deinsertion of Py-MesP and subsequent reinsertion of the smaller DPyDPP template. Large **Py-MesP** template could not be completely reinserted back into the hollow (**Zn-PP**)$_4$ cavity at room temperature based on our observation of the chemical shifts of the pyridyl protons in the template, suggesting that the initial templation was a less-than-optimal tight fit. However, the smaller 5,15-bisphenyl-10,20-bis(4-pyridyl)porphyrin (**DPyDPP**) fitted well and can be used to partition the tetramer. This can be attributed to the *E*/*Z* isomers in the 4-octen-1,8-diyl linkers, which make a large number of the assembled molecules smaller than the idealized all-cis isomer (Fig. S15).

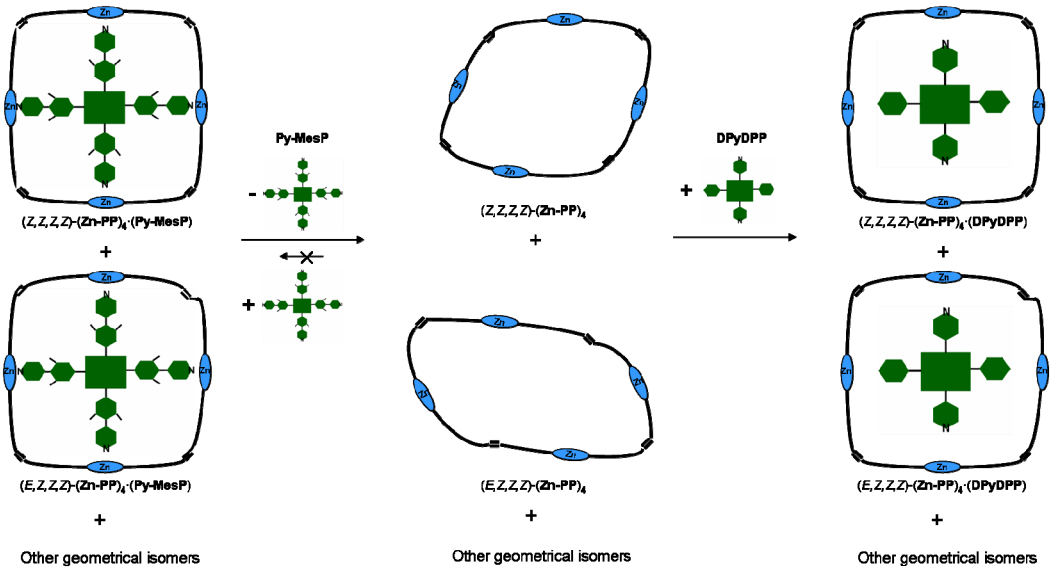

Fig. S15 Schematic description of the deinsertion of **Py-MesP** and subsequent reinsertion of the smaller **DPyDPP** template to the cavity of hollow (**Zn-PP**)$_4$.

Possible geometrical isomers of (Zn-PP)$_4$ and (MeO-Al-PP)$_4$ and their conformations. As mentioned in the caption of Fig. 4 in the main text, **(Zn-PP)$_4$** and **(MeO-Al-PP)$_4$** are far from being idealized square objects due to the flexibility of the 4-octen-1,8-diyl connectors and their *E*/*Z* isomers, a result of the ring-closing metathesis reaction. In a MeOH-rich solvent mixture, the flexible alkyl chains would allow the hydrophobic porphyrin moieties to come closer to each others and the tetramers to adopt more compact shapes than the idealized shape shown in Fig 4. Furthermore, the different E/Z configurations in the 4-octen-1,8-diyl linkages lead to a total of six geometrical isomers, many of which are elongated in shapes (Fig. S16). The end results are structures that position the coordinated methoxide closer to the coordinated phosphate than shown in Fig. 4.

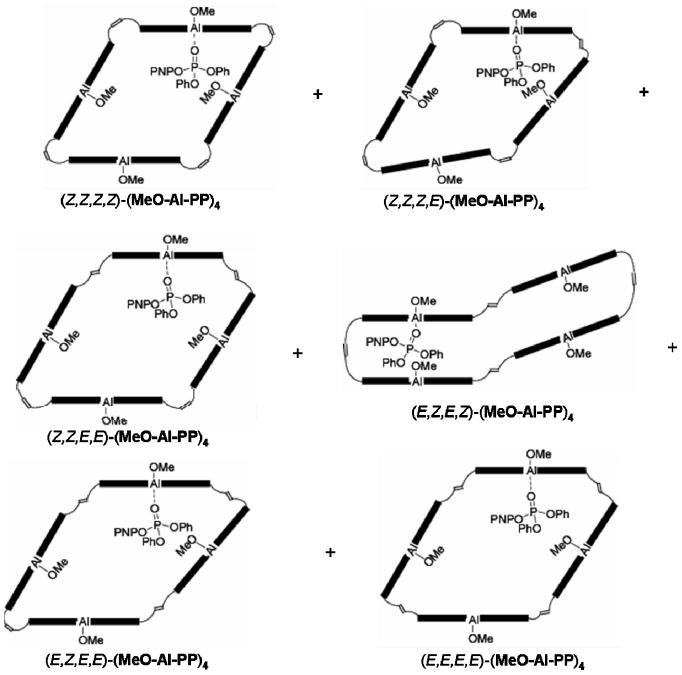

Fig. S16 Schematic description of the geometrical isomers of (**MeO-Al-PP**)$_4$ and their conformations. The elongation of these structures allow the methoxide ion to be closer to the coordinated phosphate.

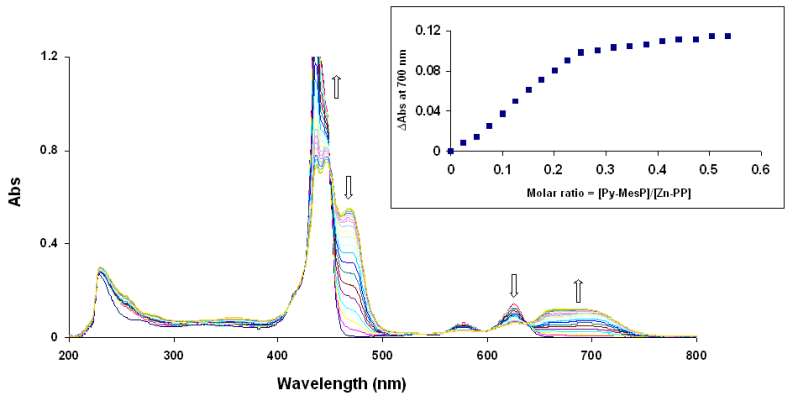

Fig. S17 Spectrophotometric titration of **Zn-PP** monomer (3.54 μM) in dichloromethane with aliquots (20 μL) of a solution of **Py-MesP** template (4.47 μM). Arrows show the directions of change in absorption with increasing **Py-MesP** concentration. Inset: absorbance change at 700 nm, showing an end point with 0.25 equiv of the template.

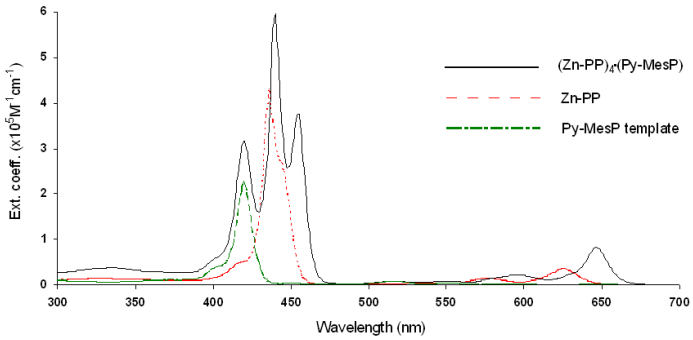

Fig. S18 Electronic absorption spectra of **Zn–PP**, **Py-MesP** template, and covalently linked (**Zn–PP**)$_4$·(**Py-MesP**).

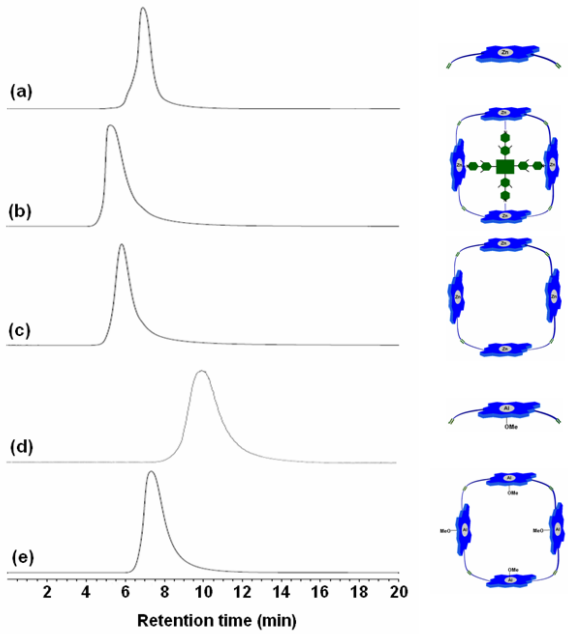

Fig. S19 Analytical GPC traces of: (a) **Zn-PP** monomer, (b) (**Zn-PP**)$_4$·(**Py-MesP**), (c) detemplated hollow (**Zn-PP**)$_4$, (d) **MeO-Al-PP** monomer (5 vol% methanol added to the CH_2Cl_2 eluant), and (e) (**MeO-Al-PP**)$_4$ (5 vol% methanol added to the CH_2Cl_2 eluent).

VI. PFG-NMR measurements. Diffusion NMR experiments were carried on a Bruker Avance-III 600 MHz spectrometer equipped with a standard Bruker BBO probe with z-axis gradients, using the convection-compensated pulse sequence dstebpgp3s.[S8-9] The spectra were acquired using a 50 millisecond diffusion delay ("big delta"), a linear ramp of gradient strengths from 2 to 95% of full strength, and an interscan delay of 20 seconds to ensure quantitative peak integrations and intensities. Data were analyzed with two methods in Bruker's Topspin program: 2D DOSY processing and line fitting analysis of individual peaks' gradient-dependent decay curves. Both method yielded comparable results. Measurements for **Zn-PP** monomer, (**Zn-PP**)$_4$·(**Py-MesP**), and hollow (**Zn-PP**)$_4$ were made at 298 K using $CDCl_3$. Measurement for (**MeO-Al-PP**)$_4$ was made at 298 K in a mixture of $CDCl_3$ and CD_3OD (8.8:1 v/v) due to insufficient solubility. The Stokes-Einstein equation, $D_s = kT/6\pi\eta a$, was used to estimate hydrodynamic radius, *a*. In this equation, *k* is Boltzmann's constant, T is the absolute temperature, and η is the temperature-dependent viscosity of the medium ($\eta(CDCl_3)$ = 0.563 cP[S10] and $\eta(CD_3OD)$ = 0.570 cP[S11]). For the 8.8:1 v/v mixture of $CDCl_3$:CD_3OD, a composite viscosity of 0.564 cP is calculated from those of the two components using the rule of mixture.

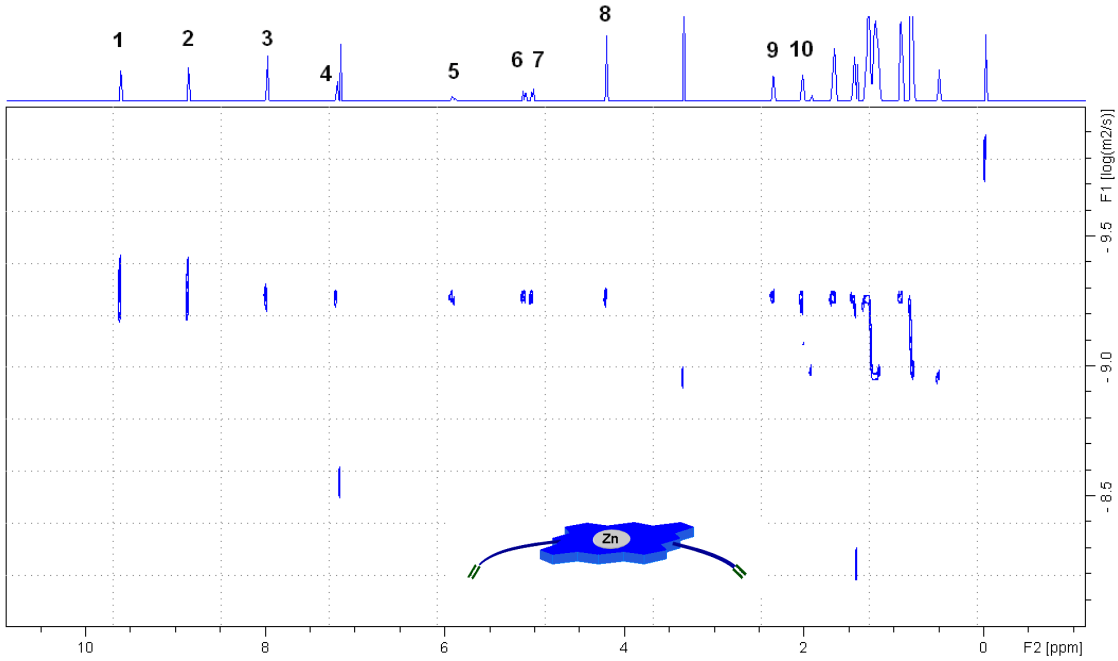

Peak number	Peak position (ppm)	Diffusion constant (D_s, 10^{-10} m^2/s)	Hydrodynamic radius (*a*, Å)
1	9.61	5.44	7.13
2	8.86	5.67	6.84
3	7.97	5.46	7.10
4	7.21	5.53	7.01
5	5.92	5.37	7.22
6	5.13	5.39	7.19
7	5.02	5.29	7.33
8	4.20	5.36	7.23
9	2.34	5.27	7.36
10	2.02	5.36	7.23
	Average		**7.16**
	Standard deviation		**0.15**

Fig. S20 Top: The DOSY spectrum of **Zn-PP** monomer at 298 K in $CDCl_3$. Bottom: Table of peak positions used in the measurement of the diffusion constant of **Zn-PP** monomer.

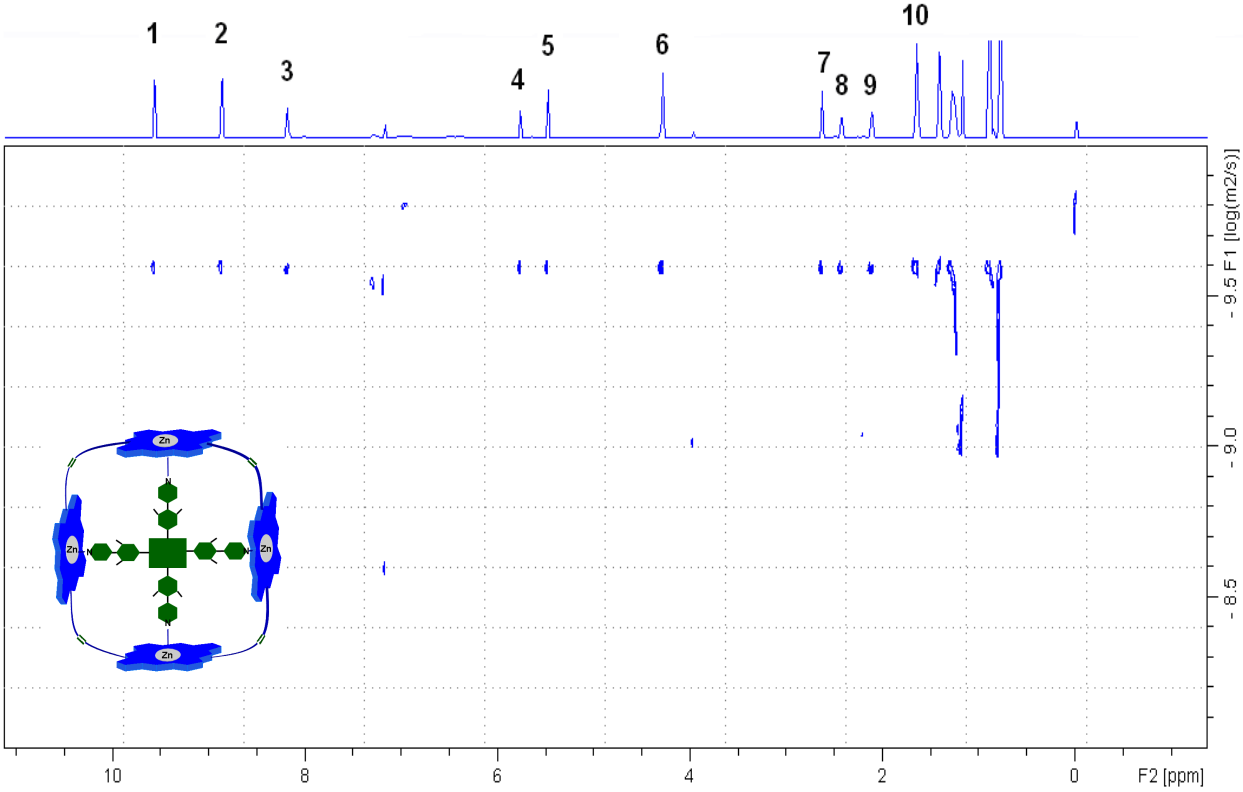

Peak number	Peak position (ppm)	Diffusion constant (D_s, 10^{-10} m^2/s)	Hydrodynamic radius (*a*, Å)
1	9.56	2.50	15.51
2	8.86	2.51	15.45
3	8.19	2.50	15.51
4	5.76	2.48	15.63
5	5.47	2.50	15.51
6	4.29	2.50	15.51
7	2.62	2.51	15.45
8	2.43	2.49	15.57
9	2.11	2.55	15.20
10	1.65	2.51	15.45
	Average		**15.48**
	Standard deviation		**0.11**

Fig. S21 Top: The DOSY spectrum of (**Zn-PP**)$_4$·(**Py-MesP**) at 298 K in $CDCl_3$. Bottom: Table of peak positions used in the measurement of the diffusion constant of (**Zn-PP**)$_4$·(**Py-MesP**).

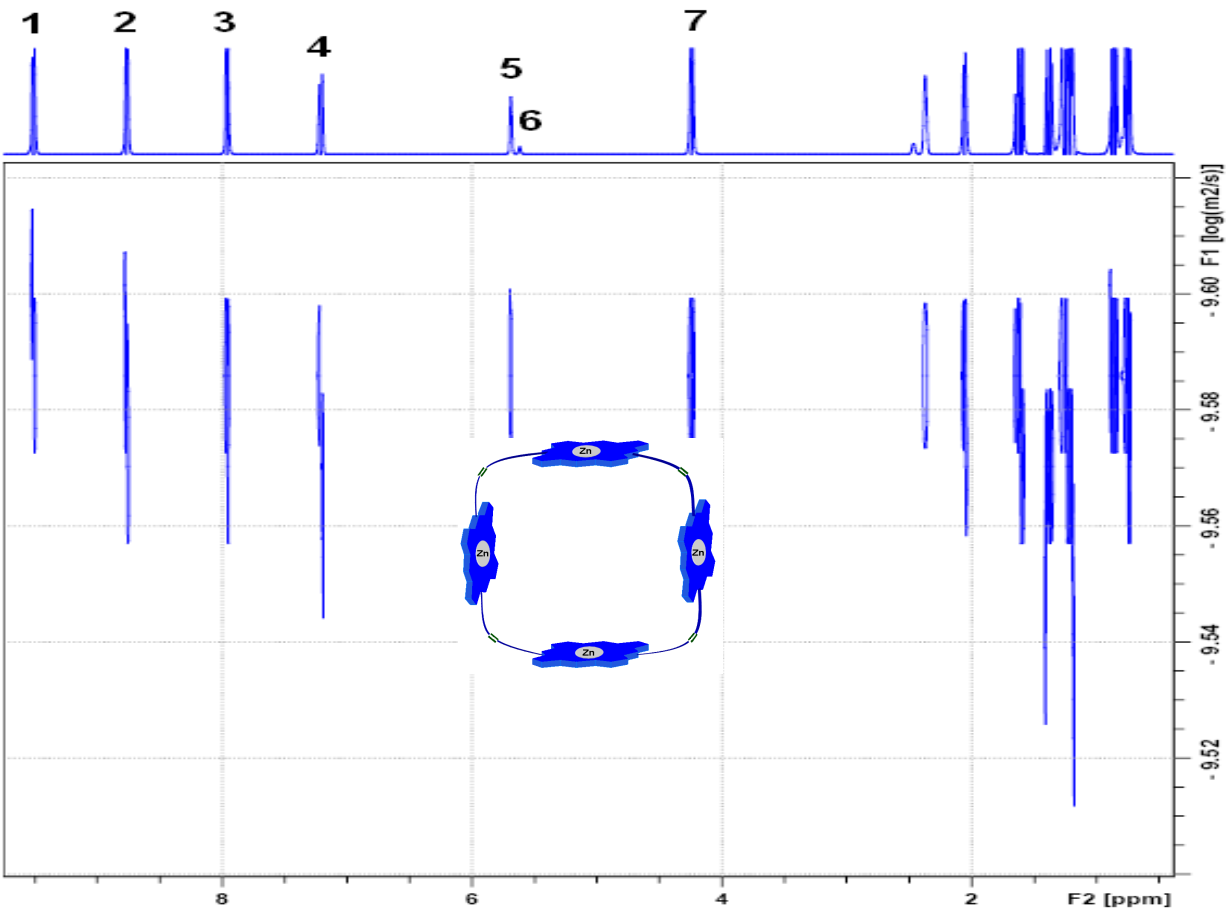

Peak number	Peak position (ppm)	Diffusion constant (D_s, 10^{-10} m^2/s)	Hydrodynamic radius (a, Å)
1	9.51	2.55	15.20
2	8.76	2.57	15.09
3	7.96	2.59	14.97
4	7.21	2.60	14.91
5	5.69	2.55	15.20
6	5.62	2.60	14.91
7	4.24	2.56	15.14
	Average		**15.06**
	Standard deviation		**0.13**

Fig. S22 Top: The DOSY spectrum of (**Zn-PP**)$_4$ at 298 K in $CDCl_3$. Bottom: Table of peak positions used in the measurement of the diffusion constant of (**Zn-PP**)$_4$.

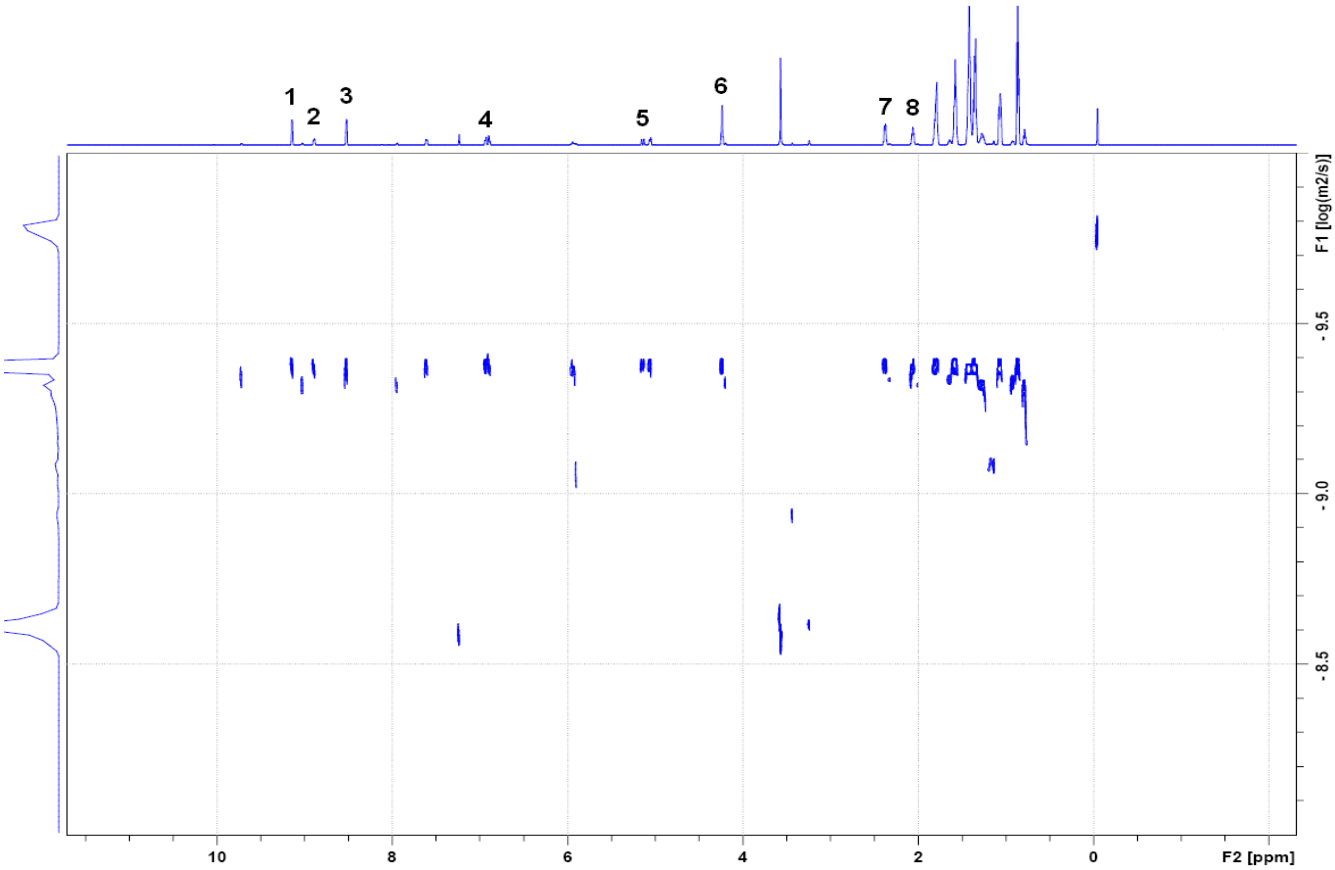

Peak number	Peak position (ppm)	Diffusion constant (D_s, 10^{-10} m^2/s)	Hydrodynamic radius (*a*, Å)
1	9.14	4.13	9.37
2	8.89	4.19	9.24
3	8.52	4.37	8.86
4	6.92	4.06	9.53
5	5.10	4.23	9.15
6	4.24	4.24	9.13
7	2.38	4.19	9.24
8	2.07	4.42	8.76
	Average		**9.16**
	Standard deviation		**0.25**

Fig. S23 Top: The DOSY spectrum of **MeO-Al-PP** monomer at 298 K in a mixture of $CDCl_3$.and CD_3OD (8.8:1 v/v). Bottom: Table of peak positions used in the measurement of the diffusion constant of **MeO-Al-PP** monomer.

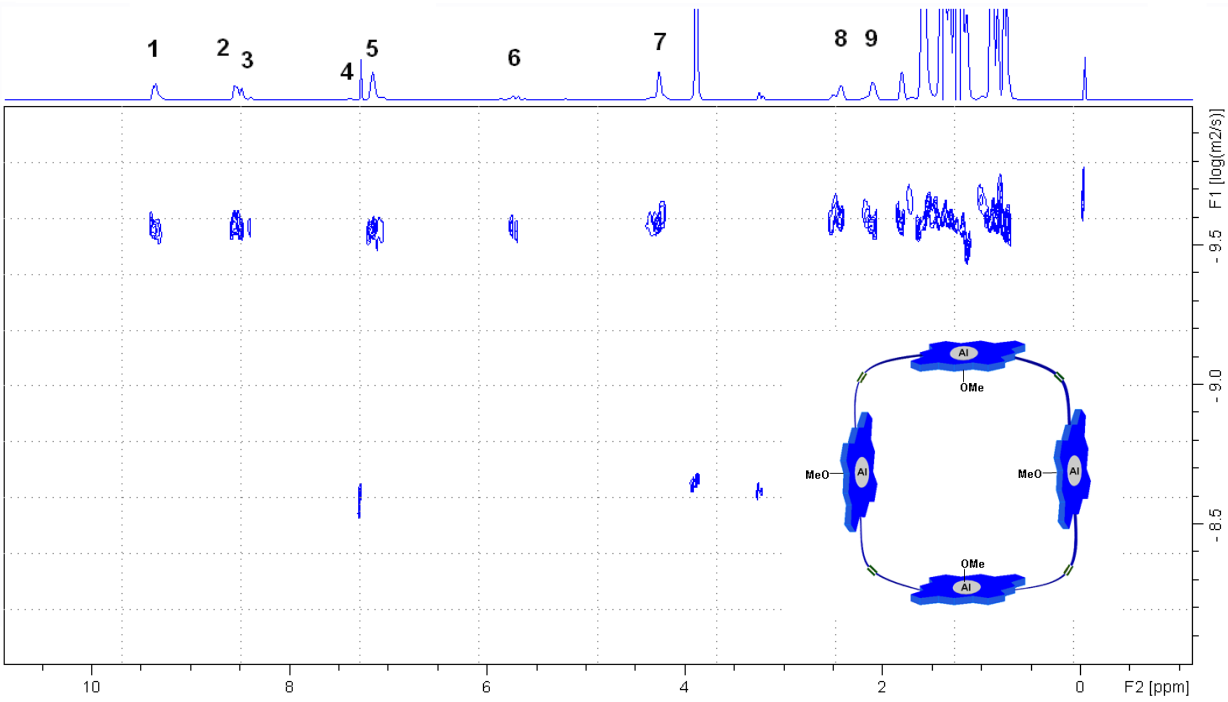

Peak number	Peak position (ppm)	Diffusion constant (D_s, 10^{-10} m^2/s)	Hydrodynamic radius (*a*, Å)
1	9.35	2.49	15.54
2	8.56	2.49	15.54
3	8.39	2.37	16.33
4	7.39	2.58	15.00
5	7.16	2.48	15.61
6	5.74	2.33	16.61
7	4.26	2.43	15.93
8	2.43	2.32	16.68
9	2.10	2.34	16.54
	Average		**15.98**
	Standard deviation		**0.59**

Fig. S24 Top: The DOSY spectrum of (**MeO-Al-PP**)$_4$ at 298 K in a mixture of $CDCl_3$.and CD_3OD (8.8:1 v/v). Bottom: Table of peak positions used in the measurement of the diffusion constant of (**MeO-Al-PP**)$_4$.

VII. General procedure for the synthesis of phosphate triesters. Phosphate triesters were synthesized following a modified literature procedure.[S12] To a magnetically stirred solution of titanium tetrachloride (16.3 µL, 148.3 µmol, 2 mol%) in anhydrous THF (40 mL) in a 100 mL Schlenk flask was added 4-nitrophenol (1.14 g, 8.2 mmol, 1.1 equiv) at room temperature under N_2. A solution of diphenyl or dialkyl chlorophosphate (7.4 mmol) in anhydrous THF (5 mL) was then added using a gas-tight syringe, followed by triethylamine (2.1 mL, 14.89 mmol, 2.0 equiv), and the resulting mixture was allowed to stir for 1 h more. The resulting yellow solution was quenched by adding water (10 mL) and extracted with EtOAc (3 × 80 mL). The combined organic extracts were dried over $MgSO_4$, filtered, and concentrated under reduced pressure. Purification via silica gel column chromatography (column dimensions = 40 mm × 300 mm, eluent = EtOAc/hexanes = 1:3 or 1:1 v/v) afforded phosphate triesters.

***p*-Nitrophenyl diphenyl phosphate (PNPDPP)**. A white solid (86%). R_f = 0.47 (EtOAc /hexanes = 1:3 v/v). ^{1}H

NMR (400.6 MHz, $CDCl_3$): δ 7.21-7.24 (m, 6H, Ar-*H*), 7.33-7.38 (m, 6H, Ar-*H*), 8.22 (d, *J* = 9.2 Hz, 2H, Ar-*H*). $\{^1H\}^{13}C$ NMR (100.7 MHz, $CDCl_3$): δ 120.2 (d, *J* = 4.4 Hz, Ar-*C*H), 121.0 (d, *J* = 5.8 Hz, Ar-*C*H), 125.9 (Ar-*C*H), 126.2 (d, *J* = 1.4 Hz, Ar-*C*H), 130.2 (Ar-*C*H), 150.2 (d, *J* = 7.4 Hz, Ar-*C*), 155.2 (d, *J* = 6.6 Hz, Ar-*C*). $\{^1H\}^{31}P$ NMR (161.9 MHz, $CDCl_3$): δ -17.84. HRESIMS: Calcd for $[C_{18}H_{14}NO_6P+H]^+$: 372.0632, found: *m/z* 372.0670 $[M+H]^+$.

Methyl diphenyl phosphate (MDPP). A colorless oil (99%). R_f = 0.25 (EtOAc /hexanes = 1:3 v/v). ^1H NMR (400.6 MHz, $CDCl_3$): δ 3.93 (d, *J* = 11.6 Hz, C*H*$_3$O), 7.15-7.24 (m, 6H, Ar-*H*), 7.30-7.34 (m, 4H, Ar-*H*). $\{^1H\}^{13}C$ NMR (100.7 MHz, $CDCl_3$): δ 55.5 (d, *J* = 6.6 Hz, *C*H$_3$O), 120.1 (d, *J* = 5.1 Hz, Ar-*C*H), 125.5 (Ar-*C*H), 129.9 (Ar-*C*H), 150.6 (d, *J* = 6.6 Hz, Ar-*C*). $\{^1H\}^{31}P$NMR (161.9 MHz, $CDCl_3$): δ -10.18. HRESIMS: Calcd for $[C_{13}H_{13}O_4P+H]^+$: 265.0624, found: *m/z* 265.0640 $[M+H]^+$.

***p*-Nitrophenyl dimethyl phosphate (PNPDMP)**. A colorless oil (88%). R_f = 0.25 (EtOAc /hexanes = 1:1 v/v). ^1H NMR (400.6 MHz, $CDCl_3$): δ 3.89 (s, 3H, C*H*$_3$O), 3.92 (s, 3H, C*H*$_3$O), 7.39 (d, *J* = 8.8 Hz, 2H, Ar-*H*), 8.24 (d, *J* = 9.2 Hz, 2H, Ar-*H*). $\{^1H\}^{13}C$NMR (100.7 MHz, $CDCl_3$): δ 55.4 (*C*H$_3$), 55.5 (*C*H$_3$) 120.7 (d, *J* = 5.9 Hz, Ar-*C*H), 125.9 (Ar-*C*H), 144.9 (Ar-*C*), 155.6 (Ar-*C*). $\{^1H\}^{31}P$NMR (161.9 MHz, $CDCl_3$): δ -4.24. HRESIMS: Calcd for $[C_8H_{10}NO_6P+H]^+$: 248.0319, found: *m/z* 248.0392 $[M+H]^+$.

***p*-Nitrophenyl dipropyl phosphate (PNPDPrP)**. A pale yellow oil (87%). R_f = 0.25 (EtOAc /hexanes = 1:3 v/v). ^1H NMR (400.6 MHz, $CDCl_3$): δ 0.96 (t, *J* = 7.6 Hz, 6H, C*H*$_3$), 1.73 (m, 4H, C*H*$_2$) 4.14 (m, 4H, C*H*$_2$O), 7.37 (d, *J* = 8.8 Hz, 2H, Ar-*H*), 8.23 (d, *J* = 9.2 Hz, 2H, Ar-*H*). $\{^1H\}^{13}C$ NMR (100.7 MHz, $CDCl_3$): δ 10.0 (*C*H$_3$), 23.6 (*C*H$_2$), 70.6 (*C*H$_2$O), 120.3 (d, *J* = 5.2 Hz, Ar-*C*H), 120.8 (d, *J* = 5.9 Hz, Ar-*C*H), 125.6 (d, *J* = 13.9 Hz, Ar-*C*H), 144.6 (Ar-*C*), 155.6 (d, *J* = 5.8 Hz, Ar-*C*). $\{^1H\}^{31}P$ NMR (161.9 MHz, $CDCl_3$): δ -6.29. HRESIMS: Calcd for $[C_{12}H_{18}NO_6P+H]^+$: 304.0945, found: *m/z* 304.0922 $[M+H]^+$.

***p*-Nitrophenyl dibutyl phosphate (PNPDBP)**. A pale yellow oil (62%). R_f = 0.35 (EtOAc /hexanes = 1:3 v/v). ^1H NMR (400.6 MHz, $CDCl_3$): δ 0.93 (t, *J* = 7.2 Hz, 6H, C*H*$_3$), 1.40 (m, 4H, C*H*$_2$), 1.69 (m, 4H, C*H*$_2$), 4.18 (m, 4H, C*H*$_2$O), 7.38 (d, *J* = 8.4 Hz, 2H, Ar-*H*), 8.24 (d, *J* = 8.8 Hz, 2H, Ar-*H*). $\{^1H\}^{13}C$ NMR (100.7 MHz, $CDCl_3$): δ 13.6 (*C*H$_3$), 18.7 (*C*H$_2$), 32.2 (d, *J* = 6.6 Hz, *C*H$_2$), 69.0 (d, *J* = 6.6 Hz, *C*H$_2$O), 120.6 (d, *J* = 5.9 Hz, Ar-*C*H), 125.8 (Ar-*C*H), 144.7 (Ar-*C*), 155.6 (d, *J* = 6.6 Hz, Ar-*C*). $\{^1H\}^{31}P$ NMR (161.9 MHz, $CDCl_3$): δ -6.40. HRESIMS: Calcd for $[C_{14}H_{22}NO_6P+H]^+$: 332.1258, found: *m/z* 332.1218 $[M+H]^+$.

VIII. Representative procedure for the methanolysis of *p*-nitrophenyl diphenyl phosphate (PNPDPP) catalyzed by a porphyrin molecular box. Under bench-top conditions, a 1 dram vial equipped with a magnetic stir bar was charged with PNPDPP (21.3 mg, 25 mM), the appropriate porphyrin catalyst ((**MeO-Al-PP**)$_4$ or (**Zn-PP**)$_4$, 3 mol%), and anhydrous $CHCl_3$ (1.15 mL). Methanol (1.15 mL to make a 12.3 M solution) was then added to the reaction mixture at room temperature. The reaction vial was capped and allowed to stir at 333 K in an oil bath. Aliquots (0.16 mL) were periodically taken and filtered through a pad of silica gel, which was then washed with ethyl acetate (3 × 2 mL). The combined filtrates were concentrated *in vacuo* at room temperature, redissolved in $CDCl_3$, and analyzed via ^{31}P NMR spectroscopy. The conversion of PNPDPP as a function of reaction time was

obtained by comparing the integrated areas under the resonances for PNPDPP and methyl diphenyl phosphate (MDPP) (Figs. S25 and S26).

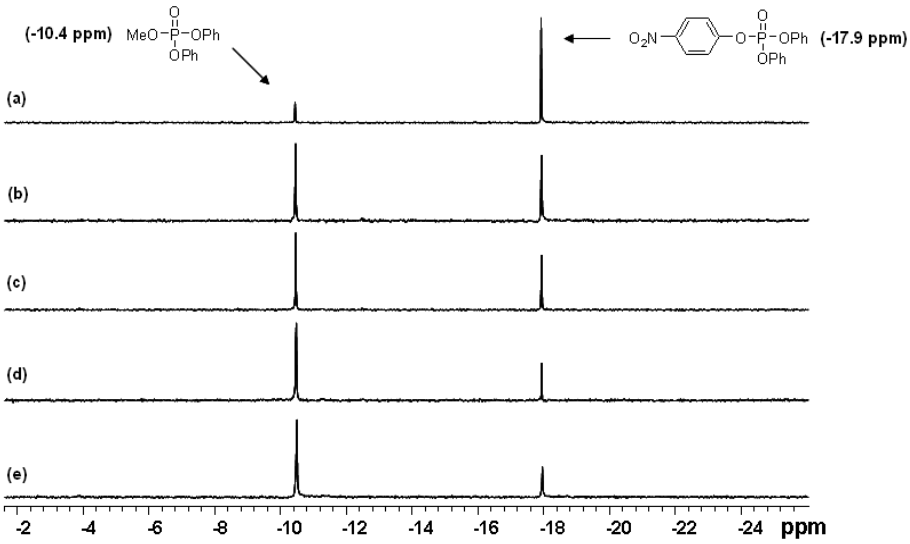

Fig. S25 ^{31}P NMR spectra showing the progress of the methanolysis of PNPDPP to MDPP in the presence of 3 mol% (**MeO-Al-PP**)$_4$ at 333 K, monitored by ^{31}P NMR spectroscopy at: (a) 3 h, (b) 10 h, (c) 15 h, (d) 28 h, and (e) 49 h.

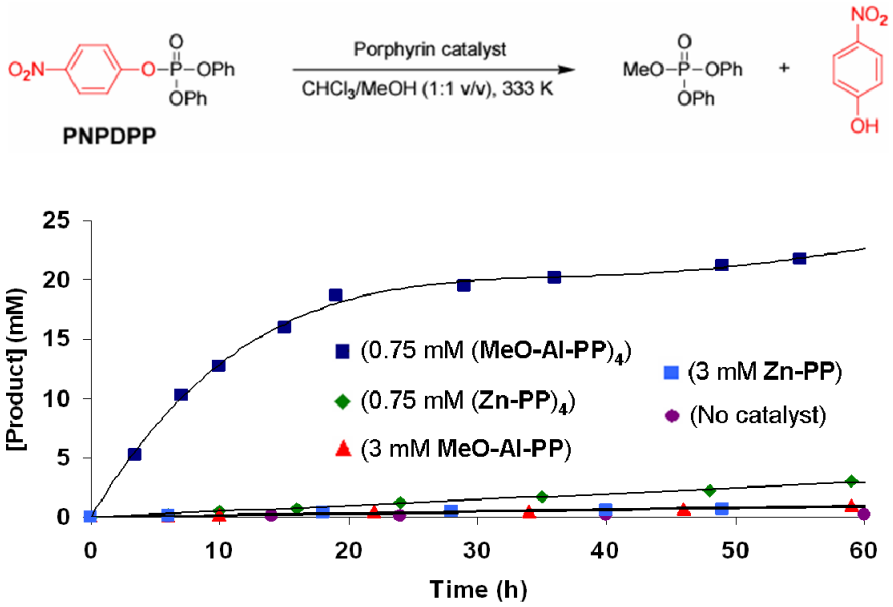

Fig. S26 Reaction profiles for the methanolysis of PNPDPP (25 mM) carried out at 333 K, in a mixture of $CHCl_3$ and CH_3OH (1:1 v/v) and in the presence of: (■) 0.75 mM (MeO-Al-PP)$_4$, (◆) 0.75 mM (Zn-PP)$_4$, (▲) 3 mM MeO-Al-PP, (■) 3 mM Zn-PP, and (●) no catalyst. This figure is a larger version of Fig. 5 in the main text.

The observation of product formation rates for the methanolysis of PNPDPP catalyzed by several porphyrin species. Reactions were carried out as described above in section VIII with several porphyrin catalysts and conversion data were collected. As an example, the determination of the product formation rate for (**MeO-Al-PP**)$_4$ was carried out as follows. To a 1 dram vial equipped with a magnetic stir bar was added PNPDPP (21.3 mg, 25 mM) and (**MeO-Al-PP**)$_4$ (8.7 mg, 3 mol%). Anhydrous $CHCl_3$ (1.15 mL) and MeOH (1.15 mL to make a 12.3 M solution) was added and the vial was sealed with a Teflon-lined cap and the reaction was allowed to stir at 333 K in an oil bath. Aliquots (0.16 mL) were withdrawn after 20, 40, 60, 80, 100, 120, 140, and 160 min and filtered through a pad of silica gel, which was then washed with ethyl acetate (3 × 2 mL). The combined filtrates were concentrated *in vacuo* at room temperature, redissolved in $CDCl_3$, and analyzed via ^{31}P NMR spectroscopy to determine the yield of MDPP (Table S1).

Table S1 Product formation rates for the methanolysis of PNPDPP in the presence or absence of a porphyrin catalyst at 12.3 M MeOH. Reported catalyzed rates were background-corrected from uncatalyzed reactions.

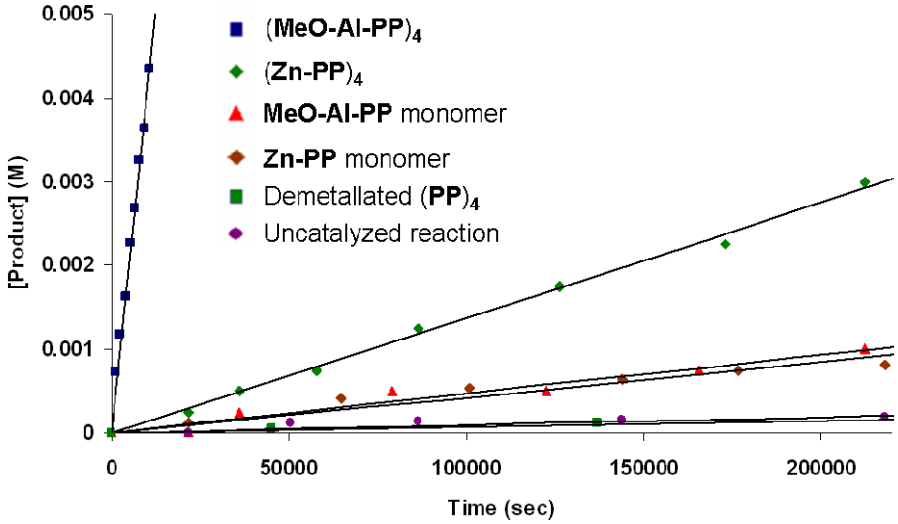

Porphyrin catalyst	Catalyst loading (mol %)	Observed initial rate (M/s)
(**MeO-Al-PP**)$_4$	3	3.9×10^{-7}
(**Zn-PP**)$_4$	3	1.3×10^{-8}
MeO-Al-PP monomer	12	3.3×10^{-9}
Zn-PP monomer	12	2.7×10^{-9}
Demetallated (**PP**)$_4$	3	9.4×10^{-10}
Uncatalyzed reaction		9.2×10^{-10}

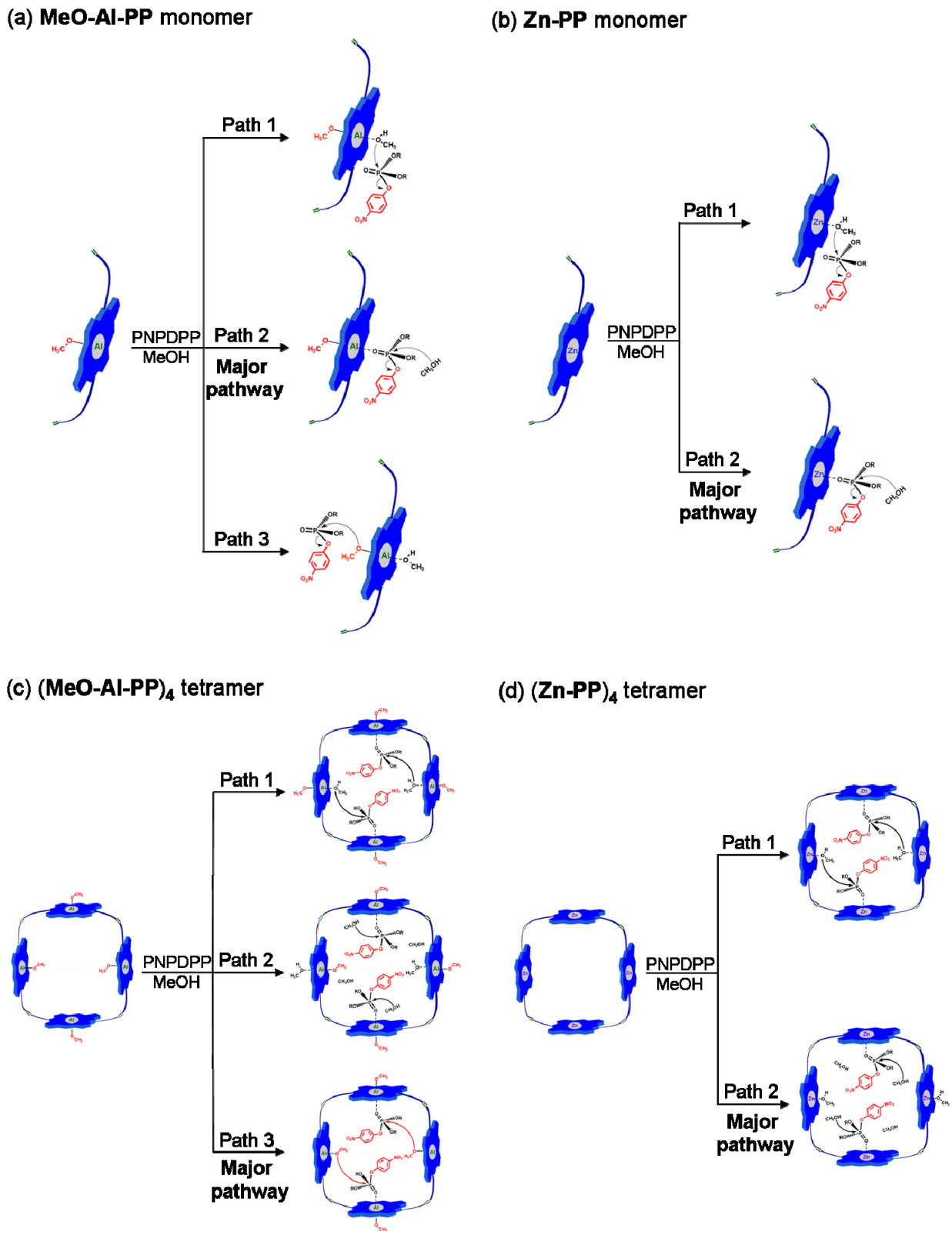

Fig. S27 Possible pathways for the methanolysis of phosphate triesters in the presence of (a) **MeO-Al-PP** monomer, (b) **Zn-PP** monomer, (c) (**MeO-Al-PP**)$_4$ tetramer, and (d) (**Zn-PP**)$_4$ tetramer.

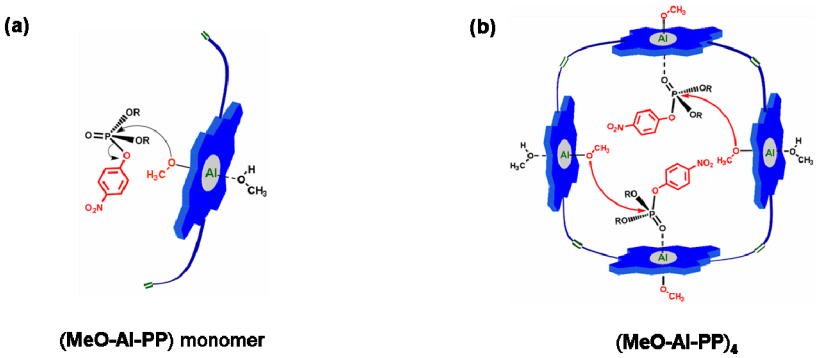

Fig. S28 The primary methanolysis of PNPDPP is proposed to be induced by methoxide in the presence of (a) **MeO-Al-PP** monomer and (b) (**MeO-Al-PP**)$_4$ tetramer.

IX. Estimation of the local concentration of methoxide in (MeO-Al-PP)$_4$.

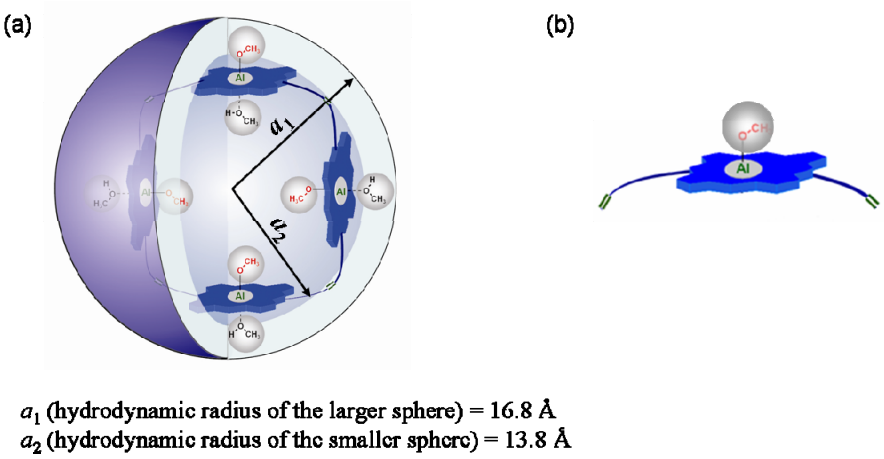

Fig. S29 Schematic description of the local concentration of methoxide in (a) (**MeO-Al-PP**)$_4$ and (b) **MeO-Al-PP** monomer.

If the shape of (**MeO-Al-PP**)$_4$ is assumed to be approximately spherical, the hydrodynamic volume is calculated by solving the equation:

$$V = (4/3)\pi \times a^3$$

where a_1 is the hydrodynamic radius (16.8 Å) obtained from PFG experiment (Fig. S30). Depending on the orientation of the methoxide ligand, two extreme situations arise. In one case, the methoxide ligands are all pointing outward from the cavity. In the other case, the methoxide ligands are all pointing inward. The local concentration *range* of methoxide in **(MeO-Al-PP)$_4$** can then be calculated by dividing the number of moles of methoxide by the spherical volumes (V) enclosed by the outer and inner radii of the spheres carved out by the assembly in each case. From the PFG experiment in a mixture of $CDCl_3$ and CD_3OD (1:1 v/v), we calculated the outer radius of **(MeO-Al-PP)$_4$** to be 16.8 Å (see data below). Subtracting ~3 Å from this give the approximate radius of the smaller sphere (13.8 Å) where all methoxides are pointing inward. Hence, the local concentration range for the methoxide is bracketed by the following quantities:

$$(6.64 \times 10^{-24}\ \text{mol})/(19.90 \times 10^{-24}\ \text{L}) = 0.334\ \text{M (larger sphere)}$$

$$(6.64 \times 10^{-24}\ \text{mol})/(11.03 \times 10^{-24}\ \text{L}) = 0.602\ \text{M (smaller sphere)}$$

This represents a 110-fold to 200-fold increase in concentration of methoxide over that of the **MeO-Al-PP** monomer concentration (0.003 M) that is used in our catalysis.

PFG-NMR measurements for (MeO-Al-PP)$_4$ in the 1:1 (v/v) mixture of $CDCl_3$ and CD_3OD. Samples were prepared by dissolving (**MeO-Al-PP**)$_4$ (0.79 mM) in a mixture of $CDCl_3$ and CD_3OD (1:1 v/v). Diffusion NMR experiments were performed under the same conditions as described above (Section VI) at 298 K on a Bruker Avance-III 600 MHz spectrometer. The Stokes-Einstein equation, $D_s = kT/6\pi\eta a$, was used to estimate hydrodynamic radius, a. In the equation, k is Boltzmann's constant, T is the absolute temperature, and η is the temperature-dependent viscosity of the medium ($\eta(CDCl_3) = 0.563$ cP[S10] and $\eta(CD_3OD) = 0.570$ cP[S11]). A composite viscosity of 0.567 cP for the 1:1 v/v mixture of $CDCl_3$:CD_3OD is calculated from those of the two components using the rule of mixture.

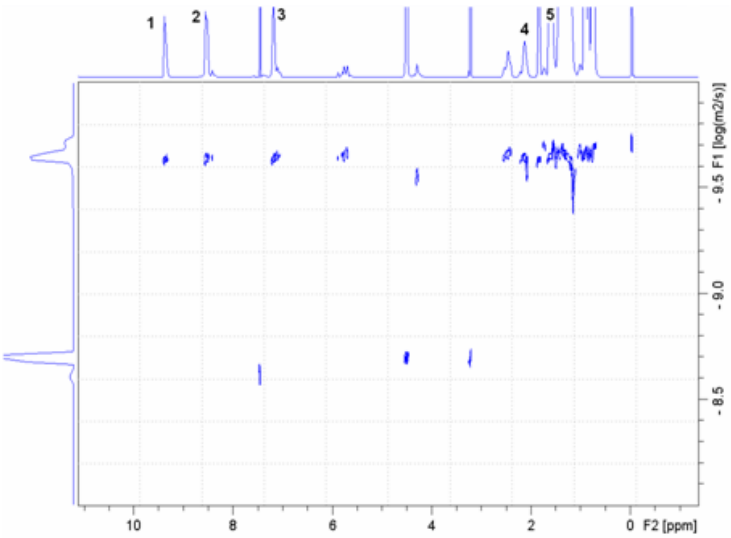

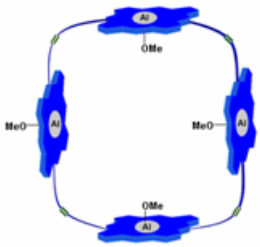

Peak number	Peak position (ppm)	Diffusion constant (D_s, 10^{-10} m^2/s)	Hydrodynamic radius (a, Å)
1	9.49	2.31	16.67
2	8.75	2.27	16.96
3	7.32	2.29	16.81
4	2.31	2.31	16.67
5	1.49	2.27	16.96
	Average		**16.81**
	Standard deviation		**0.15**

Fig. S30 Top: The DOSY spectrum of (**MeO-Al-PP**)$_4$ in a mixture of $CDCl_3$ and CD_3OD (1:1 v/v) at 298 K. Bottom: Table of peak positions used for measuring diffusion constant of (**MeO-Al-PP**)$_4$ in a mixture of $CDCl_3$ and CD_3OD (1:1 v/v).

Methoxide concentration in pure MeOH. In pure methanol, the autoprotolysis constant ($K_{auto,\ MeOH}$)[S13] at room temperature can be calculated as follows:

$$CH_3OH + CH_3OH \xrightleftharpoons{K_{auto,\ MeOH}} CH_3OH_2^+ + CH_3O^-,$$

$$K_{auto,\ MeOH} = [CH_3OH_2^+]\cdot[CH_3O^-] = 10^{-16.7}$$

where the methoxide concentration ($[CH_3O^-]$) must be equal to the protonated methanol concentration ($[CH_3OH_2^+]$).

Hence, we can replace the $[CH_3OH_2^+]$ term in the $K_{auto,\ MeOH}$ expression by another $[CH_3O^-]$ and the square root of each side gives the concentration of methoxide in pure methanol as 4.5×10^{-9} M.

$$[CH_3O^-]^2 = 10^{-16.7}\ M^2$$

$$[CH_3O^-] = 4.5 \times 10^{-9}\ M$$

Non-geometrical estimates of the effective molarity of methoxide in (MeO-Al-PP)$_4$

A simplistic way for estimate the effective methoxide molarity in (**MeO-Al-PP**)$_4$ is to compare its rate for methoxide-only pathway against that of the **MeO-Al-PP** monomer in the following manner:

$$\mathbf{Rate_{Al\text{-}monomer}} = k_{Al\text{-}monomer}[PNPDPP][MeO^-]_{Al\text{-}monomer}$$

$$\mathbf{Rate_{(MeO\text{-}Al\text{-}PP)4}} = k_{(MeO\text{-}Al\text{-}PP)4}[PNPDPP][MeO^-]_{(MeO\text{-}Al\text{-}PP)4}$$

Then the effective methoxide concentration in (**MeO-Al-PP**)$_4$ is estimated as:

$$[MeO^-]_{(MeO\text{-}Al\text{-}PP)4} = (\mathbf{Rate_{(MeO\text{-}Al\text{-}PP)4}}/\mathbf{Rate_{Al\text{-}monomer}}) \times (k_{Al\text{-}monomer}/k_{(MeO\text{-}Al\text{-}PP)4}) \times [MeO^-]_{Al\text{-}monomer}$$

However, because we do not know either the ($k_{Al\text{-}monomer}/k_{(MeO\text{-}Al\text{-}PP)4}$) or the ($\mathbf{Rate_{(MeO\text{-}Al\text{-}PP)4}}/\mathbf{Rate_{Al\text{-}monomer}}$) ratio for the methoxide-only pathway, this line of reasoning is unproductive.

Following established practices in enzymatic and supramolecular catalysis,[S14] a better way to evaluate the effectiveness of the (**MeO-Al-PP**)$_4$ tetramer is by calculating its effective molarity (EM) parameter. The EM for the methanolysis catalyzed by (**MeO-Al-PP**)$_4$ can be defined as the ratio of the intramolecular rate constant ($k_{(MeO\text{-}Al\text{-}PP)4}$) to the intermolecular rate constant ($k_{MeO\text{-}Al\text{-}PP\ monomer}$). However, because the methanolysis of PNPDPP by both the monomer and tetramer comprises several pathways (Fig. S27), several assumptions must be made before these two rate constants can be obtained. Our analysis is described below:

- The rate equations for the intermolecular methanolysis of PNPDPP catalyzed by **MeO-Al-PP** monomer, based on the reaction pathways shown in Fig. S27a, are:

  $\mathbf{Rate_{path1}}$(Al monomer) = $k_{path1}[PNPDPP][MeOH\text{-}Al_{monomer}]$

  ($[MeOH\text{-}Al_{monomer}]$ = concentration of the coordinated MeOH to $Al_{monomer}$ = $[Al_{monomer}]$)

  $\mathbf{Rate_{path2}}$(Al monomer) = $k_{path2}[PNPDPP\text{-}Al_{monomer}][MeOH]$

  ($[PNPDPP\text{-}Al_{monomer}]$ = concentration of the coordinated PNPDPP to $Al_{monomer}$ = $[Al_{monomer}]$)

  $\mathbf{Rate_{path3}}$(Al monomer) = $k_{path3}[PNPDPP][MeO^-]$

  ($[MeO^-] = [Al_{monomer}]$)

  Overall rate(Al monomer) = $\mathbf{Rate_{path1}}$(Al monomer) + $\mathbf{Rate_{path2}}$(Al monomer) + $\mathbf{Rate_{path3}}$(Al monomer)

  $= 3.3 \times 10^{-9}$ M/s (Table S1)

- The rate equations for the intermolecular reactions catalyzed by the **Zn-PP** monomer, based on the reaction pathways shown in Fig. S27b, are:

  $\mathbf{Rate_{path1}}$(Zn monomer) = $k_{path1}[PNPDPP][MeOH\text{-}Zn_{monomer}]$

  $\mathbf{Rate_{path2}}$(Zn monomer) = $k_{path2}[PNPDPP\text{-}Zn_{monomer}][MeOH]$

  Overall rate(Zn monomer) = $\mathbf{Rate_{path1}}$(Zn monomer) + $\mathbf{Rate_{path2}}$(Zn monomer)

  $= 2.7 \times 10^{-9}$ M/s (Table S1)

Assuming that the Lewis acidity of **MeO-Al-PP** and **Zn-PP** are the same, we can then consider the reaction rates

induced by the coordinated MeOH and free MeOH to be the same for both **MeO-Al-PP** (path 1 and path 2 in Fig. S27a) and **Zn-PP** (path 1 and path 2 in Fig. S27b) monomers. Thus, the rate constant (k_{path3}) induced by the methoxide in **MeO-Al-PP** monomer (path 3 in Fig. S27a) can be calculated by subtracting the $\mathbf{Rate_{path1}}$ and $\mathbf{Rate_{path2}}$ of the **Zn-PP** monomer from the overall reaction rate for **MeO-Al-PP** monomer.

$\mathbf{Rate_{path3}}$(Al monomer) = k_{path3}[PNPDPP][MeO$^-$] ≈ $3.3 \times 10^{-9} - 2.7 \times 10^{-9} = 0.6 \times 10^{-9}$ M/s

OR: k_{path3}(Al monomer) ≈ $0.6 \times 10^{-9}/(0.025)(0.003) = 8.0 \times 10^{-6}$ $M^{-1} \cdot s^{-1}$

We note that this is actually a gross overestimate of the importance of the methoxide pathway for **MeO-Al-PP** monomer. As shown in the main text, the slightly higher catalyzed-methanolysis rate for **MeO-Al-PP** is actually due to a combination of its higher Lewis acidity than **Zn-PP** and the presence of the methoxide.

- The rate equations for the intramolecular reactions catalyzed by (**MeO-Al-PP**)$_4$, based on the reaction pathways shown in Fig. 4 (reproduced in an alternate form in Fig. S27c for convenience) and the 2:1 encapsulation stoichiometry of PNPDPP obtained from our binding studies, are:

$$\text{PNPDPP}_2\text{-}(\mathbf{MeO\text{-}Al\text{-}PP})_4\,(\text{MeOH})_2 \xrightarrow{k_{path1}} 2\ \text{MDPP}$$

$\mathbf{Rate_{path1}}$ = ½ k_{path1}[PNPDPP$_2$-(**MeO-Al-PP**)$_4$·(MeOH)$_2$]

assuming that there are only two vacant sites in the tetramer for coordinating MeOH, this is a minor pathway induced by coordinated MeOH

$$\text{PNPDPP}_2\text{-}(\mathbf{MeO\text{-}Al\text{-}PP})_4 + \text{MeOH} \xrightarrow{k_{path2}} 2\ \text{MDPP}$$

$\mathbf{Rate_{path2}}$ = ½ k_{path2}[PNPDPP$_2$-(**MeO-Al-PP**)$_4$][MeOH]

assuming that the concentration of encapsulated MeOH inside the tetramer does not change significantly from that in the reaction solution, this is a minor reaction pathway induced by free MeOH

$$\text{PNPDPP}_2\text{-}(\mathbf{MeO\text{-}Al\text{-}PP})_4 \xrightarrow{k_{path3}} 2\ \text{MDPP}$$

$\mathbf{Rate_{path3}}$ = d[P]/dt = ½ k_{path3}[PNPDPP$_2$-(**MeO-Al-PP**)$_4$]

this is the major pathway induced by localized methoxide

Overall rate(Al tetramer) = $\mathbf{Rate_{path1}}$(Al tetramer) + $\mathbf{Rate_{path2}}$(Al tetramer) + $\mathbf{Rate_{path3}}$(Al tetramer)

= 3.9×10^{-7} M/s (Table S1)

- By a similar analysis, the rate equations for the intramolecular reactions catalyzed by (**Zn-PP**)$_4$, based on the reaction pathways shown in Fig. 4 (reproduced in an alternate form in Fig. S27d for convenience) and the 2:1 encapsulation stoichiometry of PNPDPP obtained from our binding studies (see section XII below), are:

$$\text{PNPDPP}_2\text{-}(\mathbf{Zn\text{-}PP})_4\,(\text{MeOH})_2 \xrightarrow{k_{path1}} 2\ \text{MDPP}$$

$\mathbf{Rate_{path1}}$(Zn tetramer) = ½ k_{path1}[PNPDPP$_2$-(**Zn-PP**)$_4$·(MeOH)$_2$]

assuming that there are only two vacant sites in the tetramer for coordinating MeOH

$$\text{PNPDPP}_2\text{-}(\mathbf{Zn\text{-}PP})_4 + \text{MeOH} \xrightarrow{k_{path2}} 2\ \text{MDPP}$$

Rate$_{path2}$(Zn tetramer) = ½ k_{path2}[PNPDPP$_2$-(**Zn-PP**)$_4$][MeOH]

assuming that the concentration of encapsulated MeOH inside the tetramer does not change significantly from that in the reaction solution

Overall rate(Zn tetramer) = **Rate$_{path1}$**(Zn tetramer) + **Rate$_{path2}$**(Zn tetramer)

= 1.3×10^{-8} M/s (Table S1)

As in the monomer case, we can assume that the reaction rates induced by the coordinated MeOH and free MeOH are the same for both (**MeO-Al-PP**)$_4$ (path 1 and path 2 in Fig. S27c) and (**Zn-PP**)$_4$ (path 1 and path 2 in Fig. S27d) tetramers, the rate constant (k_{path3}) induced by the methoxide in (**MeO-Al-PP**)$_4$ tetramer (path 3 in Fig. S27c) can be calculated by subtracting the **Rate$_{path1}$** and **Rate$_{path2}$** of the (**Zn-PP**)$_4$ tetramer from the overall reaction rate for (**MeO-Al-PP**)$_4$ tetramer:

Rate$_{path3}$(Al tetramer) = ½ k_{path3}[PNPDPP$_2$-(**MeO-Al-PP**)$_4$] ≈ $3.9 \times 10^{-7} - 1.3 \times 10^{-8} = 3.77 \times 10^{-7}$ M/s

OR: k_{path3}(Al teramer) ≈ $2 \times 3.77 \times 10^{-7}/(0.00075) = 1.005 \times 10^{-3}$ s^{-1}

Again, we note that this is probably a gross overestimate of the importance of the methoxide pathway for (**MeO-Al-PP**)$_4$. As shown in the main text, the slightly higher catalyzed-methanolysis rate of **MeO-Al-PP** monomer (compared to **Zn-PP**) is actually due to a combination of its higher Lewis acidity (than **Zn-PP** monomer) and the presence of the methoxide. In the line of reasoning, we expect that the (**MeO-Al-PP**)$_4$ tetramer would also have higher Lewis acidity than (**Zn-PP**)$_4$ and Lewis acid activation of the PNPDPP substrate would be important.

From the estimated data for k_{path3}(Al teramer) and k_{path3}(Al monomer), the EM parameter for the methoxide-induced-only pathway catalyzed by (**MeO-Al-PP**)$_4$ can be calculated as follows:

$$k_{(\text{MeO-Al-PP})4}/k_{\text{MeO-Al-PP monomer}} \approx (1.005 \times 10^{-3}\ \text{s}^{-1})/(8.0 \times 10^{-6}\ \text{M}^{-1}\cdot\text{s}^{-1}) = 125\ \text{M}$$

This EM value is in the same range as the 110-200 fold increase in the localized methoxide concentrations that we estimated from geometrical considerations (see above). Although this EM value is a simple number that can be used for comparing the catalytic efficiency of (**MeO-Al-PP**)$_4$ against that of the **MeO-Al-PP** monomer and other supramolecular catalyst systems, it oversimplifies the uniqueness of the large (**MeO-Al-PP**)$_4$ cavity in being able to position up to 4 methoxide ions around 2 encapsulated PNPDPP substrates. In addition, while our geometrical estimate of the local methoxide concentration reported at the beginning of this section IX may seem a bit naïve, it allows for a separate estimate of the local methoxide concentration apart from the encapsulated PNPDPP. Lastly, we note that the geometrical estimate does not require us to assume that the other two methanolysis pathways are the same for the Zn and Al-OMe systems.

X. Product formation rates for the methanolysis of *p*-nitrophenyl dimethyl phosphate (PNPDMP), *p*-nitrophenyl dipropyl phosphate (PNPDPrP), and *p*-nitrophenyl dibutyl phosphate (PNPDBP). Reactions were carried out as described above in section VIII with several porphyrin catalysts and conversion data was collected. The progress for the methanolysis of *p*-nitrophenyl dialky phosphates (25 mM) at 333 K in a mixture of $CHCl_3$/MeOH (1:1 v/v) was analyzed via ^{31}P NMR spectroscopy to determine the yield of methanolyzed product. At different times, aliquots (0.16 mL) were withdrawn from the reaction mixtures and filtered through a pad of silica gel, which was then washed with ethyl acetate (3 × 2 mL). ^{31}P NMR spectra were acquired with at least 500

scans on each sample. The chemical shifts of the methanolyzed product for each phosphate substrate were compared with the authentic samples synthesized by following a modified literature procedure.[S12]

Table S2 Product formation rates for the methanolysis of PNPDMP, PNPDPrP, and PNPDBP in the presence of 3 mol% of (**MeO-Al-PP**)$_4$ at 12.3 M MeOH.

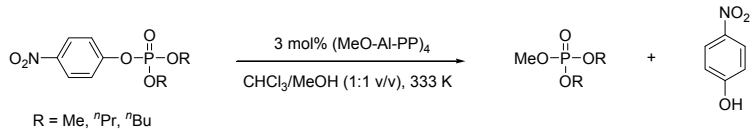

Phosphate triester	(MeO-Al-PP)$_4$ (mol %)	Observed initial rate (M/s)
PNPDMP	3	1.03×10^{-7}
PNPDPrP	3	4.23×10^{-8}
PNPDBP	3	3.14×10^{-8}

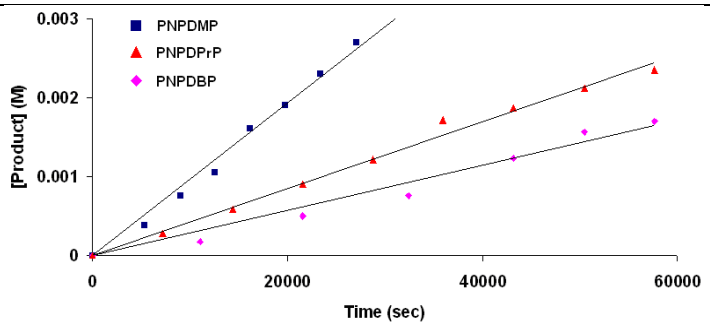

Table S3 Product formation rates for the methanolysis of PNPDMP and PNPDBP in the presence of 3 mol% of (**Zn-PP**)$_4$ at 12.3 M MeOH.

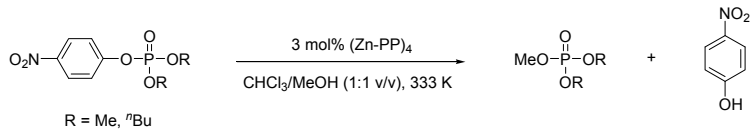

Phosphate triester	(Zn-PP)$_4$ (mol %)	Observed initial rate (M/s)
PNPDPP	3	1.26×10^{-8}
PNPDMP	3	1.05×10^{-8}
PNPDBP	3	9.62×10^{-9}

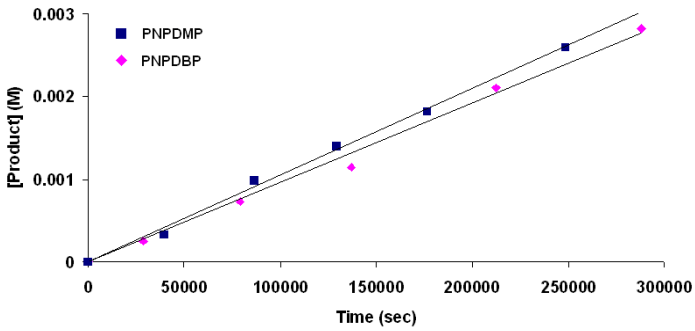

Table S4 Product formation rates for the methanolysis of PNPDMP and PNPDBP in the presence of 12 mol% of **MeO-Al-PP** or **Zn-PP** monomers at 12.3 M MeOH.

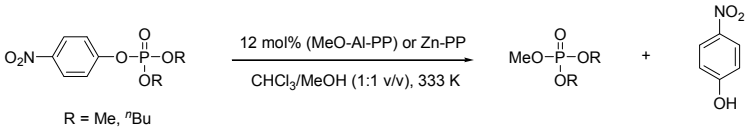

Phosphate triester	Zn-PP (12 mol %)	(MeO-Al-PP) (12 mol %)
	Observed initial rate (M/s)	Observed initial rate (M/s)
PNPDPP	2.66×10^{-9}	3.28×10^{-9}
PNPDMP	2.20×10^{-9}	2.98×10^{-9}
PNPDBP	1.87×10^{-9}	2.63×10^{-9}

XI. Product formation rates for the methanolysis of PNPDPP catalyzed by (MeO-Al-PP)$_4$ or MeO-Al-PP monomer at various MeOH concentrations. Reactions were carried out as described above in section VIII with 3 mol% of (**MeO-Al-PP**)$_4$ or 12 mol% of **MeO-Al-PP** at various MeOH concentrations (4.3, 8.3, 12.3, 15.3, and 18.3 M MeOH). The initial yields of MDPP were monitored by ^{31}P NMR spectroscopy and the resulting initial rates for porphyrin catalysts were obtained after background-corrected with the rates for the uncatalyzed reactions (Table S5).

Table S5 Product formation rates for the methanolysis of PNPDPP in the presence of 3 mol% of (**MeO-Al-PP**)$_4$ (a) or 12 mol% of **MeO-Al-PP** monomer (b). The ratio of initial rates between (**MeO-Al-PP**)$_4$ and **MeO-Al-PP** monomer at various MeOH concentrations (c). Reported catalyzed rates were background-corrected from uncatalyzed reactions.

MeOH (M)	Initial rate (M/s) with (MeO-Al-PP)$_4$	Initial rate (M/s) with MeO-Al-PP monomer	Ratio of the initial rates ($Rate_{(MeO\text{-}Al\text{-}PP)_4}/Rate_{MeO\text{-}Al\text{-}PP}$)
18.3	6.55×10^{-7}	4.23×10^{-9}	155
15.3	5.27×10^{-7}	4.07×10^{-9}	129
12.3	3.91×10^{-7}	3.28×10^{-9}	119
8.3	2.29×10^{-7}	2.18×10^{-9}	105
4.3	1.17×10^{-7}	1.17×10^{-9}	100

(a)

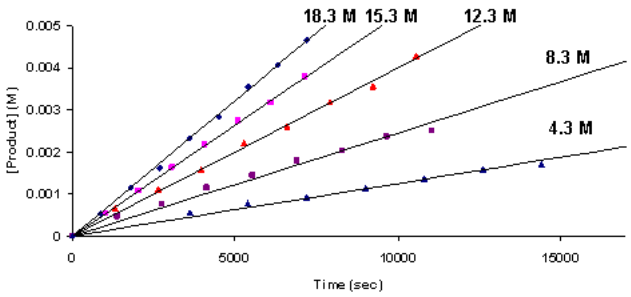

(b)

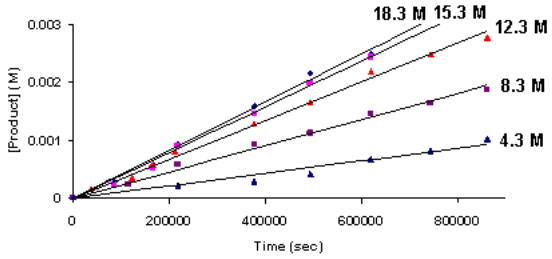

(c)

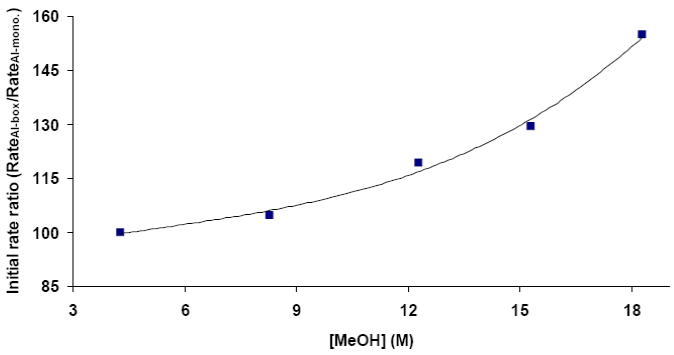

XII. Measurement of binding constants by UV-vis and fluorescence titrations. The UV-vis spectrophotometric titrations were conducted by progressively adding small aliquots (5 μL) of guest solution (15.6 M for neat MeOH or 1.3 M for PNPDPP in $CHCl_3$), using a 25 μL microsyringe, to a cuvette containing the porphyrin tetramer solution (2.3 mL of a 0.39 μM solution in $CHCl_3$) or the porphyrin monomer solution (2.3 mL of a 1.54 μM solution in $CHCl_3$). To minimize the change of the solution volume, the maximum total added volume for all aliquots of the guest solutions was less than 100 μL. As an example for the analysis of UV-vis titration data, the difference in absorbance (ΔA) of the (**MeO-Al-PP**)$_4$ in the presence and absence of the guest was calculated and the data were plotted against [guest] (guest = MeOH or PNPDPP, Fig. S31 and Fig. S32). Simultaneous binding of the guest to the host was assumed to vary in the 1:n stoichiometries ((**MeO-Al-PP**)$_4$:guest) and the binding constants K_a for these species were derived using the Marquardt least-squares minimization[S15] based on the equations:

$$(\text{MeO-Al-PP})_4 + nL \xrightleftharpoons{K_a} (\text{MeO-Al-PP})_4\cdot L_n$$

$$K_a = \frac{[(\text{MeO-Al-PP})_4\cdot L_n]}{[(\text{MeO-Al-PP})_4][L]^n} \quad \text{(S1)}$$

$$C_{(\text{MeO-Al-PP})_4} = [(\text{MeO-Al-PP})_4] + [(\text{MeO-Al-PP})_4\cdot L_n] \quad \text{(S2)}$$

$$C_L \approx [L] \quad \text{(S3)}$$

$$[(\text{MeO-Al-PP})_4\cdot L_n] = \frac{C_{(\text{MeO-Al-PP})_4} K_a}{K_a + (1/C_L)^n} \quad \text{(S4)}$$

K_a : Binding constant of MeOH or PNPDPP to (MeO-Al-PP)$_4$
n : Binding number of MeOH or PNPDPP to (MeO-Al-PP)$_4$
[(MeO-Al-PP)$_4$] : Concentration of (MeO-Al-PP)$_4$
[L] : Concentration of MeOH or PNPDPP
$C_{(\text{MeO-Al-PP})_4}$: Total concentration of (MeO-Al-PP)$_4$
C_L : Total concentration of MeOH or PNPDPP

Eq S4 indicates that [(**MeO-Al-PP**)$_4$·L$_n$] is a function of n (the number of guest binding) and K_a when C_L and $C_{(\text{MeO-Al-PP})_4}$ are known. Two unknown parameters (n and K_a) in Eq S4 for single-guest (n = 1), two-guest (n = 2), three-guest (n = 3), and four-guest (n = 4) binding models were fitted from the UV titration data with the Marquardt algorithm in OriginPro 8.0 software to minimize the value of $\Sigma([(\textbf{MeO-Al-PP})_4\cdot L_n]_{exp} - [(\textbf{MeO-Al-PP})_4\cdot L_n]_{calc})^2$.[S15] To obtain the speciation distribution diagrams shown as an inset in Fig. S31a and Fig. S32a, we performed MCR-ALS (multivariable curve resolution-alternative least square) analysis.[S16] The quality of the fitting between calculated curve and experimental titration data indicates that single-guest-binding mode for [(**MeO-Al-PP**)$_4$·MeOH] and two-guest-binding mode for [(**MeO-Al-PP**)$_4$·(PNPDPP)$_2$] are reasonable in $CHCl_3$.

Fitting the speciation distribution of [(**MeO-Al-PP**)$_4$·(MeOH)] for the MeOH binding to Eq S4 gave a good fit with a binding constant of K_a = 7.5 M^{-1} (n = 1). Additionally, fitting the speciation distribution of [(**MeO-Al-PP**)$_4$·(PNPDPP)$_2$] for the PNPDPP binding to Eq S4 gave a good fit with a binding constant of K_a = 2570 M^{-2} (n = 2), indicating that two PNPDPP are simultaneously coordinating to one (**MeO-Al-PP**)$_4$. This fitting result reveals that the binding constant for one PNPDPP could be $K_a = (2570\ M^{-2})^{1/2} = 50.7\ M^{-1}$. Similarly, the speciation distributions for (**Zn-PP**)$_4$ are [(**Zn-PP**)$_4$·MeOH] and [(**Zn-PP**)$_4$·(PNPDPP)$_2$]. As expected, the speciation distributions for the **Zn-PP** monomer are [(**Zn-PP**)·MeOH] and [(**Zn-PP**)·(PNPDPP)]; and those for the **MeO-Al-PP** monomer are [(**MeO-Al-PP**)·(MeOH)] and [(**MeO-Al-PP**)·(PNPDPP)]; respectively.

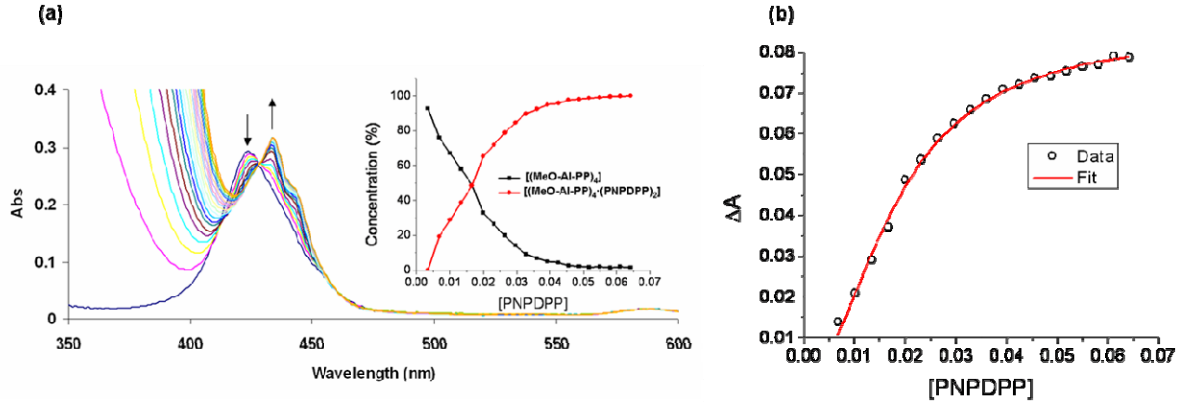

Fig. S31 (a) The changes in the absorption spectra of (**MeO-Al-PP**)$_4$ in $CHCl_3$ upon titration with PNPDPP at 296 K. Arrows show the directions of change in absorption with increasing PNPDPP concentration. Inset: speciation distribution diagram for the binding of PNPDPP to (**MeO-Al-PP**)$_4$ by MCR-ALS. (b) The absorption changes at 445 nm and the result of fitting the data to Eq S4.

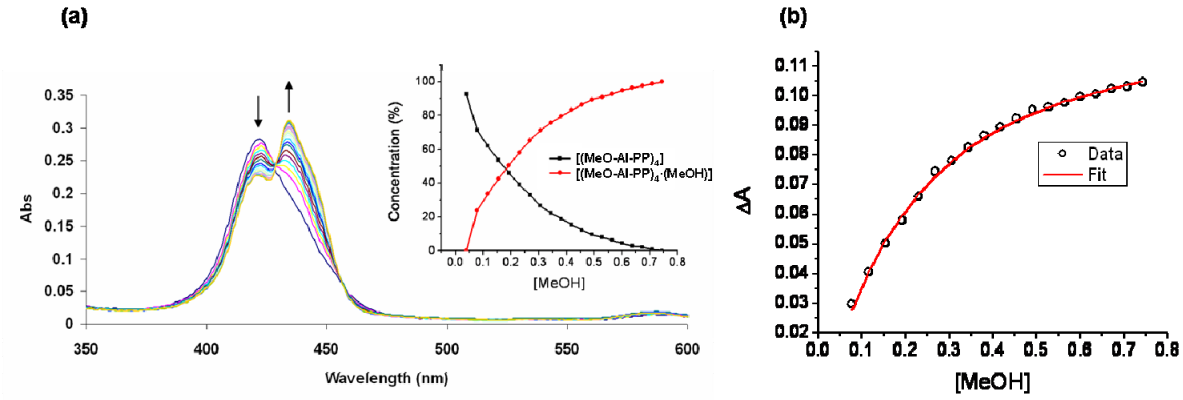

Fig. S32 (a) The changes in the absorption spectra of (**MeO-Al-PP**)$_4$ in $CHCl_3$ upon titration with MeOH at 296 K. Arrows show the directions of change in absorption with increasing MeOH concentration. Inset: speciation distribution diagram for the binding of MeOH to (**MeO-Al-PP**)$_4$ by MCR-ALS. (b) The absorption changes at 440 nm and the result of fitting the data to Eq S4.

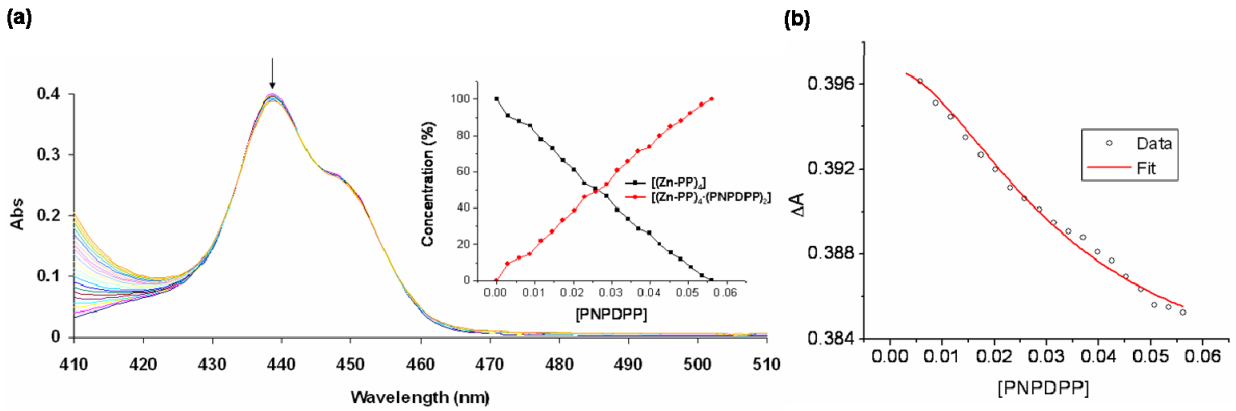

Fig. S33 (a) The changes in the absorption spectra of (**Zn-PP**)$_4$ in $CHCl_3$ upon titration with PNPDPP at 296 K. The arrow shows the direction of change in absorption with increasing PNPDPP concentration. Inset: speciation distribution diagram for the binding of PNPDPP to (**Zn-PP**)$_4$ by MCR-ALS. (b) The absorption changes at 438 nm and the result of fitting the data to Eq S4.

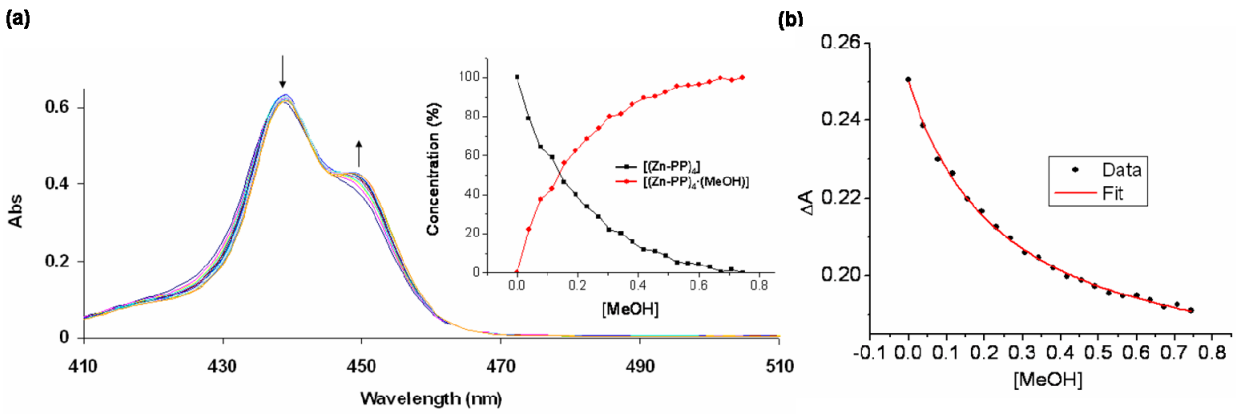

Fig. S34 (a) The changes in the absorption spectra of (**Zn-PP**)$_4$ in $CHCl_3$ upon titration with MeOH at 296 K. Arrows show the directions of change in absorption with increasing MeOH concentration. Inset: speciation distribution diagram for the binding of MeOH to (**Zn-PP**)$_4$ by MCR-ALS. (b) The absorption changes at 430 nm and the result of fitting the data to Eq S4.

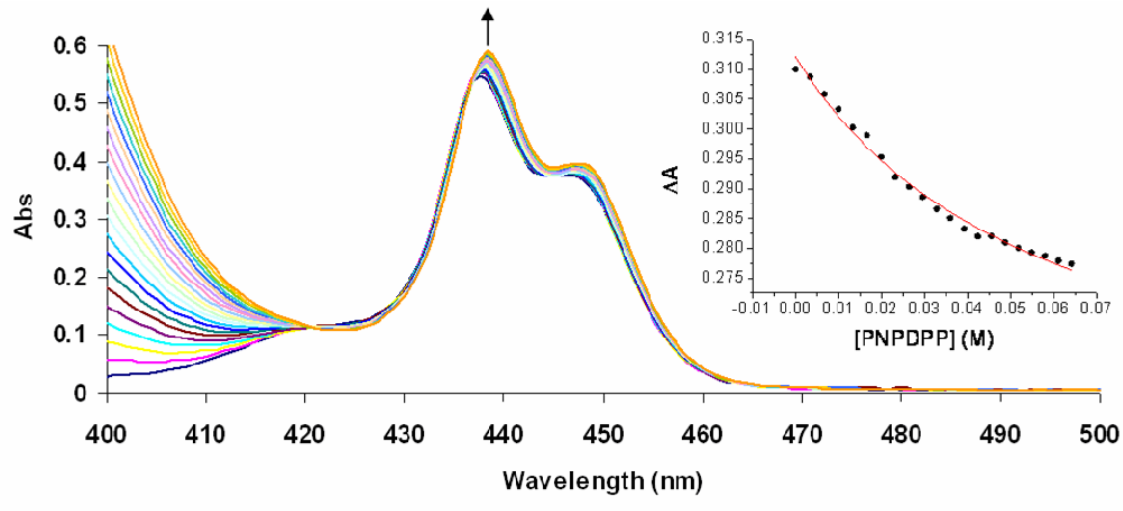

Fig. S35 The changes in the absorption spectra of the **MeO-Al-PP** monomer in $CHCl_3$ upon titration with PNPDPP at 296 K. The arrow shows the direction of change in absorption with increasing PNPDPP concentration. Inset: the absorption changes at 434 nm and the result of fitting the data to Eq S4.

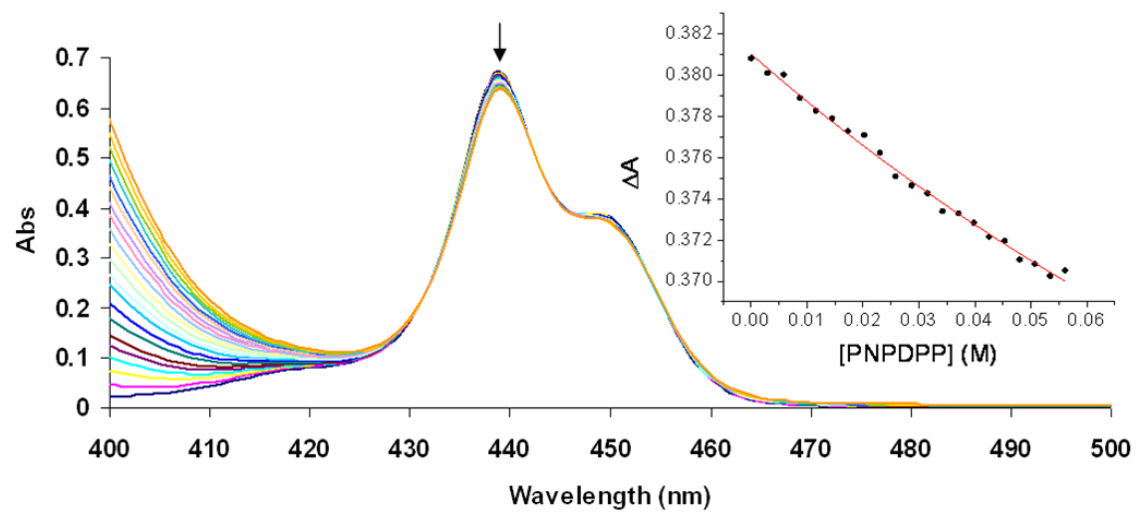

Fig. S36 The changes in the absorption spectra of the **Zn-PP** monomer in $CHCl_3$ upon titration with PNPDPP at 296 K. The arrow shows the direction of change in absorption with increasing PNPDPP concentration. Inset: the absorption changes at 450 nm and the result of fitting the data to Eq S4.

Table S6 UV-vis-measured binding constants of MeOH and PNPDPP to porphyrin boxes and monomers in $CHCl_3$.

Porphyrin species	Binding constant of MeOH ($K_{a(MeOH)}$, M^{-1})[a]	Binding constant of PNPDPP ($K_{a(PNPDPP)}$, M^{-1})[a]
(MeO-Al-PP)$_4$	7.5 ± 0.5	50.7 ± 1.7
(Zn-PP)$_4$	4.0 ± 0.2	30.4 ± 1.9
MeO-Al-PP monomer	–	17.1 ± 2.6
Zn-PP monomer	–	8.0 ± 2.8

[a]UV-vis titration experiments of MeOH and PNPDPP were carried out at 296 K in $CHCl_3$. The solutions of the porphyrin boxes were 0.39 μM and the solutions of the porphyrin monomers were 1.54 μM.

The fluorescence titrations were carried out by progressively adding small aliquots (5 μL) of PNPDPP solution (1.3 M, PNPDPP stock solutions in $CHCl_3$/MeOH (1:1 v/v)), using a 25 μL microsyringe, to a quartz fluorescence cuvette containing the porphyrin box solution (1 mL of a 0.02 μM solution in $CHCl_3$/MeOH (1:1 v/v)) or the porphyrin monomer solution (1 mL of a 0.04 μM solution in $CHCl_3$/MeOH (1:1 v/v)). To minimize the change of the solution volume, the maximum total added volume for all aliquots of the guest solution was less than 100 μL. The solution was excited at 442 nm and the fluorescent emission intensity was recorded from 500 to 800 nm after each addition of PNPDPP. A plot of intensity versus [PNPDPP] was carried out to yield the binding constant (K_a) by the nonlinear fitting method described above.[S15]

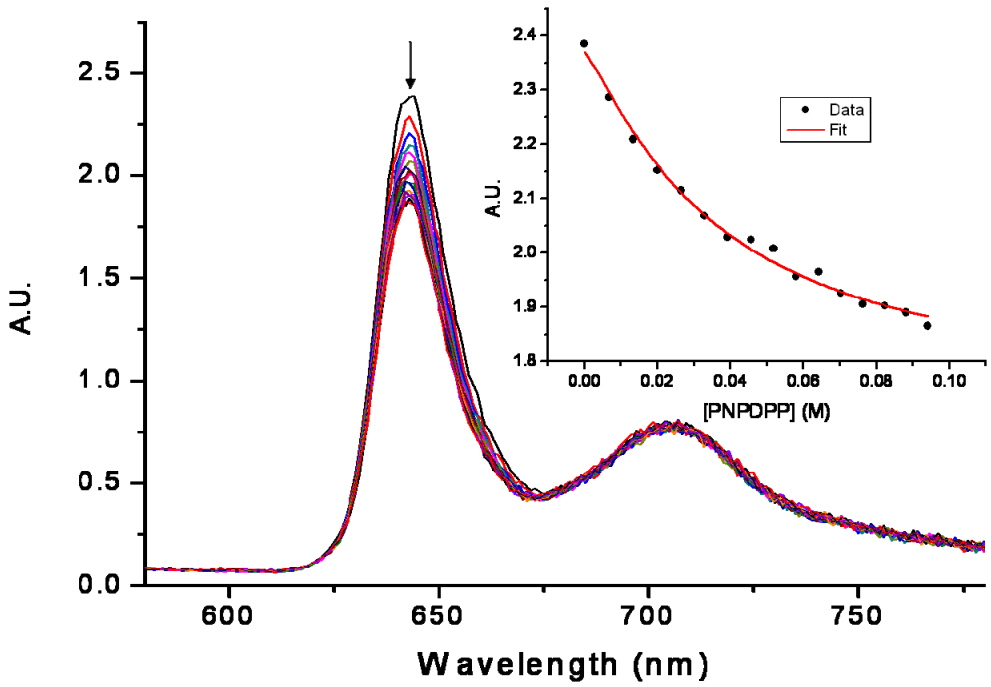

Fig. S37 The changes in the fluorescence emission spectra of (**MeO-Al-PP**)$_4$ in a mixture of $CHCl_3$/MeOH (1:1 v/v) upon titration with PNPDPP at 296 K. The arrow shows the direction of change in fluorescence emission with increasing PNPDPP concentration. Inset: the fluorescence emission changes at 643 nm and the result of fitting the data to Eq S4.

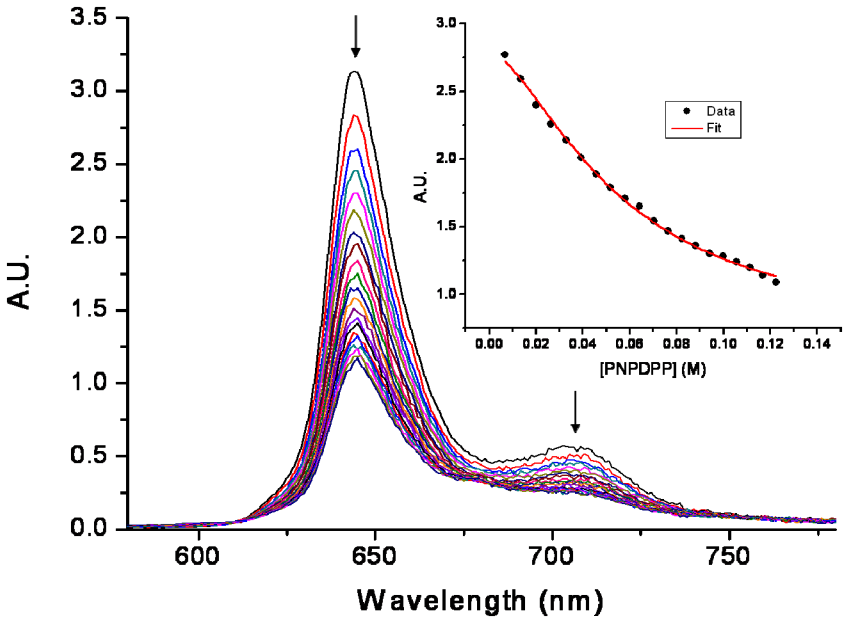

Fig. S38 The changes in the fluorescence emission spectra of (**Zn-PP**)$_4$ in a mixture of $CHCl_3$/MeOH (1:1 v/v) upon titration with PNPDPP at 296 K. Arrows show the directions of change in fluorescence emission with increasing PNPDPP concentration. Inset: the fluorescence emission changes at 643 nm and the result of fitting the data to Eq S4.

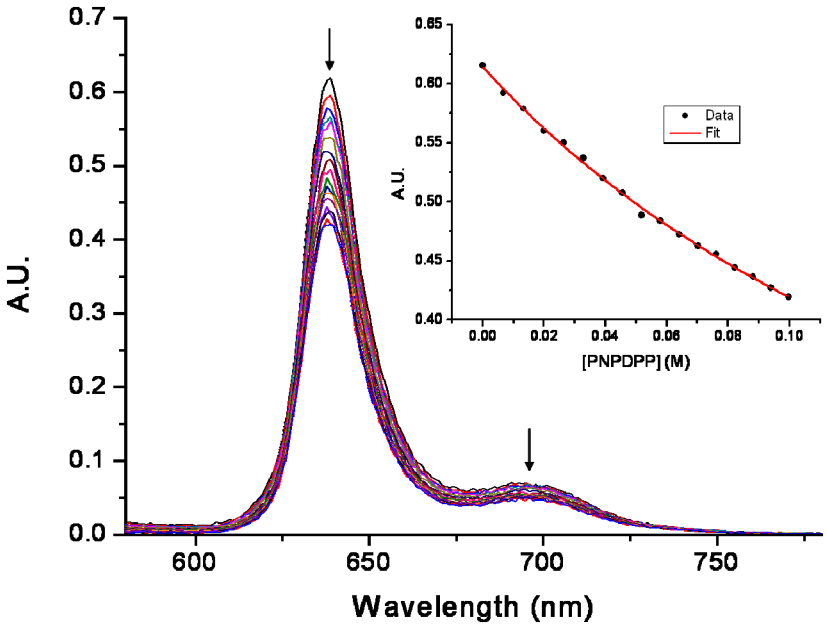

Fig. S39 The changes in the fluorescence emission spectra of the **MeO-Al-PP** monomer in a mixture of $CHCl_3$/MeOH (1:1 v/v) upon titration with PNPDPP at 296 K. Arrows show the directions of change in fluorescence emission with increasing PNPDPP concentration. Inset: the fluorescence emission changes at 638 nm and the result of fitting the data to Eq S4.

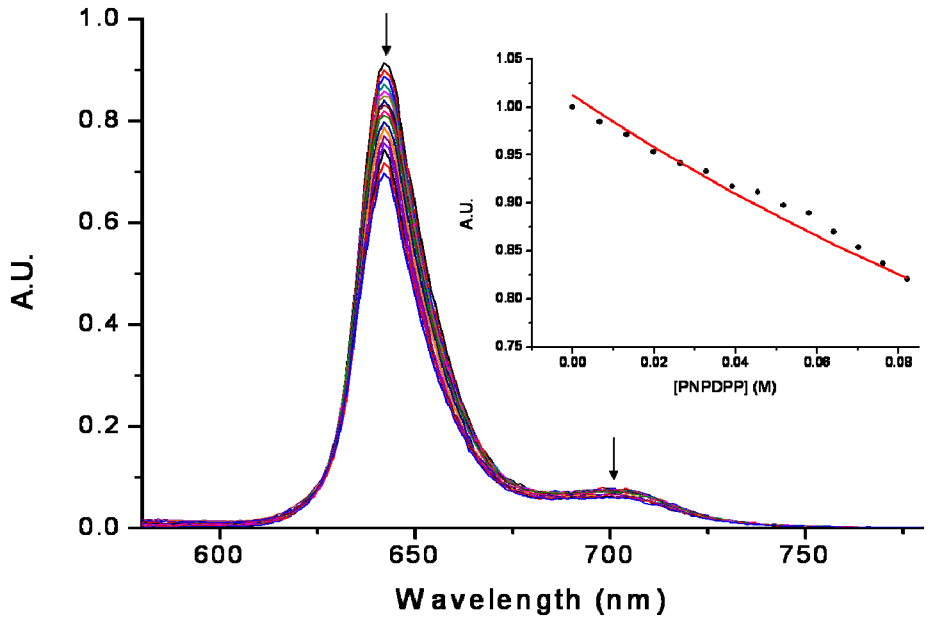

Fig. S40 The changes in the fluorescence emission spectra of the **Zn-PP** monomer in a mixture of $CHCl_3$/MeOH (1:1 v/v) upon titration with PNPDPP at 296 K. Arrows show the directions of change in fluorescence emission with increasing PNPDPP concentration. Inset: the fluorescence emission changes at 642 nm and the result of fitting the data to Eq S4.

Table S7 Fluorescence-based binding constants of PNPDPP to porphyrin boxes and monomers in a mixture of $CHCl_3$/MeOH (1:1 v/v).

Porphyrin species	Binding constant of PNPDPP ($K_{a(PNPDPP)}$, M^{-1})[a]
(MeO-Al-PP)$_4$	26.9 ± 2.6
(Zn-PP)$_4$	17.3 ± 0.7
MeO-Al-PP monomer	4.5 ± 0.6
Zn-PP monomer	2.8 ± 1.3

[a]Fluorescence titration experiments of PNPDPP were carried out at 296 K in a mixture of $CHCl_3$/MeOH (1:1 v/v). The solutions of the porphyrin boxes were 0.02 μM and the solution of the porphyrin monomers were 0.04 μM.

The predicted binding constants of PNPDPP ($K_{a(PNPDPP)}$) to (MeO-Al-PP)$_4$ and (Zn-PP)$_4$ in a mixture of CHCl$_3$/MeOH (1:1 v/v) based on the $K_{a(PNPDPP)}$ and $K_{a(MeOH)}$ in pure CHCl$_3$. The speciation distributions obtained from MCR-ALS (multivariable curve resolution-alternative least square) analysis[S16] (Figs. S31-S34) indicate two-guest-binding mode for [**H**·(PNPDPP)$_2$] and single-guest-binding mode for [**H**·MeOH] (**H** = (**MeO-Al-PP**)$_4$ and (**Zn-PP**)$_4$ hosts). Thus, the binding constant of PNPDPP to the porphyrin tetramer host (**H**) in pure CHCl$_3$ (K_{PNPDPP}(CHCl$_3$)) can be calculated as follows:

$$\mathrm{H} + 2\,\mathrm{PNPDPP} \xrightleftharpoons{K_{PNPDPP}} \mathrm{H{\cdot}PNPDPP_2}$$

$$K_{PNPDPP}(\mathrm{CHCl_3}, \mathrm{M^{-2}}) = \frac{[\mathrm{H{\cdot}PNPDPP_2}]}{[\mathrm{H}][\mathrm{PNPDPP}]^2} \qquad \text{(S5)}$$

From Table S6, K_{PNPDPP}(CHCl$_3$), the experimental binding constant of PNPDPP to the porphyrin tetramer host (**H**) in pure CHCl$_3$ is 2570 ± 173 M^{-2} for (**MeO-Al-PP**)$_4$ and 924 ± 118 M^{-2} for (**Zn-PP**)$_4$.

The binding constants of MeOH to the porphyrin tetramer host (**H**) in pure CHCl$_3$ (K_{MeOH}(CHCl$_3$)) can be calculated as follows:

$$\mathrm{H} + \mathrm{MeOH} \xrightleftharpoons{K_{MeOH}} \mathrm{H{\cdot}MeOH}$$

$$K_{MeOH}(\mathrm{CHCl_3}, \mathrm{M^{-1}}) = \frac{[\mathrm{H{\cdot}MeOH}]}{[\mathrm{H}][\mathrm{MeOH}]}$$

$$\frac{[\mathrm{H{\cdot}MeOH}]}{[\mathrm{H}]} = K_{MeOH}[\mathrm{MeOH}] \qquad \text{(S6)}$$

From Table S6, K_{MeOH}(CHCl$_3$), the experimental binding constant of MeOH to porphyrin boxes (**H**) in pure CHCl$_3$ is 7.5 ± 0.5 M^{-1} for (**MeO-Al-PP**)$_4$ and 4.0 ± 0.2 M^{-1} for (**Zn-PP**)$_4$.

In a mixture of CHCl$_3$/MeOH (1:1 v/v), the association constant of PNPDPP to the porphyrin box (H) at room temperature (K_{PNPDPP}(CHCl$_3$/MeOH)) can be expressed as:

$$(\mathrm{H} + \mathrm{H{\cdot}MeOH}) + 2\,\mathrm{PNPDPP} \xrightleftharpoons{K_{PNPDPP}} \mathrm{H{\cdot}PNPDPP_2}$$

$$K_{PNPDPP}(\mathrm{CHCl_3/MeOH}, \mathrm{M^{-2}}) = \frac{[\mathrm{H{\cdot}PNPDPP_2}]}{([\mathrm{H}]+[\mathrm{H{\cdot}MeOH}])[\mathrm{PNPDPP}]^2}$$

$$= \frac{[\mathrm{H{\cdot}PNPDPP_2}]}{(1+K_{MeOH}(\mathrm{CHCl_3})[\mathrm{MeOH}])[\mathrm{H}][\mathrm{PNPDPP}]^2}$$

$$= \frac{K_{PNPDPP}(\mathrm{CHCl_3})}{1+K_{MeOH}(\mathrm{CHCl_3})[\mathrm{MeOH}]} \qquad \text{(S7)}$$

In a mixture of CHCl$_3$/MeOH (1:1 v/v, 12.3 M MeOH),

K_{PNPDPP}(CHCl$_3$/MeOH) for (**MeO-Al-PP**)$_4$ = (2570 M^{-2})/(1 + (7.5 M^{-1} × 12.3 M)) = 27.6 M^{-2}

From this, the predicted association constant of one PNPDPP to (**MeO-Al-PP**)$_4$ at 12.3 M MeOH is:

$K_{a(PNPDPP)} = (K_{PNPDPP})^{1/2} = (27.6\ M^{-2})^{1/2} = 5.3\ M^{-1}$.

In a mixture of $CHCl_3$/MeOH (1:1 v/v, 12.3 M MeOH),

K_{PNPDPP} for (**Zn-PP**)$_4$ = (924 M^{-2})/(1 + (4.0 M^{-1} × 12.3 M)) = 18.4 M^{-2}

From this, the predicted association constant of one PNPDPP to (**Zn-PP**)$_4$ at 12.3 M MeOH is:

$K_{a(PNPDPP)} = (K_{PNPDPP})^{1/2} = (18.4\ M^{-2})^{1/2} = 4.3\ M^{-1}$

Standard error of predicted K_a values. To calculate the standard error of predicted K_a values based on the uncertainty of experimental K_a, established error propagation equations were used.[S17] The calculation process for the predicted $K_{a(PNPDPP)}$ to (**MeO-Al-PP**)$_4$ is described as follows.

$$K_{PNPDPP}\ (CHCl_3/MeOH,\ M^{-2}) = \frac{2570 \pm 173\ M^{-2}}{1 + (7.5 \pm 0.5\ M^{-1} \times 12.3 \times 0.1\ M)} = (27.6 \pm \delta_d)\ M^{-2} \qquad \text{(S8)}$$

$$K_{a(PNPDPP)}\ (CHCl_3/MeOH,\ M^{-1}) = (K_{a(PNPDPP)}\ M^{-2})^{1/2} = (5.3 \pm \delta_f)\ M^{-1} \qquad \text{(S9)}$$

To determine the uncertainty (δ_f) of the predicted $K_{a(PNPDPP)}$ in Eq S9, we first calculate the uncertainty (δ_m) of the denominator (7.5 ± 0.5 M^{-1} × 12.3 ± 0.1 M) in Eq S8. If dependent variables x and y are related to the measured quantities a and c by the relations:

$$x = a \pm b$$

$$y = c \pm d$$

(± b and ± d are standard errors)

then the uncertainty (δ_m) of the multiplication of these variables ($z = x \times y = (a \pm b \times c \pm d)$) is given by:

$$\delta_m = (a \times c) \times (b^2/a^2 + d^2/c^2)^{1/2}$$

So the δ_m value of the denominator is $(7.5 \times 12.3) \times (0.5^2/7.5^2 + 0.1^2/12.3^2)^{1/2} = 6.2$

OR:

$$K_{PNPDPP}\ (CHCl_3/MeOH,\ M^{-2}) = \frac{2570 \pm 173\ M^{-2}}{93.3 \pm 6.2}$$

Similarly, if $x = a \pm b$ and $y = c \pm d$, then the uncertainty (δ_d) of division ($z = x/y = (a \pm b)/(c \pm d)$) is given by:

$$\delta_d = (a/c) \times (b^2/a^2 + d^2/c^2)^{1/2}$$

So the δ_d value is $(2570/93.3) \times (173^2/2570^2 + 6.2^2/93.3^2)^{1/2} = 2.6$.

OR:

$$K_{PNPDPP}\ (CHCl_3/MeOH,\ M^{-2}) = (27.6 \pm 2.6)\ M^{-2}$$

Finally, if $x = a \pm b$, then the uncertainty (δ_f) of z powered by 1/2 ($z = x^{1/2} = (a \pm b)^{1/2}$) is given by:

$$\delta_f = (1/2) \times (a)^{1/2} \times (b/a)$$

Thus, the final δ_f value is $(1/2) \times (27.6)^{1/2} \times (2.6/27.6) = 0.3$.

$$K_{a(PNPDPP)}\ (CHCl_3/MeOH,\ M^{-1}) = (5.3 \pm 0.3)\ M^{-1}$$

The same calculation procedure for **(Zn-PP)$_4$** provides the uncertainty (δ_f) of the predicted $K_{a(PNPDPP)}$ as 0.3.

Table S8 The predicted binding constants of PNPDPP ($K_{a(PNPDPP)}$) to **(MeO-Al-PP)$_4$** and **(Zn-PP)$_4$** in a mixture of $CHCl_3$/MeOH (1:1 v/v).

Porphyrin species	Binding constant of PNPDPP ($K_{a(PNPDPP)}$)	
	Predicted $K_{a(PNPDPP)}$ (M^{-1})	Experimental $K_{a(PNPDPP)}$ (M^{-1})[a]
(MeO-Al-PP)$_4$	5.3 ± 0.3	26.9 ± 2.6
(Zn-PP)$_4$	4.3 ± 0.3	17.3 ± 0.7

[a]Experimental $K_{a(PNPDPP)}$ values were obtained from the room-temperature fluorescence titration of PNPDPP to 0.02 μM solution of the porphyrin boxes in a mixture of $CHCl_3$/MeOH (1:1 v/v). See the complete data set in Table S7.

XIII. NMR studies of the encapsulation of PNPDPP in (MeO-Al-PP)$_4$ or (Zn-PP)$_4$.

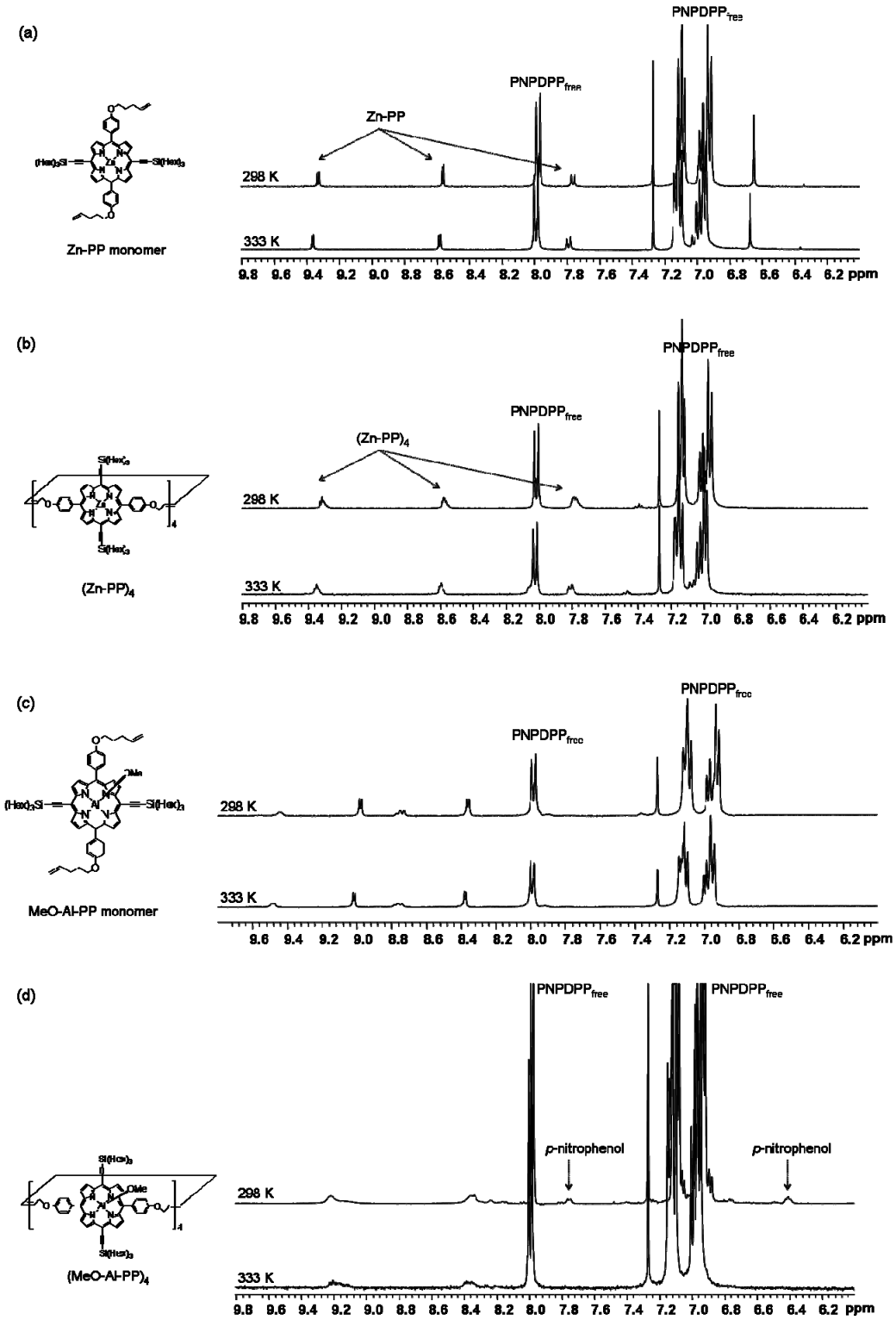

Fig. S41 Variable-temperature (VT) ^{1}H NMR (400 MHz) spectra of a combination of porphyrin species (0.03 or 0.12 equiv) and PNPDPP (1.0 equiv) in a mixture of $CDCl_3$ and CD_3OD (1:1 v/v) at 298 and 333 K: (a) [**Zn-PP**] = 3.0 mM and [PNPDPP] = 25 mM, (b) [(Zn-PP)$_4$] = 0.75 mM and [PNPDPP] = 25 mM, (c) [**MeO-Al-PP**] = 3.0 mM and [PNPDPP] = 25 mM, (d) [(**MeO-Al-PP**)$_4$] = 0.75 mM and [PNPDPP] = 25 mM. Spectra were collected within 1 h of sample preparation to ensure that no signi-ficant conversion has occurred.

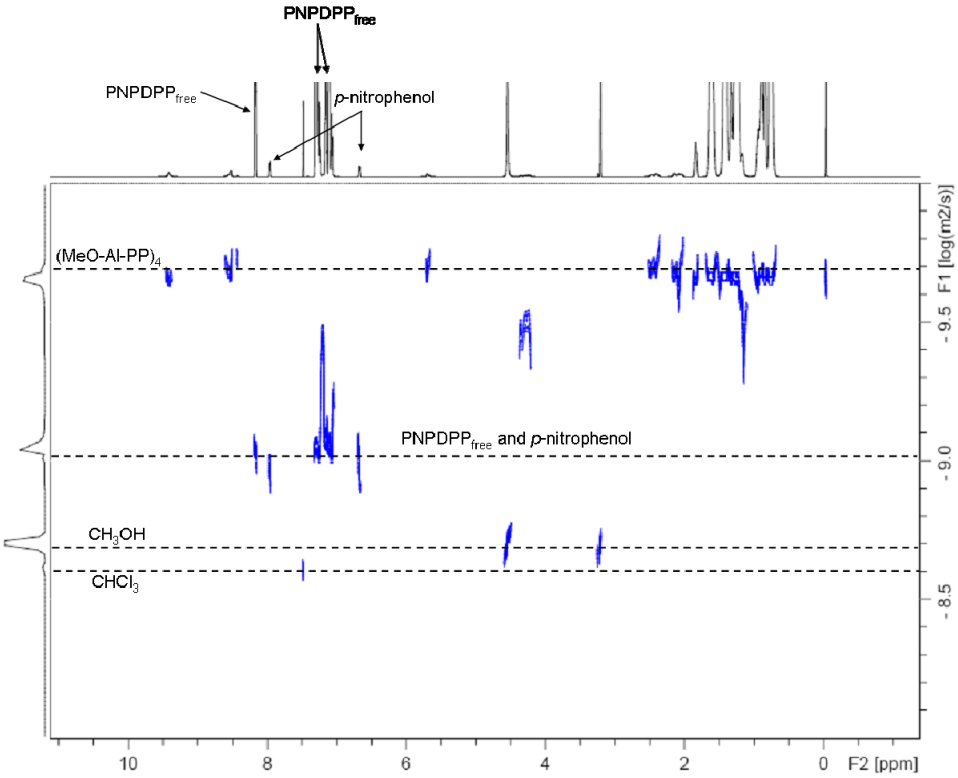

Fig. S42 The DOSY NMR (600 MHz) spectrum of a combination of (**MeO-Al-PP**)$_4$ (0.03 equiv) and PNPDPP (1.0 equiv) in a mixture of $CDCl_3$ and CD_3OD (1:1 v/v) at 298 K; [(**MeO-Al-PP**)$_4$] = 0.75 mM and [PNPDPP] = 25 mM. Spectrum was collected within 2 h of sample preparation to ensure that no significant conversion has occurred.

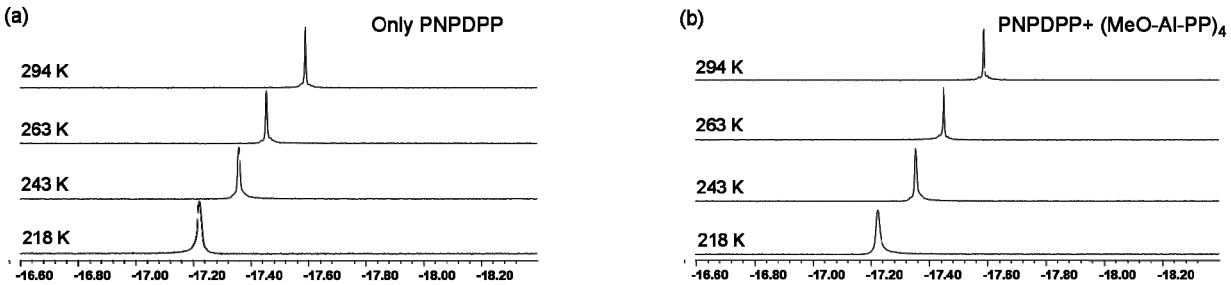

Fig. S43 ^{31}P NMR (161.9 MHz) spectra at different temperatures for: (a) PNPDPP (25 mM) in a mixture of $CDCl_3$ and CD_3OD (1:1 v/v), (b) a combination of (**MeO-Al-PP**)$_4$ (0.75 mM) and PNPDPP (25 mM) in a mixture of $CDCl_3$ and CD_3OD (1:1 v/v). Spectra were collected within 2 h of sample preparation to ensure that no significant conversion has occurred.

Table S9 The full width at half maximum (FWHM) of the ^{31}P NMR signals for the spectra shown in Fig. S43.

Temperature (K)	FWHM of the ^{31}P NMR signal (Hz)	
	Only PNPDPP	Combination of PNPDPP and (**MeO-Al-PP**)$_4$
294	0.63	0.46
263	0.93	0.79
243	1.95	1.38
218	2.87	2.51

XIV. Author contributions audit: B.K. and S.T.N. conceived the experiments presented herein. B.K. synthesized all compounds except tetrakis(4(4'-pyridyl)-3,5-dimethylphenyl))porphyrin (**Py-MesP**), which was synthesized by K.T.Y. B.K. carried out the characterization of all compounds, the catalysis experiments, and the UV-vis and fluorescence titration experiments. J.W.K carried out the PFG-NMR experiments. R.K.T. carried out several control experiments. J.T.H. and S.T.N. supervised the project. B.K. wrote the initial draft of the paper and received inputs and corrections from all co-authors. B.K. and S.T.N. finalized the manuscript.

XV. References

S1. A. B. Pangborn, M. A. Giardello, R. H. Grubbs, R. K. Rosen and F. J. Timmers, *Organometallics* 1996, **15**, 1518-1520.

S2. T. Itoh, K. Matsuda, H. Iwamura and K. Hori, *J. Am. Chem. Soc.* 2000, **122**, 2567-2576.

S3. M. Beinhoff, W. Weigel, M. Jurczok, W. Rettig, C. Modrakowski, I. Brüdgam, H. Hartl and A. D. Schlüter, *Eur. J. Org. Chem.* 2001, 3819-3829.

S4. G. Subramaniam and R. K. Gilpin, *Macromolecules* 1990, **23**, 693-697.

S5. K.-T. Youm, S. T. Nguyen and J. T. Hupp, *Chem. Commun.* 2008, 3375-3377.

S6. M. Hu, J. Li and S. Q. Yao, *Org. Lett.* 2008, **10**, 5529-5531.

S7. J. E. Reeve, H. A. Collins, K. D. Mey, M. M. Kohl, K. J. Thorley, O. Paulsen, K. Clays and H. L. Anderson, *J. Am. Chem. Soc.* 2009, **131**, 2758-2759.

S8. A. Jerschow and N. Müller, *J. Magn. Reson. Ser. A* 1996, **123**, 222-225.

S9. A. Jerschow and N. Müller, *J. Magn. Reson.* 1997, **125**, 372-375

S10. E. Bock and E. Tomchuk, *Can. J. Chem.* 1969, **47**, 4635-4638.

S11. B. A. Bushuk, A. N. Rubinov and A. P. Stupak, *Sov. J. Quantum Electron.* 1987, **17**, 578-579.

S12. S. Jones and D. Selitsianos, *Org. Lett.* 2002, **4**, 3671-3673.

S13. S. Glab and A. Hulanicki, *Talanta* 1981, **28**, 183-186.

S14. R. Cacciapaglia, S. Di Stefano and L. Mandolini, *Acc. Chem. Res.* 2004, **37**, 113-122.

S15. OriginPro 8.0, OriginLab Corp., Northampton, MA, USA.

S16. J. Jaumot, R. Gargallo, A. de Juan and R. Tauler, *Chemometr. Intell. Lab. Syst.* 2005, **76**, 101-110.

S17. P. R. Bevington and D. K. Robinson, *Data Reduction and Error Analysis for the Physical Sciences*, 2nd Ed., McGraw-Hill, New York, 1992, pp 38-52.